POLITECNICO DI TORINO

Collegio di Ingegneria Chimica e dei Materiali

Corso di Laurea Magistrale
in Ingegneria Chimica e dei Processi Sostenibili

Tesi di Laurea Magistrale

Techno-economic analysis of CO_2 fermentation to acetic acid

Relatori

dott. Francesco Regis
prof. Alessandro Hugo Antonio Monteverde
prof. Debora Fino

Candidato

Noemi Pace

Dicembre 2024

Abstract

Acetic acid is one of the most widely used carboxylic acid, with applications in textile, fibre, pharma and food industries. Nowadays, most of this chemical is produced via energy-intensive and fossil fuel-based processes, contributing to greenhouse gas emissions and environmental pollution. As a consequence, interest in the production of bio-acetic acid is growing. A promising route could be gas fermentation using CO_2 and H_2 as gaseous substrates. This path could potentially overcome the limits associated to sugar fermentation, i.e. the competition with food production and deforestation associated with first-generation biomass and the expensive pretreatment linked to second-generation one. Although CO_2 fermentation is already practiced at an industrial scale for ethanol production, to the best of our knowledge scientific literature lacks any techno-economic analyses focused on the manufacture of acetic acid through the same approach. Therefore, the aim of this work is to present a techno-economic analysis for the production process of acetic acid via fermentation, using captured CO_2 from a waste stream and green hydrogen as substrates.

The process was simulated on Aspen Plus® and is aimed at the production of 37 kton.y^{-1} of glacial acetic acid (99.9 wt%). The fermentation section is preceded by an upstream phase to obtain the reactants at the required purity and is followed by a downstream step to concentrate the very diluted culture broth until glacial acetic acid is obtained. H_2 is produced with alkaline water electrolysis (AEL), whereas CO_2 is captured with chemical absorption with mono ethanolamine (MEA). In particular, CO_2 derives from the upgrade process of biogas into bio-methane of an anaerobic biodigester starting from OFMSW (Organic Fraction of Municipal Solid Waste). The fermentation step has been simulated based on the results of a study in which the fermenter was simulated as a bubble column. The purification of acetic acid occurs with a hybrid process, which combines liquid-liquid extraction and azeotropic distillation using methyl tert-butyl ether (MTBE) as solvent. To maximize energy recovery minimizing utilities consumption, an energy integration was conducted using Aspen Energy Analyzer (HX-NET). Subsequently, an economic analysis was carried out using the Net Present Value (NPV) method to determine a minimum selling price for acetic acid that would cover all investment costs during the plant-life. The estimated price is more than twice the actual market price of glacial acetic acid. Although less economical than traditional methods, gas fermentation offers a sustainable alternative reducing fossil fuels consumption and utilizing CO_2 otherwise emitted to the atmosphere.

Riassunto

L'acido acetico è uno degli acidi carbossilici più utilizzati, con applicazioni principalmente nell'industria tessile, delle fibre, farmaceutica e alimentare. Attualmente, la maggior parte di questo composto è prodotta tramite processi ad alta intensità energetica e basati sull'impiego di combustibili fossili, contribuendo alle emissioni di gas serra e all'inquinamento ambientale. Di conseguenza, cresce l'interesse per la produzione di bio-acido acetico. Una via promettente potrebbe essere la fermentazione di gas utilizzando CO_2 e H_2 come substrati gassosi. In tale contesto, i cosiddetti batteri acetogeni sono in grado di metabolizzare questi gas per produrre acido acetico attraverso la via metabolica Wood-Ljungdahl. Questo approccio potrebbe potenzialmente superare i limiti associati alla fermentazione di zuccheri, come la competizione con la produzione alimentare e la deforestazione legate alla biomassa di prima generazione, nonché il costoso pretrattamento della biomassa di seconda generazione. La fermentazione della CO_2 è già praticata su scala industriale per la sintesi di etanolo, ma, secondo le conoscenze dell'autore, nella letteratura scientifica mancano analisi tecnico-economiche focalizzate sulla produzione di acido acetico tramite lo stesso approccio. Pertanto, l'obiettivo del presente lavoro è presentare un'analisi tecno-economica per il processo di produzione di acido acetico tramite fermentazione, utilizzando come substrati anidride carbonica catturata da una corrente di scarto e idrogeno verde.

Il processo è simulato su Aspen Plus® ed è finalizzato alla produzione di 37 kton.y^{-1} di acido acetico glaciale (99.9% in peso). La sezione di fermentazione è preceduta da una fase a monte per ottenere i reagenti ed è seguita da una fase a valle per concentrare il brodo di coltura molto diluito fino ad ottenere acido acetico glaciale.

L'idrogeno viene prodotto tramite elettrolisi alcalina dell'acqua (AEL). L'elettrolizzatore è stato simulato con una potenza di 0.5 MW, una densità di corrente di 0.4 A.cm^{-2} e un'area attiva delle celle di 1000 cm^2. L'elettrolita utilizzato è una soluzione di idrossido di potassio (KOH) al 30% in peso. Questa simulazione ha consentito di produrre di 166.39 ton.y^{-1} di idrogeno. Per raggiungere l'obiettivo di produttività richiesto dal fermentatore sono necessari 35 moduli simili a quello appena descritto.

Il processo selezionato per la cattura della CO_2 è l'assorbimento chimico con monoetanolammina (MEA). Il gas di alimentazione proviene da una corrente di scarto di un biodigestore, altrimenti rilasciata nell'atmosfera. Contiene tracce di H_2S che vengono preventivamente eliminate con il processo LO-CAT; tale approccio prevede l'utilizzo di una colonna di assorbimento gas-liquido in cui viene alimentata una soluzione catalitica a base di ferro per ossidare H_2S in zolfo elementare. La sezione di assorbimento della CO_2 è composta da due colonne impaccate, un assorbitore ed un rigeneratore. Nel primo, l'anidride carbonica viene catturata dal flusso di gas, mentre nel secondo, l'ammina ricca di CO_2 viene riscaldata per rilasciare l'anidride carbonica ad elevata purezza e rigenerare il solvente. A seguito del processo di cattura, l'ossigeno presente nel flusso ricco di CO_2 viene eliminato in un reattore catalitico in modo da non ostacolare la successiva fase fermentativa, che avviene in condizioni anaerobiche. Dalla simulazione vengono catturati 7407.87 kg.h^{-1} di una corrente di CO_2 al 99.5% in peso.

I reagenti così ottenuti vengono alimentati alla sezione di fermentazione, simulata a due differenti pressioni dello spazio di testa nel fermentatore (2 bar e 10 bar) con lo scopo di identificare la configurazione ottimale. Si è osservato che operando con una pressione di

testa di 2 bar, nonostante una minore produttività del singolo fermentatore, il costo dell'acido acetico risulta ridotto. Inoltre, viene sintetizzato acido formico in quantità trascurabili rispetto a quella prodotta operando a 10 bar.

Per quanto riguarda il processo a valle, la purificazione dell'acido acetico dal brodo di fermentazione altamente diluito richiede due passaggi fondamentali preliminari: filtrazione e scambio ionico. L'effettiva purificazione dell'acido acetico viene effettuata utilizzando un processo ibrido in cui si combinano l'estrazione liquido-liquido con metil terz-butil etere (MTBE) e la distillazione azeotropica. Tale sezione è stata modellata con l'obiettivo di raggiungere un recupero di acido acetico del 99.80% in peso e una purezza del 99.90% in peso.

Per massimizzare il recupero energetico riducendo al minimo il consumo delle *utilities*, è stata condotta un'integrazione energetica utilizzando Aspen Energy Analyser (HX-NET), seguita da un'analisi economica per determinare un prezzo minimo di vendita dell'acido acetico azzerando il *Net Present Value* (NPV). Per una produttività dell'impianto di 37.41 $kton.y^{-1}$ è stato ottenuto un prezzo minimo di vendita di acido acetico glaciale pari a 1.58 $€.kg^{-1}$. A contribuire maggiormente a tale risultato sono la sezione di purificazione per il 37.83% e la sezione di produzione di idrogeno per il 36.35%, seguite dalla fase di fermentazione per il 18.94% e dalla cattura della CO_2 per il 6.88%. In termini di costi capitali, l'investimento associato all'elettrolizzatore costituisce oltre il 34% del Costo Totale delle Apparecchiature (TEC). Invece, più della metà delle spese operative totali è attribuibile alle *utilities*, a causa principalmente dell'alto consumo di elettricità per la produzione di idrogeno.

Inoltre, è stata effettuata un'analisi di scalabilità per valutare le implicazioni economiche derivanti dall'aumento della produzione di acido acetico attraverso l'impiego di più fermentatori in parallelo. Con una scala superiore a 500 $kton.y^{-1}$, che rispecchia quella dei grandi impianti industriali tradizionali, il prezzo di acido acetico è sceso a 1.17 $€.kg^{-1}$. La simulazione è stata ripetuta considerando di produrre idrogeno in accordo con gli obiettivi del 2030 e, nonostante la diminuzione del prezzo in acido acetico, questo risulta decisamente superiore rispetto al valore di mercato dell'acido acetico glaciale nel 2023 pari a 0.6 $€.kg^{-1}$.

Sebbene meno economica rispetto ai metodi tradizionali, la fermentazione gassosa offre un'alternativa sostenibile riducendo il consumo di combustibili fossili e utilizzando CO_2 altrimenti emessa in atmosfera. Infatti, quasi l'80% del carbonio in ingresso alla cattura viene convertito nel prodotto di interesse.

Contents

1. Introduction

1.1 Acetic acid uses and market

Acetic acid (CH_3COOH) is the most widely used and second simplest aliphatic carboxylic acid, whose applications mainly concern textile, fibre, pharma and food industry.

Its main uses deal with the production of vinyl acetate monomer (VAM), followed by terephthalic acid (TPA), acetate anhydride and acetate esters. VAM is used to make latex emulsion resins for paints, adhesives, paper coatings and textile finishing agents. The terephthalic acid market is aimed at making poly (ethylene terephthalate) solid state packaging resins, film and fibres, whereas acetic anhydride is employed for the manufacture of cellulose acetate textile fibers, cigarette filter tow and cellulose plastics [1]. The expansive spectrum of final products and applications is showed in Figure 1.1 [1].

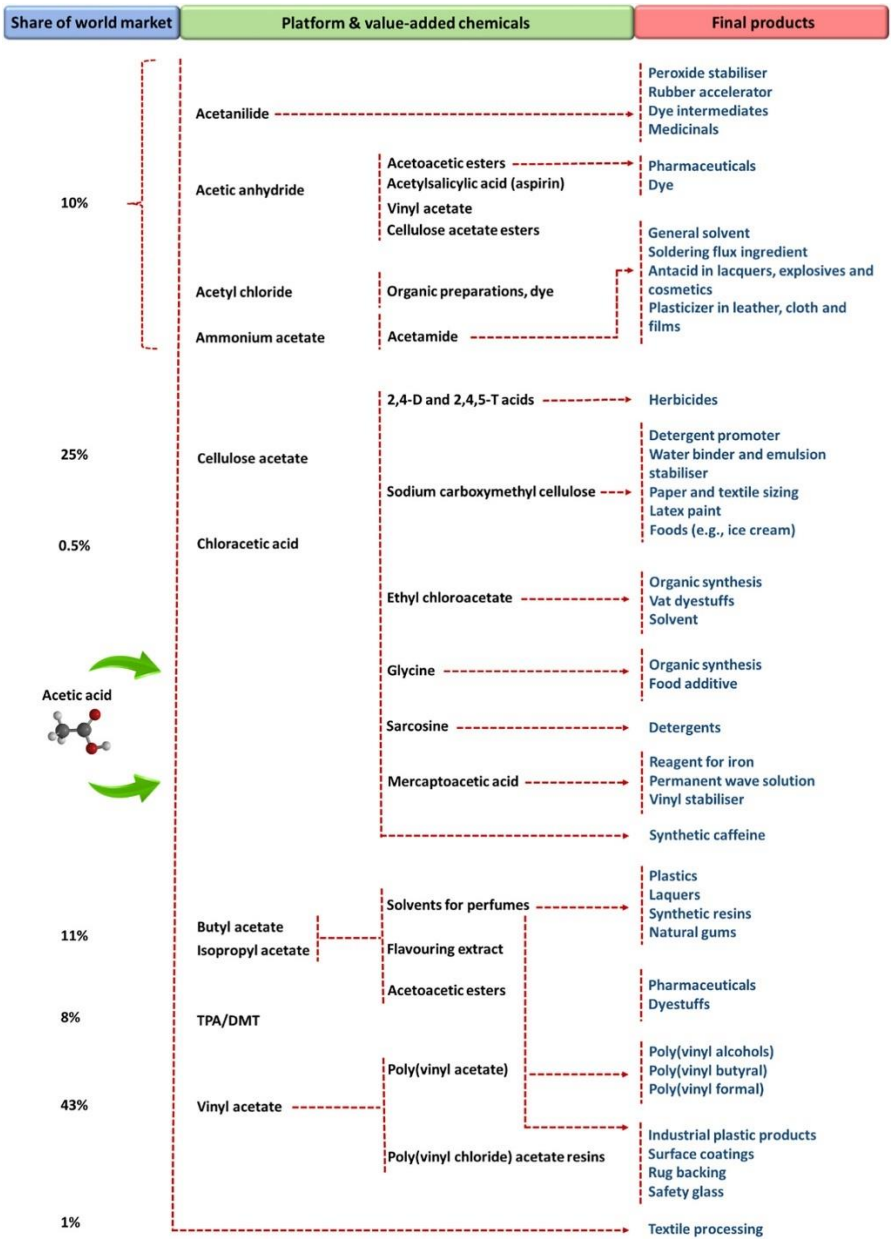

Figure 1.1. Final products and applications of acetic acid.

That of acetic acid is a rapidly growing market. In 2019 the world production reached 9.1 million tons and a rapid increase is predicted [2]. The global acetic acid market size reached 11.2 Billion US$ in 2022 and analysts expect a 6.2% growth rate in the 2023-2028 time frame, reaching 16.1 Billion US$ by 2028. Among the biggest consumers, Asia-Pacific countries consumed around 60% of the total global production in 2014 and China plays the role of the world's largest consumer, whose market between 2014 and 2020 was characterized by a growth rate of 5.6%. On the other hand, European and American countries markets are more mature, with a growth rate lower than the global average one. The reasons for this extension are linked to an increasing demand for TPA for the textile and packaging industry, in addition to the rising use of ester solvents in paints and coatings [3] [4].

Being required to adapt to this fast development, producers of acetic acid are adopting technologies aiming at the creation of a positive outlook for the growth of industry, with the objectives of savings in capital and operative costs, increasing at the same time plant capacity, production efficiency and reducing energy consumption [1].

Nowadays, most of glacial acetic acid (GAA), i.e. acetic acid with a purity higher than 99.5%, is produced by fossil fuels exploitation. Among these processes, the main one is methanol carbonylation with a market share of 75%, followed by the oxidation of ethylene or acetaldehyde and partial oxidation of ethane [5]. Methanol carbonylation is based on the reaction of carbon monoxide (CO) and methanol (CH_3OH) to produce acetic acid, with temperatures between 150-200 °C and pressures between 30 and 50 bar. The most relevant processes which exploits this synthesis route are the Monsanto Process, which involves the use of a rhodium-based catalyst and the more innovative Cativa process, developed by BP chemicals, in which the employed catalyst consists of iridium [2]. Acetic acid can also be manufactured with acetaldehyde oxidation, in which petroleum stock derived acetaldehyde is oxidized to acetic acid. The reaction occurs at temperatures around 150 °C and pressure of 55 bar and uses metal catalysts, such as cobalt or chromium. Another synthesis path is partial oxidation of ethane to acetic acid utilising molybdenum-vanadium based catalyst with temperatures between 220 and 300 °C and pressures between 12 and 15 bar [6].

In all cases raw materials derive from petroleum stocks and they are very energy-intensive processes, contributing to global warming through greenhouse gas (GHG) emissions. Moreover, they require huge involvement of manpower and proper process safety. In addition, the employed catalysts are expensive and the release of wastes and by-products occurs causing environmental pollution [5].

As a result, there's a growing interest in bio-acetic acid production processes, following a biorefinery perspective to convert biomass into chemicals. The development of these routes will play a significant role in the future acetic acid market [7]. These are processes characterized by many drawbacks, linked both to the nature itself of the biomass, which could be used for other purposes and necessary pretreatment to be carried out, respectively for first-generation and for second-generation biomass. To address these limits, one potential promising pathway could be gas fermentation, which utilizes CO_2 and H_2, fed to a fermentation reactor to produce acetic acid. To ensure environmental sustainability, it would be essential that raw materials did not derive from fossil sources. Consequently, it would be appropriate to exploit CO_2 captured from a production plant and green hydrogen, synthetised with electrolysis of water.

1.2 Process simulations and technical economic studies in literature

In recent years, there has been a considerable interest in biorefinery strategies to convert non fossil sources to biofuels or chemical intermediates. This concern is driven by the necessity to reduce global dependency on fossil resources, cut green-house gas emissions (GHG) and meet global energy and chemical demand.

Therefore, fermentation is becoming increasingly interesting. In fact, low-carbon fuel can be produced from biomass. Although a renewable resource is employed, which also contributes to a diversification of energy sources, it's a process that still has numerous disadvantages. First, the use of second-generation biomass is preferable to first-generation one in order not to hinder food supply. However, in this case expensive multiple pretreatment and hydrolysis steps are required to separate cellulose and hemicellulose from lignin and break down polysaccharides into fermentable monosaccharides [8].

A possible alternative is gas fermentation which consists of the gasification of biomass and the employment of the produced syngas as a feedstock for the fermentation step [9]. In fact, the exploitation of all biomass fractions, including lignin, leads to high product yield. It is also a flexible process because it allows the use of a wide range of feedstocks, including municipal solid waste and industrial waste [10]. Another advantage is the possibility of operating at mild pressures and temperatures. On the other hand, low gas-liquid mass transfer rates and the cost of the biological medium are the main drawbacks. These themes were deeply evaluated by Gao et al., 2013 and Phillips et al., 2017 ([11], [12]). Alternatively, gas fermentation can also be applied starting from CO_2 and hydrogen which don't derive from gasification. For example, it is possible to employ captured CO_2 from the atmosphere or concentrated flows from companies and H_2 from water electrolysis.

Process simulations represent the basis for future technical feasibility assessments and in literature most of gas fermentation simulations regard the manufacture of ethanol via fermentation of syngas. For example, Ardila et. al, 2014 simulated this process with the use of Aspen Plus starting from sugarcane bagasse which is later gasified [13]. Here, the fermentation step was modelled in a stoichiometric reactor (RSTOIC) where a medium and syngas are introduced. In particular, the medium feed stream is assumed to be pure water since biomass, which is necessary for microbial growth, is neglected for simplicity. Rao et al., 2005 presented a process simulation following this production route, although it was based on a small scale. Here both an equilibrium model based on Gibbs free energy minimization and a stoichiometric one were used [14]. Chen et al., 2015 developed a metabolic model for a bubble column reactor for the fermentation step, where the inlet gas could derive from biomass gasification [15]. They determined that increasing superficial gas velocities, ethanol titer and ethanol/acetate ratio improved at the expense of low CO and H2 conversions, indicating the possible advantage of recycling unused gas to achieve higher conversions. In addition, efficient gas-liquid mass transfer was identified as essential for achieving high ethanol production. Michailos et al., 2017 modelled a biological reactor employing Aspen Plus to simulate the fermentation step with the utilization of bagasse-derived syngas to obtain ethanol. The reactor is modelled as a CSTR operating at 311 K and 0.15 MPa. An undesired by-product is acetic acid, which is recycled back in the fermentation broth to the inlet of the reactor, as well as the cells (which are not simulated in detail). In addition, unreacted gases are separated from the liquid product and, in order to avoid accumulation, a part of it is split and sent to a combined gas-steam turbine to produce electricity. However, at the best of author's knowledge, one of the most complete works is the one published by Pardo-Planas et al., 2017 which laid the foundation for future techno-economic feasibility studies [16]. They modelled a hybrid gasification-syngas fermentation

plant for the production of ethanol starting from switchgrass taking into account also the distillation and drying steps. Here, the fermenter was modelled using a stoichiometric reactor BIOREACT in Aspen Plus.

As regards techno-economic analysis, at the best of the author's knowledge, the majority of the studies were focused on the production of bio ethanol [17], [18], [19], [20], [21], [22], [23].

Piccolo et al., 2009 compared the enzymatic hydrolysis of lignocellulosic biomass followed by fermentation (EHF) and the gasification of lignocellulose followed by syngas fermentation (GF) to produce bioethanol [18]. The first process is more mature than the second one and pilot plants and preindustrial facilities have recently been brought to operation. Moreover, this analysis shows that further technological improvements are needed to lower the selling price in a significant way and make the technology attractive also on a large-scale business. As regards the second technology, the large capital costs, the energy expensive product recovery and the moderate final yield are linked to very high production costs and the need of a very high ethanol selling price, which make the GF process a less interesting alternative when compared to the EHF one. Swanson et al., 2010 simulated with the use of Aspen Plus a hybrid gasification-syngas fermentation process to obtain anhydrous ethanol [21]. The results demonstrated that higher yields of ethanol are reached (3.70 liter of ethanol per dry kilogram of biomass) compared to the currently one achieved by the biochemical platform. Furthermore, it was highlighted that distillation is the most expensive step in the process and an increase in CO and H2 uptake rate by the microbial strain will result in a smaller reactor volume. Roy et al., 2015 assessed the potential environmental and cost benefits that could be achieved from the manufacture of ethanol via syngas fermentation process, starting from the biomass Miscanthus. It was enlightened that heat recovery has a significant effect on the net production cost, as well as the choice of the feedstock and conversion technologies. The obtained production cost varies from 0.72 to 0.83 €. L-1 [23]. The result conforms to those of previous bibliographic studies, such as that of Piccolo et at., 2009 in which the cost fluctuates between 0.28 and 0.56 €. L-1 [18]. In addition, it was concluded that the exploitation of untreated feedstock is a better alternative in terms of GHG emissions and production costs compared with treated feedstocks. Michailos et al., 2017 performed a technical and economic feasibility study on ethanol, simulating the gasification of bagasse with subsequent fermentation. A minimum ethanol selling price (MESP) of 0.58 €. L-1 is obtained. In particular, it was mentioned that the reasons of the low yield of ethanol are caused by the low solubility and mass transfer limitation of CO and H_2 gaseous substrates. Moreover, it was concluded that the implementation of a two-stage continuous fermentation could lead to higher yields [17]. De Medeiros et al., 2020 modelled the operation of a bubble column reactor for syngas fermentation to produce ethanol, selecting operating conditions and design variables for an optimal production of ethanol [20]. The reaction unit was integrated with the purification unit and the global process was optimized in terms of economic variables (CAPEX and MESP) as well as energy efficiency. This study showed that the optimised results are strongly correlated with mass transfer, proving that the improving the mass transfer coefficient (kla) is a promising strategy for global process enhancement. Regis et al, 2023 conducted a technical economic analysis of bioethanol production from switchgrass through biomass gasification and syngas fermentation [19]. Even though the estimated ethanol selling price is higher than the present market one, a high yield of ethanol per tonne of biomass is obtained as well as an increasing carbon yield of the process due to the addition of green hydrogen produced through water electrolysis. In addition, it is also reported that

improvements can be expected by changing the reactor configuration and using less expensive nutrients.

Choi et al., 2009 conducted a TEA to study the feasibility of a gasification-fermentation combined process for the manufacture of Polyhydroxyalkanoate (PHA), biodegradable material which could be an alternative to petrochemical plastics, starting from switchgrass. This process has hydrogen as a co-product and therefore the final cost strongly depends on the sale of hydrogen gas. In particular, it was concluded that the production cost of PHA via syngas fermentation is cheaper than producing it via sugar fermentation [24].

None of the processes of these works mentioned above are commercially competitive. In fact, not only is a technological improvement required but also it is needed a reduction in the cost of reactants, such as hydrogen (as reported by Piccolo et al., 2009 and Regis et al., 2023), to achieve competitive product prices [18], [19].

At the best of the author's knowledge, as regards to acetic acid manufacture via gas fermentation, no complete flowsheet analysis as well as techno-economic assessment has been published in the scientific literature yet.

1.3 Hydrogen production

Hydrogen is the lightest element in the universe and the tenth most abundant one in the Earth's crust. However, it is rarely readily available directly in our planet in the form of deposits, but it is mostly found in chemically combined forms of water, fossil fuels and biomass. Consequently, the primary task is to economically and efficiently extract hydrogen from the naturally occurring molecules.

Since hydrogen can store and deliver energy in a usable form, it is considered as a crucial energy source for the future. With the highest specific energy density (140 MJ/kg), more than double that of typical solid fuels, it is the most efficient energy carrier [25]. However, it is characterized by a low density, requiring then compression and cooling to be stored and transported in reasonable quantities.

One of the primary reasons of the growth of interest towards this chemical is that its combustion does not require special disposal procedures and does not pollute the environment, since water is the only waste produced. Therefore, it offers a viable alternative to relying on fossil fuels. Nevertheless, the production of this element does not always occur in sustainable ways. In fact, nowadays 96% of hydrogen is still manufactured using fossil fuels and its synthesis was accountable for the emissions of 830 million tons of CO_2 in 2020 [26]. More specifically, 48% of the hydrogen used in its manufacture comes from natural gas, 30% from fossil oil, 18% from coal and the remaining portion (4%) is produced using electricity through water electrolysis.

Hydrogen is classified into different colour shades i.e., grey, blue, green, pink, brown and white depending on the technology used for its production, the energy source and its environmental impact [27]:

- *grey hydrogen* is produced from the steam reforming process of methane, which is currently the most employed technology;
- *blue hydrogen* is also manufactured from steam reforming but coupled with carbon capture and storage (CSS) of carbon dioxide to reduce greenhouse gas (GHG) emissions;
- *green hydrogen* is synthesized through water electrolysis by utilising the energy peaks from renewable sources, such as wind and solar power;
- *pink hydrogen* also relies on water electrolysis, but in this context, electricity is provided by nuclear plants;
- *brown hydrogen* is produced from coal gasification;
- *white hydrogen is naturally* occurring hydrogen that is found in underground deposits;

The entire spectrum of hydrogen production methods is summarised in Table 1.1, along with their respective advantages, disadvantages, efficiency and cost. These information are taken from Table 1 of the work of Kumar et al., 2019 [25].

Table 1.1. Hydrogen production methods, their advantages, disadvantages, efficiency and cost.

Hydrogen production method	**Advantages**	**Disadvantages**	**Efficiencies (%)**	**Cost ($. kg^{-1})**
Steam reforming	Well established technology Existing infrastructure	Produced CO_2 and CO as a by product Unstable supply	74-85	2.27
Partial oxidation	Established technology	Produced heavy oils and petroleum coke	60-75	1.48
Autothermal reforming	Well established technology Existing infrastructure	Produced CO_2 as a by product Use of fossil fuels	60-75	1.48
Bio photolysis	Consume CO_2 O_2 is a byproduct Working under mild conditions	Low yields of H_2 Sunlight needed Large reactor required O_2 sensitivity High cost of material	10-11	2.13
Dark fermentation	Simple method H_2 produced without light No limitation O_2 CO_2 neutral Involves to waste recycling	Fatty acids elimination Low yields of H_2 Low efficiency Necessity of huge volume of reactor	60-80	2.57
Photo fermentation	Involves to wastewater recycling Used different	Low efficiency	0.1	2.83

	organic waste waters CO_2 neutral	Low H_2 production rate Sunlight required Necessity of huge volume of reactor O_2 sensitivity		
Gasification	Abundant Cheap feedstock CO_2 neutral	Tar formation Fluctuating H_2 amount because of feedstock impurities and seasonal availability	30-40	1.77-2.05
Pyrolysis	Abundant Cheap feedstock CO_2 neutral	Tar formation Fluctuating H_2 amount because of feedstock impurities and seasonal availability	35-50	1.59-1.70
Thermolysis	Clean and sustainable O_2 as a byproduct Copious feedstock	High capital costs Elements toxicity Corrosion problems	20-45	7.98-8.40
Photolysis	O_2 as a byproduct Abundant feedstock No emissions	Low efficiency Non effective photocatalytic material Requires sunlight	0.06	8-10
Electrolysis	Established technology Zero emission	Storage and transportation problem	60-80	10.30

	Existing infrastructure O_2 as a byproduct			

1.3.1 Hydrogen production via electrolysis

Electrolysis of water is one of the most promising routes to produce green hydrogen. It has been known since the 18th century and since then efforts have been made to improve its performance. This has led to an ever-increasing employment of this technology, although still limited. It's an already established process, contributing to the global production of hydrogen with a percentage that is no longer negligible (4%), even if it needs to be increased in the near future in parallel with the use of renewable sources for the production of electricity [25].

This process only requires electricity and water. Through the application of a certain potential difference between two electrodes immersed in an electrolyte, water is split into hydrogen (H_2) and oxygen (O_2).

The global reaction of water electrolysis is indicated in Equation 1.1 [28]:

$$1\ H_2O + Electricity\ + Heat\ \rightarrow H_2 + {}^{1}/_{2}\ O_2 \qquad (1.1)$$

This reaction can be schematized into two half reactions which occur at the anode and cathode of the electrochemical cell.

To split water into hydrogen and oxygen at ambient temperature, the above reaction requires 1.23 V of theoretical thermodynamic voltage. Nonetheless, additional voltage is needed to overcome the kinetics and ohmic resistance of the electrolyte and cell components of the electrolyze. Therefore, the actual required voltage is 1.48 V.

According to the employed electrolyte, operating conditions and ionic agents (OH^-, H^+, O^{2-}) water electrolysis technologies can be grouped into: Alkaline water electrolysis (AEL), Anion exchange membrane (AEM), Proton exchange membrane (PEM) and Solid oxide water electrolysis cell (SOEC).

Alkaline water electrolysis (AEL)

The cell consists of two halves in which the two half reactions take place: at the cathode the hydrogen evolution reaction (HER) and at the anode the oxygen evolution reaction (OER). The alkaline solution consisting of water and potassium hydroxide (KOH) is initially fed to the cathode which is reduced to form hydrogen gas (H_2) and OH^- ions. Hydrogen can be removed, while generated ions pass through a porous septum, called diaphragm, and undergo the oxidation reaction which leads to the formation of water and oxygen, as it is shown in Figure 1.2 [29].

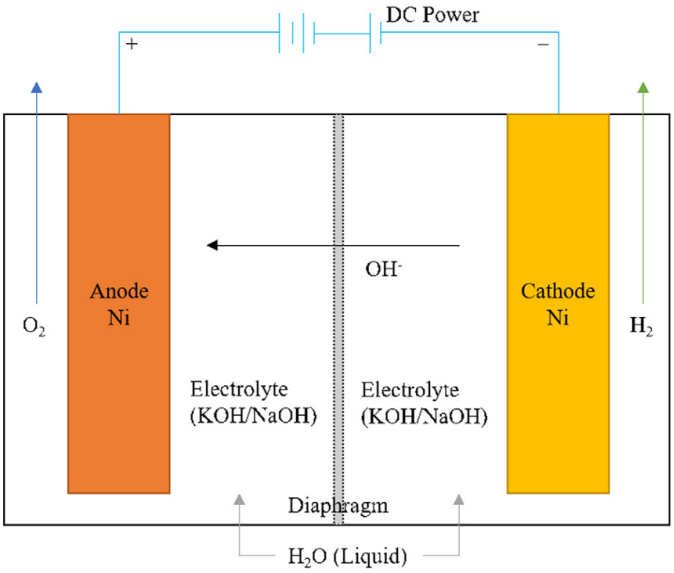

Figure 1.2. Schematic representation of alkaline water electrolysis working principle, taken from Pinsky et al., 2019.

Among the advantages, the maturity of technology (TRL-9 [30]) and the absence of noble electrocatalysts are the most relevant ones. The former, in fact, enables its application in industrial processes while the latter avoids the employment of rare and expensive materials, since the plates present inside the apparatus are usually made of Ni-Mo or Ni-Co alloys.

On the other hand, the application of AEL technology brings some critical issues. Within its limits, low current densities (0.1-0.5 A. cm^{-2}), caused by the moderate OH^- mobility, lead to the necessity of large surface areas for the production of sufficient quantities of hydrogen [28]. In addition, another problem regards the usage of corrosive KOH electrolytes and the reaction of KOH electrolytes with ambient CO_2, producing K_2CO_3 which causes a reduction of the number of OH^- ions. Moreover, K_2CO_3 salts close the pores of the anode gas diffusion layer, decreasing then ion transfer and consequently the production of hydrogen. In addition, the diaphragm does not completely prevent the crossover between the cells. This last aspect must be strictly kept under control, given the simultaneous presence of hydrogen and oxygen which can be responsible of the formation of an explosive atmosphere which can be very dangerous especially during the startup.

Table 1.2 summarizes occurring reactions, as well as the main characteristics and operating conditions of commercial alkaline electrolysers [31].

Table 1.2. Reactions and operating conditions of AEL taken from Arsad et al.,2023.

Anode reaction	$2\,OH^- \rightarrow H_2O + \frac{1}{2}O_2 + 2\,e^-$
Cathode reaction	$2\,H_2O + 2\,e^- \rightarrow H_2 + 2\,OH^-$
Overall reaction	$H_2O \rightarrow H_2 + \frac{1}{2}\,O_2$
T (°C)	50-90
P (bar)	2-10
Voltage range (V)	1.8-2.4
Current density (A. cm^{-2})	0.2-0.4
Electrolyte	KOH/NaOH (5M)
Efficiency (%)	62-82
Energetic consumption (kWh. Nm^{-3})	4.5-7
Capacity (Nm^3. h^{-1})	<760
Lifetime (years)	20-30

Proton exchange membrane (PEM)

In this process, pure water is fed at the anode, where it decomposes to oxygen, H^+ ions and electrons e^-. Oxygen is removed while H^+ ions are transported via the polymeric membrane and the electrons through the external circuit. At the cathode, ions and electrons recombine to form hydrogen. Its schematic representation and working principle are shown in Figure 1.3 [29].

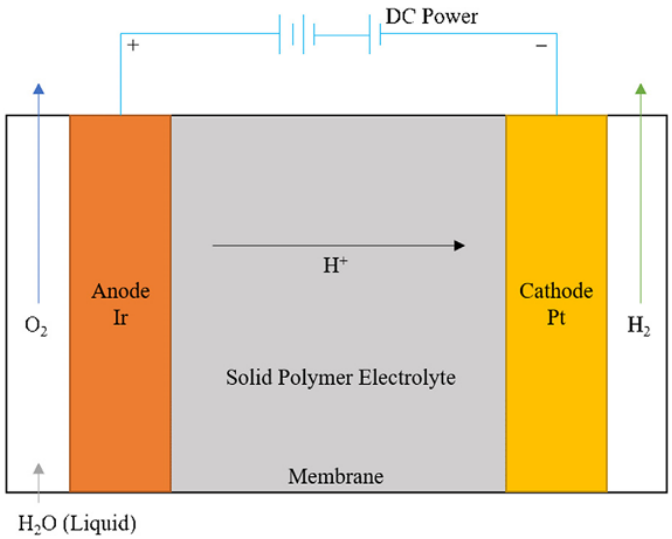

Figure 1.3. Schematic representation of PEM water electrolysis working principle, taken from Pinsky et al., 2019's work.

This technology is well developed and commercially available (TRL-8 [30]) for applications in industrial and transport sector. Among the advantages, it boasts higher current densities (1-2 $A.cm^{-2}$), leading to greater compactness of the stack and fast response to startup [28]. Moreover, gases are characterized by high purity and the risk of mixing them is absent.

On the other hand, the cost of the cell components and the presence of noble metal electrocatalysts are the main drawbacks. In fact, expensive titanium plates coated with platinum or gold are used as separators and IrO_2 for the OER and carbon-supported Pt for the HER are employed. Therefore, research is mainly aimed at replacing these materials from a sustainable perspective.

In Table 1.3 occurring reactions, as well as the main characteristics and operating conditions of commercial PEM electrolyser are listed [31].

Table 1.3. Reactions and operating conditions of PEM electrolyser taken from Arsad et al., 2023.

Anode reaction	$H_2O \rightarrow 2\,H^+ + \frac{1}{2}O_2 + 2\,e^-$
Cathode reaction	$2\,H^+ + 2\,e^- \rightarrow H_2$
Overall reaction	$H_2O \rightarrow H_2 + \frac{1}{2}\,O_2$
T (°C)	60-90
P (bar)	15-30
Voltage (V)	1.8-2.2
Current density ($A.\,cm^{-2}$)	0.6-2
Electrolyte	Solid polymer electrolyte
Efficiency (%)	67-82
Energetic consumption ($kWh.\,Nm^{-3}$)	4.5-7
Capacity ($Nm^3.\,h^{-1}$)	<40
Lifetime (years)	10-20

Solid oxide water electrolysis cell (SOEC)

This hydrogen production technology differs from the others described previously in terms of operating conditions. In fact, in this case temperatures are very high, between 500 °C and 900 °C [28]. Water, as steam, is fed at the cathode, where water molecules are reduced to hydrogen and O^{2-} ions. These ions are then transported to the anode via membrane, where oxygen formation takes place and two electrons e^- are produced and pass through the external circuit to be used then at the cathode. The membrane is made up of a solid electrolyte, usually a ceramic material based on yttria and zirconia.

Its schematic representation and working principle are shown in Figure 1.4 [29].

The most significant advantage of the employment of this technology is the possibility of operating at high temperatures, reducing power consumption to convert water into hydrogen and oxygen. This turns into an increase in energy efficiency, leading to a potential decrease

in hydrogen price. In addition, this technology can be easily thermally integrated with downstream processes, for the production of chemicals such as methanol and ammonia. Another advantage concerns the lack of use of noble metals. Unfortunately, the inadequate long-term stability has hindered its commercial use and it's still characterized by a low TRL, equal to 5 [30].

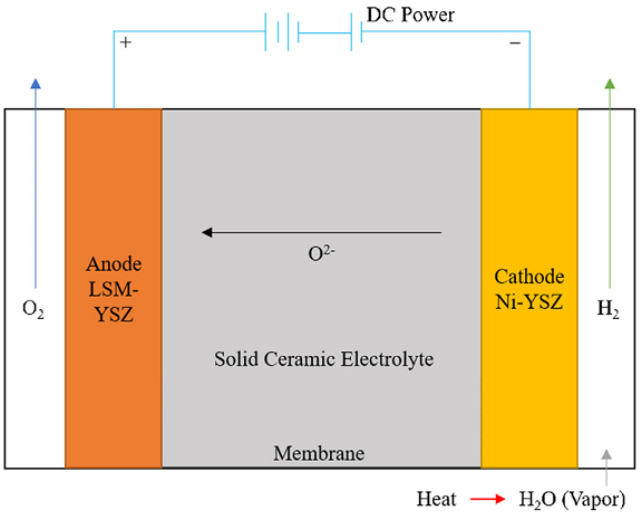

Figure 1.4. Schematic representation of SOEC working principle, taken from Pinsky et al., 2019.

In Table 1.4. occurring reactions, as well as the main characteristics and operating conditions of commercial SOEC are listed [31].

Table 1.4. Reactions and operating conditions of SOEC taken from Arsad et al.,2023.

Anode reaction	$O^{2-} \rightarrow \frac{1}{2} O_2 + 2\, e^-$
Cathode reaction	$H_2O + 2\, e^- \rightarrow O^{2-} + H_2$
Overall reaction	$H_2O \rightarrow H_2 + \frac{1}{2} O_2$
T (°C)	500-1000
P (bar)	<30
Voltage (V)	0.7-1.5
Current density (A. cm^{-2})	0.3-1
Electrolyte	Yttria stabilized Zirconia
Efficiency (%)	81-86 (laboratory)
Energetic consumption (kWh. Nm^{-3})	2.5-3.5
Capacity (Nm^3. h^{-1})	<40
Lifetime (years)	-

1.4 CO_2 capture

It is broadly known that climate change is at the centre of the debate and that greenhouse gas (GHG) emissions should be drastically reduced to achieve the objectives set for the near future.

Among greenhouse gases, CO_2 is responsible for 65% of GHG emissions worldwide, with China being the main emitter followed by USA.

Due to the strong increase in human population (8.1 Billion in 2023 [32]), infrastructure, industry and transport sector are expanding, leading to an important hike in GHG emissions.

Based on NOAA's Global Monitoring Laboratory, in 2023 the global average atmospheric CO_2 concentration was 419.3 ppm and it's the 12^{th} consecutive year in which the quantity of carbon dioxide in the atmosphere increases more than 2 ppm. This is an alarming scenario if compared to pre-Industrial Revolution levels, when CO_2 concentration in the atmosphere was halved. The annual Global Carbon Budget stated that CO_2 emissions in 2023 were 36.8 billion tonnes, up 1.1% from 2022 [33]. This is a worrying data if compared with those of 1960s, around 11 billion tons [34].

The significant increase in CO_2 emissions is responsible for cascading effects for our planet and life. In fact, carbon dioxide is a greenhouse gas, and this means that it absorbs and radiates heat in all directions. By adding more CO_2 in the atmosphere this effect is enhanced causing a rise in global temperature [34]. This causes weather events such as tropical storms, wildfires, droughts, heat waves, melting glaciers and sea level rise [35].

Consequently, the reduction of these emissions is of fundamental importance and chemical industry plays a significant role, as it is the third largest contributor to CO_2 emissions, after power generation and agricultural sector. To fight against climate change, the Paris Agreement of 2015 established to reduce carbon emissions to maintain Earth's temperature rise below 2 °C compared to pre-industrial levels. For this purpose, the Intergovernmental Panel on Climate Change (IPCC) proposed an 80% reduction in global CO_2 emissions by 2050 to achieve that target [36].

Currently, the use of renewable sources to replace the exploitation of fossil fuels is insufficient to cover the entire energy requirement. Solutions capable of mitigating CO_2 emissions are needed during this transition period, especially as regards *hard-to-abate sectors*. These are energy-intensive industries that are difficult to decarbonise and reconvert, such as cement and glass factories, steel and paper mills.

In this scenario, direct air capture (DAC) as well as carbon capture and storage (CCS) are crucial, acting as a bridge between our current fossil-fuel based economy and a renewable one. They both consist in the capture of CO_2 from gas mixtures, but CCS also involves its storage in geological sites, reducing the overall rate of release. As an alternative, carbon dioxide can also be used as a feedstock for the manufacture of chemicals and fuels. While DAC technologies extract CO_2 directly from the atmosphere, CCS is usually carried out at the point of emissions, for example at the exit of cement factories. Therefore, in the first case air is not very concentrated in CO_2 (around 400 ppm) whereas in the second case it is.

Although DAC is still less industrially developed than CCS, there are companies that already exploit this technology. An example is the Swiss company Climeworks which employs direct air capture (DAC) technology reducing the atmospheric concentration of CO_2. In particular, air after being drawn passes through a filter which traps carbon dioxide particles. When the filter is completely saturated with CO_2, the collector is closed and by increasing the temperature the filter releases CO_2 which is mixed with water and pumped

down underground [37]. The company boasts in Iceland the largest CO_2 capture system with a capacity of up to 36 000 ton.y^{-1}[38]. Nevertheless, it should be underlined that DAC requires much more energy compared to CCS, being CO_2 in the atmosphere much more dilute than a flue gas [39].

The development and optimization of CSS is fundamental and, among others, is expected to contribute to 20% of the reduction in humans GHG emissions by 2050 [40]. Nowadays, the most relevant technologies for CCS are three: post-combustion, pre-combustion and oxy-fuel capture systems [41], [42].

- In post combustion capture most of the CO_2 is extracted from a concentrated waste gas before it is released into the atmosphere. In this case, the most commercially developed techniques involve wet scrubbing with aqueous amine solutions. At low temperature (around 50 °C) the amine solvent absorbs CO_2 from the waste gas. In order to reuse it, the saturated solvent is later regenerated by heating it to around 120 °C. In this case, low concentration of CO_2 (4-14%) represents a limit for the capture because a powerful chemical solvent is needed and, consequently, high energy for regeneration.

- Pre combustion capture involves gasification of a fuel at high pressures (between 30 and 70 atm) to produce a synthesis gas which is mostly a mixture of CO and H_2. At this point steam is added to promote *water gas shift reaction* $CO + H_2O \rightleftarrows CO_2 + H_2$. CO_2 is later separated by absorption, adsorption or membranes to generate a hydrogen-rich fuel gas. This technology enables the achievement of higher outlet CO_2 concentration and pressures, at the expense of very high investment costs.

- Oxyfuel process, instead, requires an expensive separation of oxygen from air (realised with cryogenic separation or membranes). A fuel is burnt with oxygen and produces a gas of mainly CO_2 and condensable water vapour which can be separated and cleaned in the compression step. Since the combustion is performed with pure oxygen higher temperatures are reached but CO_2-rich flue gas is recirculated reducing the temperature to normal values. Consequently, the concentration of CO_2 in the output stream is very high, reaching 80% v/v. It is very important to underline the influence of the type of fuel: in fact, for example by using coal, NO_x and SO_x must be removed from the waste gas before the compression process. The main disadvantage is the expensive separation of O_2 and N_2 from air.

Considering the most applied technology in industrial plants, i.e. post-combustion capture, the processes which separation can be achieved with are:

- Chemical absorption;
- Physical absorption;
- Adsorption;
- Separation with membranes;
- Cryogenic distillation.

In addition, hybrid systems can be utilized such as membranes associated with cryogenic distillation or membranes with solvent absorption [41].

The advantages and disadvantages of the mentioned technologies are summarized in in Table 1.5 [43], [44].

Table 1.5. Comparison between different separation technologies in terms of advantages and disadvantages [43].

Separation Technologies	Advantages	Disadvantages
Absorption	High absorption efficiency (>90%) Solvents can be regenerated by heating and/or depressurisation High capacity at low temperature and high pressure Low-cost solvent Most mature technology Chemical absorption is suitable for treating diluted-CO_2 gases Possibility of implementing a hybrid absorption	Energy-intensive solvent regeneration Chemical absorption involves the use of solvents that are corrosive, and they can degrade by contaminants High operating costs Low capacity at high temperature and low pressure Physical absorption is not economically convenient with low CO_2 partial pressure Hybrid absorption involves high investments in building physical and chemical absorption facilities
Adsorption	High adsorption efficiency (> 85%) Reversible physical adsorption process Adsorbent can be recycled High capacity at low temperature and high pressure for physical adsorbents High capacity at low CO_2 pressure for solid amine sorbents Less corrosion	Process using physical adsorbents has low CO_2 selectivity and capacity decreases with temperature and the presence of moisture Process using chemical adsorbents has high energy consumption due to high temperature requirement for CO_2 sorption and adsorbent regeneration Solid amine sorbents degrade by thermal, oxidation and contaminants
Membrane	High separation efficiency (> 80%) Relatively low operation cost Easy handling and operation	High manufacturing cost Low permeability Fouling Relatively low separation selectivity

		May be not stable in the presence of moisture
Cryogenic	High separation efficiency (> 85%) Mature technology	Very energy-intensive process due to very low temperature and high-pressure operation Requires moisture pre-removal May accumulate solidified CO_2 on the surface of heat exchanger

1.4.1 Chemical absorption with amines

Absorption with amines is the most employed technology for CO_2 capture, with around 60% of CCS plants exploiting this technique [45]. In fact it boasts robustness and ease of operation as well as high absorption rate, large CO_2 capacity, low viscosity and high chemical and thermal stability [46]. The process consists in the uptake of CO_2 into the bulk phase of a basic liquid solution, where a temperature dependent acid-base reaction occurs at flue gas temperature (40-60 °C). After the reaction with CO_2, the solution is regenerated at higher temperatures (100-120 °C) liberating gaseous CO_2 that is later sent to a storage reservoir. The removal efficiency that is normally achieved is around 90% [46]. The process is schematized in Figure 1.6 [47].

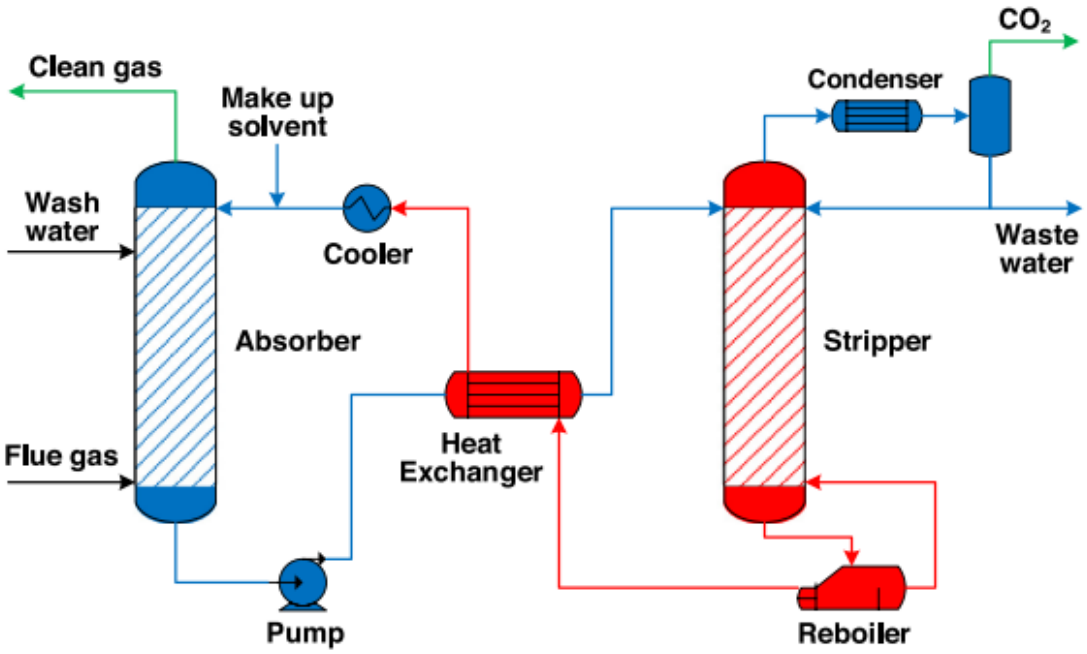

Figure 2.6. Chemical absorption process diagram.

Although it is the cheapest CCS technology available, it is associated with expensive operative costs caused by the energy demand for solvent regeneration. In this regard, Gao et al., 2020 concluded that the regeneration process consumes above 60% of the entire energy demand requested for carbon capture [46]. In addition, an important obstacle is

amine degradation since it increases operation cost by 10%. Moreover, degradation products are responsible for an increase in corrosion [46].

Alkanolamines are the most commonly used solvents for CO_2 absorption and they can be grouped into primary (monoethanolamine, i.e. MEA), secondary (diethanolamine, i.e. DEA), tertiary (methyldiethanolamine, i.e. MDEA) and cyclic (piperazine, i.e. PZ). Most primary and cyclic amines are characterized by a high reaction enthalpy and reaction rate with CO_2, whereas tertiary amines show a high absorption capacity and low cost of regeneration [47].

Chemical absorption with MEA is the most studied and mature technology due to MEA's fast kinetics, high water solubility and low price. However, it's a very energy-intensive process due to the significant amount of steam needed for amine regeneration [48]. In addition, the presence of impurities is responsible for a decrease in efficiency due to solvent losses, corrosion, foaming and fouling [49].

Therefore, the major challenge is the development of solvents that require less regeneration energy and the attempt to reduce, at the same time, the risk of corrosion. This is complicated because typically low regeneration energy solutions are characterized by low heat of absorption that involves poor CO_2 absorption. Bhown et al., 2020 concluded that a possible solution is to increase solvent's concentration above 30 wt % in order to reduce the working volume of solvent needed to capture CO_2. In addition corrosion inhibitors and additives can be added to deal with the negative effects of working at higher concentrations [45]. This results in lower sensible heating requirements, less water evaporation in the reboiler and consequently lower regeneration energy. A further solution is the utilization of blended amines instead of pure solvents to find a compromise between high removal efficiency and a lower regeneration heat [47].

Recently the analysis of the performance of various amino blends is gaining greater interest. However, it is difficult to establish which amino blend is most effective because it strongly depends on the system and its operative conditions. In this regard, in the literature techno-economic feasibility studies are present. Idem et al., 2006 and Law et al., 2018 concluded that by using the blend MEA/MDEA a significant heat-duty reduction can be obtained [50], [51]. Ding et al., 2023 stated that the employment of this blend turned into a higher total annualised cost (TAC) than that of single MEA. In this case, the best alternative according to this study is the utilization of the blend PZ/ MDEA [47].

Therefore, by using other amines than MEA capital and energy cost could be potentially reduced. Despite this, it must be enlighten that it's complicated to make further significant improvements because the existing processes already provide 50% of thermodynamic efficiency [49].

Another approach that has yet to be commercialized involves using catalysts to accelerate the kinetics of aqueous CO_2 reactions.

1.5 Fermentation in bubble columns

Biological production of acetic acid has been known since ancient times and widely used in food industry to obtain vinegar, in which acetic acid concentration is between 4 and 12% by weight. However, only 10% of acetic acid world production is manufactured by bacterial fermentation to produce vinegar [52]. This method involves the use of renewable carbon sources such as apple, grape, pears, honey, cane, coconut, date, syrup cereals, hydrolysed starch, beer and wine as nourishment for the bacteria. In particular, ethanol, obtained from alcoholic fermentation of sugars, is subsequently converted into acetic acid by the activity of specific bacteria. The latter belong to two main species: *Acetobacter* and *Gluconacetobacter*. They are capable of carrying out the oxidation of ethanol in the presence of atmospheric oxygen, first obtaining acetaldehyde and, subsequently, acetic acid. To produce vinegar on an industrial scale three methods are usually employed [53]:

- *Orleans method*, which is well established, utilized for low volume production of vinegar and uses wooden barrels to ferment the feed.
- *Tricking process,* which was developed to overcome the slow rate of acidification of the previous method. Here, process intensification is aimed at improving bacteria and substrate interaction. Nevertheless, the main disadvantage is the accumulation of gelatinous material, which reduces the rate of reaction.
- *Continuous submerged process,* which is characterized by high yields and it is 30 times faster than Orleans method. It's economical, with a simple design and easy process control. However, pure substrates are required to achieve high quality of acetic acid.

Given the increasing dangers of global warming and the rising demand for acetic acid, it is essential to develop new technological methods to find sustainable raw materials for its manufacture. Given the limits of sugar fermentation, interest in the use of syngas as feedstock for the production of acetic acid has recently increased providing better alternatives in terms of sustainability. Furthermore, acetic acid can also be manufactured from CO_2 and H_2, enabling the use of CO_2 as a value-added feedstock [53]. For this purpose, acetogens bacteria can be employed.

Acetic acid production via acetogenesis

Acetic acid can be produced by various species of bacteria, which are called acetogens. The currently most studied ones are *Clostridium aceticum*, *Acetobacterium wooddi*, *C. thermoaceticum*, *Thermoanaerobacter kivui* and *A. wieringae* [54]. Among the acetogens mentioned, the most promising are the thermophilic ones, as they present a lower risk of contamination, greater metabolic and diffusive capacities, lower cooling costs and, in the case of volatile products, a lower recovery cost [7]. These microorganisms are strongly anaerobic and can support both autotrophic and heterotrophic metabolism. Therefore, they can grow in the presence of a wide variety of organic substrates, such as hexoses, pentoses, alcohols, methyl groups and formic acid, or through consumption of inorganic substances such as carbon monoxide (CO), carbon dioxide (CO_2) and hydrogen (H_2) [52]. The bacteria from which acetic acid is obtained as the main product of fermentation starting from CO_2 are generally called CO_2-reducing acetogens and follow the Wood-Ljungdahl metabolic mechanism (WLP), whose schematic representation is shown in Figure 1.7 [55]. Here, two moles of CO_2 are reduced to one mole of acetlyl-CoA and then further to acetate. In particular, one mol of CO_2 is reduced to formate and then bound to the C1-carrier tetrahydrofolate (THF), with the energy provided by ATP hydrolysis. From the formyl-THF, water is removed and the produced methenyl-THF is further reduced to methyl-THF.

The latter condenses with CO and coenzyme A on the enzyme acetyl-CoA synthase/CO dehydrogenase to form acetyl-CoA. The CO comes from the reduction of another CO_2 by the CO dehydrogenase. Acetyl-CoA is then converted to acetate and ATP [54].

The main advantage of this approach is that microorganisms have the potential to convert flows of CO_2 otherwise released in the atmosphere. In addition, compared to thermochemical processes, less severe operating conditions are sufficient, leading to a decrease in energy expenses. Furthermore, biological catalysts are characterized by lower sensitivity to impurities, which makes upstream processes less complicated [56]. The disadvantages are, instead, low yields mainly caused by the low solubility of CO_2 and H_2 in the fermentation broth and also the difficulty of purifying the product of interest due to its dilute concentration, making then the downstream process complex [6].

In this regard, Regis et al., 2024 conducted experimental tests in a pressurized stirred tank reactor on a laboratory scale to maximise the specific productivity of acetic acid, produced from H_2 and CO_2 using the bacterium *Thermoanaerobacter kivui* [57]. This acetogen is a Gram-negative, strictly anaerobic, thermophilic bacterium that grows optimally at 66 °C and pH 6.5. Tests indicated that the optimal acetic acid cell-specific productivity was achieved at 10 bar, providing a 3:1 H_2:CO_2 blend. Subsequently, supplying this blend at high pressure into the vessel of the reactor, an in-flow gas rate screening was performed to identify the gas flowrate that allowed the maximum acetic acid productivity. The optimal rate was 60 $mL.min^{-1}$, and the acetic acid cell specific productivity reached 2.90 $g.g^{-1}.h^{-1}$. In another work Regis, 2024 derived biological kinetic equations from experimental data to simulate *T.kivui*'s growth and metabolic production rates. The model analysed various operational parameters such as pressure, inlet gas composition, flow rate and impeller speed to maximise acetic acid production [58]. As a result, accurate predictions of the quantities of biomass, acetic acid and formic acid produced over time were achieved. It was, then, concluded that this bacterium could be a viable candidate for future large-scale fermentations exploiting CO_2.

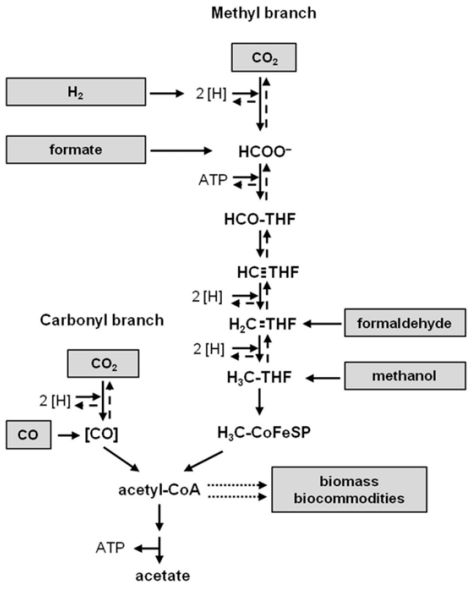

Figure 1.7. Wood-Ljungdahl metabolic pathway for the production of acetic acid from CO_2 and H_2. The figure is taken from Katsyv and Müller, 2020.

Fermentation in bubble reactors

At laboratory scale continuous stirred tank reactors (CSTRs) are usually employed, because of their efficient gas-liquid mixing and homogeneous substrate distribution to microrganisms [59]. Nevertheless, the significant energy needed for stirring makes large-scale commercial operations particularly difficult. As a consequence, alternative bioreactors designs with lower energy demands should be used. Among these, bubble columns, immobilized cell columns and packed-bed biofilm reactors are studied for their potential use in larger-scale applications [8].

In multiphase systems, bubble columns are widely utilised because of the benefits they offer, including high heat and mass transfer rates, compactness and low operating and maintenance costs. The high mass transfer rate is influenced by various factors, including the superficial gas velocity, the properties of both the gas and liquid phases, the solid concentration, the reactor design, the gas diffuser and the operating conditions [60]. Moreover, bubble size and gas holdup have a significant influence on buoyancy effects which cause mixing [61].

Computational fluid dynamics (CFD) simulations and mathematical models are used in conjunction with experimental studies in order to better characterize the phenomena occurring inside a bubble column reactor. In fact, modelling bubble columns is challenging because multiphase flow, mass transfer and bioreactions are interconnected phenomena that involve multiple physical processes. In this regard, Regis, 2024 developed an industrial-scale bubble column 1D model to produce acetic acid starting from CO_2 and H_2. At the biomass concentrations of 5 g. L^{-1} two optimal values for head pressure in the bubble column have been identified. At a pressure of 10 bar, the productivity of acetic acid and the conversion rates of H_2 and CO_2 are maximised, but the presence of formic acid complicates the purification of the fermentation broth. At a lower pressure of 2 bar, formic acid production is negligible and compression costs are lower. However, the specific production rate of acetic acid is 63% of what is achieved at 10 bar [58].

The employment of bubble column reactors for gas fermentation processes on an industrial scale is well-established. An example is represented by Lanzatech plants in which gas fermentation takes place in bubble columns [62]. This company matured a process that allows the production of chemicals, in this case ethanol, from waste emissions, thus also contributing to a reduction of the same. This company has already five commercial plants. In 2018, in collaboration with the Chinese Shougang Group, LanzaTech initiated operations with an ethanol capacity of 45 000 ton.y^{-1} [63]. In 2022, a 64 000 ton.y^{-1} commercial-scale facility in Gent, Belgium, has been launched in collaboration with ArcelorMittal which captures CO_2 from waste gases produced during steelmaking and biologically converts them into ethanol [64]. Moreover, the largest full-scale biological methanation demonstration plant in the world, located in Avedore (Denmark), exploits the advantages provided by bubble reactors to ensure the correct fermentation behaviour [65]. This project, called *Electrochaea GmbH*, consists in the conversion of hydrogen obtained by water electrolysis and captured CO_2 from a biogas plant into CH_4 and H_2O. The plant converts 5 700 million tons of CO_2 a year and produces around 2 000 ton.y^{-1} of synthetic methane [66].

1.6 Purification of acetic acid

The purification of organic acids, including acetic acid, from fermentation is an extremely complicated process, because of the high solubility and dilute concentration [67]. The primary challenge in the extensive use of bio-based chemicals and fuels is the absence of efficient and affordable separation techniques. In fact, typically, over 60-80% of the total production cost in fermentation-based processes is spent on purifying the final product [68].

There are several technologies available for separating a mixture of acetic acid and water, including distillation, liquid-liquid extraction, adsorption, ion exchange, precipitation and membrane processes. The primary benefits and drawbacks of each purification technology are shown in Table 1.7 [67], [69], [70], [71], [72], [73].

Table 1.7. Advantages and disadvantages of purification technologies.

Methods	Advantages	Disadvantages
Distillation	Easy installation High purity of the product	Large difference in volatility is necessary High energy expenditure High capital costs
Extraction with solvent	High recovery of the product High purity of the product	Need to regenerate the solvent
Adsorption	Simplicity of operations	Short life of the adsorbent Low capacity
Ionic exchange	Simplicity of operation Selective separation Less energy intensive	Consumption of a large amount of acids, bases and water to regenerate the resin
Precipitation	Simplicity of operations	Low purity of the product High consumption of lime and sulphuric acid Production of polluting solid waste (e.g. $CaSO_4$)
Electro-membranes	High purity of the product	Fouling formation High energy expenditure
Pressure membranes	High selectivity Simplicity of operations Simple scale-up	Fouling formation

Common distillation is used in traditional acetic acid purification processes, but it's not suitable for very dilute mixtures such as fermentation broths, as the volatilities of water and acetic acid for very low acid concentrations have similar values. It derives that the process would require columns with many stages and high reflux ratio. Consequently, separating acid and water by simple distillation is energy-intensive and is not practical for industrial use [74].

To address this challenge, azeotropic distillation or extractive distillation can be employed. They both involve the addition of a third component, which is able to modify the relative volatility of the species of the mixture, thereby facilitating their separation. In azeotropic distillation an organic liquid immiscible with water is used as the third component. The latter, called *entrainer*, forms an azeotrope with one of the original compounds of the mixture, in this case water. Pure acetic acid is then collected from the bottom of the column, while water exits at the top as an azeotrope with the third component. The latter must then be separated from water so that it can be recirculated [75]. Another option is extractive distillation. In this case, the third component is characterized by a higher boiling point than acetic acid and water and is not vaporized inside the column. The solvent and acetic acid constitute the extract and are recovered from the bottom of the column while water is taken from the head. To carry out this operation, both a column for extractive distillation and an ordinary distillation column, to separate the solvent used and acetic acid, are required [76].

Liquid-liquid extraction consists in the use of a suitable liquid solvent to extract acetic acid from the mixture of acetic acid and water. In this instance as well, downstream operations are necessary to recover pure acetic acid and the solvent. In fact, usually one or more distillation columns are required, depending on the extractive agent involved [70]. However, a fraction of water will still be extracted from the solvent along with acetic acid and distillation cannot remove it from the acid, so a lower acid purity will be obtained.

One strategy adopted to purify acetic acid in chemical conversion processes is to integrate liquid-liquid extraction with azeotropic distillation. In this way, following the extraction column, the extract containing the solvent, acetic acid and a fraction of water is sent to an azeotropic distillation column, in which the solvent and water form an azeotrope and are recovered at the top, while the acid comes out from the bottom. An additional distillation columns serves to purify the water and further recover the solvent [77].

The discussed technologies have been thoroughly studied for the purification of acetic acid coming from conventional chemical processes. However, there is limited research on applying these technologies after fermentation processes. At the best of the author's knowledge, there are few studies on the use of these technologies downstream of fermentation processes and the only one that involves a deep techno-economic analysis is that of Morales-Vera et al., 2020, in which the starting concentration of acetic acid in the fermentation broth is 5% [68]. The key difference between the development of traditional processes and fermentation-based processes lies in the concentration of acetic acid entering the purification section. In the case of conventional processes, the acid is obtained with a purity of 30-40% by weight [76], while in the fermentation broth the final concentration depends on various factors, but is usually less than 10% by weight [71].

A fundamental factor for the effectiveness of the technologies just described is the choice of solvent, which must have a high affinity with acetic acid, given that this is highly hydrophilic. Furthermore, it must have a low cost, a low environmental impact and the ability to be easily separated from both water and acid downstream of distillation or extraction [76].

In the case of azeotropic distillation, it is essential to use a compound that has a lower point than both water and acetic acid. This compound should form an azeotrope with water at a temperature lower than that of pure water, creating a significant volatility difference between the azeotrope and acetic acid. It is also preferable for the compound to be immiscible with water to allow for easy separation using a decanter, which simplifies the recovery process after distillation. A critical factor influencing the energy consumption of the azeotropic distillation process is the enthalpy of vaporization of the azeotropic mixture, which depends on the water content in the azeotrope. The lower the water content, the lower the energy costs of the operation, especially as regards the condenser of the azeotropic distillation columns. Several organic agents suitable for this process are mentioned in the literature, including vinyl acetate (VA), isobutyl acetate (IBA), methyl acetate (MA), ethyl acetate (EA) and methyl-tert-butyl ether (MTBE) [76].

As regards extractive distillation, however, it is convenient to use an extractive agent with a higher boiling point than both acetic acid and water and which does not form azeotropes with them. The higher the boiling point of the solvent the easier it will be to recover it following extractive distillation. Classic examples are adiponitrile, sulfolane [76], ketone compounds starting from C_7 and tertiary amines [52].

For liquid-liquid extraction followed by simple distillation, both low molecular weight and high molecular weight compounds can be used. Morales Vera et al., 2020 [68] compared two solvents with very different properties: ethyl acetate and alanine dissolved in di-iso-butyl kerosene (DIBK). In the first case, two distillation columns are necessary downstream of the extraction. The first acts as a dehydration column to remove traces of water in the extract, while the second serves to purify acetic acid and recover the solvent. In the case of alanine and DIBK, however, three columns are necessary: the first one for dehydration, the second one to recover the alanine and the third one to recover DIBK. This second solution is convenient from both an energy and economic point of view. If the extraction is followed by azeotropic distillation, the principles described for the choice of solvent in the azeotropic distillation process apply, first of all the ability to form azeotropes with water. Furthermore, the enthalpy of vaporization of the azeotropic mixture which depends on the water content in the azeotrope, affects the energy costs downstream of extraction. Finally, the distribution coefficient of acetic acid in the two phases must be taken into consideration. This is an index of the affinity of acetic with the organic phase compared to the aqueous one. The higher the distribution coefficient the greater the quality of acetic acid that passes from the aqueous phase to the organic phase during the extraction phase. Possible solvents are vinyl acetate, ethyl acetate and methyl-tert-butyl ether [76].

1.7 Objectives of the thesis

The objective of this work is to propose an in-depth techno-economic analysis for the production process of acetic acid via fermentation, starting from captured CO_2, from a waste stream destined for the atmosphere, and H_2 generated by water electrolysis.

As regards the synthesis of hydrogen, the choice is fallen on the exploitation of alkaline electrolysis, being currently the most developed process for obtaining green hydrogen.

Concerning the manufacture of CO_2, it is captured from a waste stream deriving from the upgrade process of biogas into bio-methane starting from OFMSW (Organic Fraction of Municipal Solid Waste). Among the available capture technologies, chemical absorption with amines has been selected. In particular, the choice of the solvent fell on the utilization of the benchmark MEA.

With respect to the fermentation step, the reactor is modelled as a bubble column. The unconverted CO_2 and H_2 are recycled to the head of the reactor to limit their demand. The simulation has been conducted at two distinct pressures, 2 bar and 10 bar to identify the optimal configuration. This decision stemmed from the observation that higher pressures maximise acetic acid productivity and reduce the number of fermenters in parallel. However, this increase in pressure turns is higher capital expenditure (CAPEX) for each fermenter and a non-negligible production of formic acid, making the downstream operation more complicated. On the other hand, when operating at lower pressure, a collapse in productivity is being observed, necessitating the use of additional fermenters. Despite this, formic acid synthesis is minimal, the capital expenditure for each individual fermenter is lower and the cost of acetic acid is reduced.

As for the downstream process, the purification of acetic acid from the highly diluted solution of acetic acid and water is carried out using a hybrid process with solvent extraction and azeotropic distillation. In fact, even if the two components do not form an azeotrope, the liquid- vapour diagram of this mixture presents a pinch point at low concentrations of acetic acid. Consequently, modelling the dehydration step via evaporation or using simple distillation columns is not sustainable. This choice derives from a literature analysis, in which this combination appears to be the most efficient for the purification of the fermentation broth.

The entire process is simulated using the software Aspen Plus®, with the aim of producing high purity acetic acid (99.9%) in quantities comparable with current plants for the manufacture of this chemical. An estimate of the operating and capital expenses required for the process is subsequently carried out.

Additionally, a scalability analysis is being conducted to assess the cost implications of scaling up acetic acid production through the operation of multiple fermenters in parallel. Hence, the selected process aims to strike a balance between innovation and real application in the chemical industry.

2. Methods

2.1 Overview of the entire process

The process is simulated on Aspen Plus® Version 10 (AspenTech, Inc.), to solve material and energy balances as well as to carry out the sizing of the equipment necessary to conduct a techno-economic analysis.

The entire process diagram is shown in Figure 2.1 and aims at the production of bio acetic acid. In particular, the fermentation step (S-500) is preceded by an upstream phase (from S-100 to S-400) to obtain the reactants, hydrogen and carbon dioxide, and is followed by a downstream phase (from S-600 to S-800) for the purification of acetic acid from a highly dilute solution.

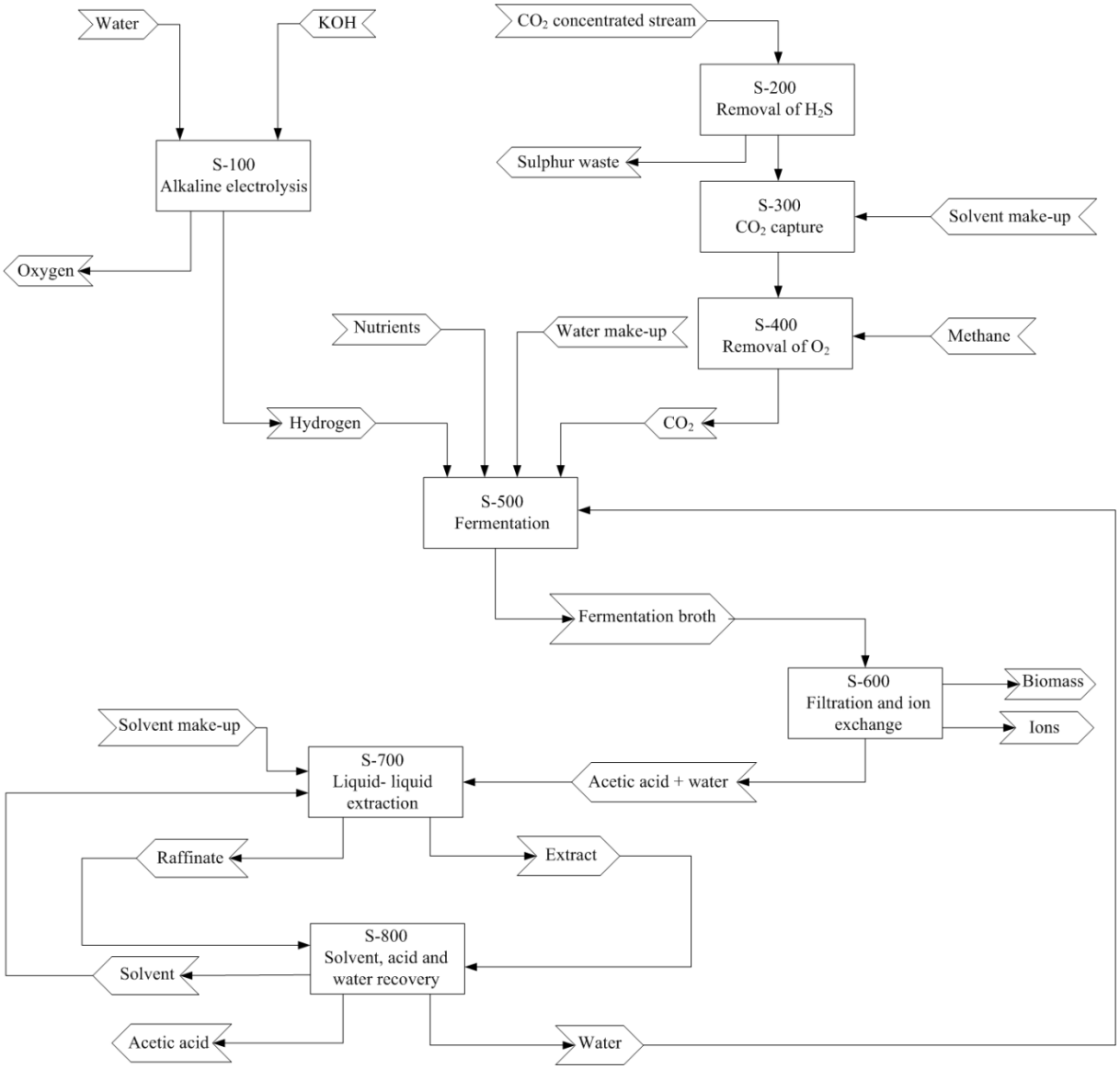

Figure 2.1. Descriptive diagram of the production process of bio acetic acid.

The process was modelled to achieve an annual production of 37.41 kton of glacial acetic acid. This production scale corresponds to the capacity of the single bubble column reactor used in the model developed by Regis, 2024 [58]. Furthermore, this size is comparable to that of single bubble columns that utilize gas fermentation for ethanol production [78]. For acetic acid manufacture, this size corresponds to a conventional small-scale plant, but it can be scaled up by adopting multiple fermenters in parallel, analogous to LanzaTech's approach in Gent, Belgium, where they are already employing this strategy for the production of ethanol [64].

2.2 Hydrogen production

The selected hydrogen production method is alkaline electrolysis. Since the aim of this work is the simulation of an industrial-scale process, the choice fell on the most mature technology with a lower manufacturing cost, i.e. AEL [79]. Furthermore, unlike PEM, the pressure conditions of AEL conform to those at which fermentation occurs.

The simulation and modelling of the hydrogen production process, as well as the resolution of material and energy balances is performed using Aspen Plus® Version 10 (AspenTech, Inc.).

The electrolyte employed in the alkaline electrolyser is an aqueous solution consisting of potassium hydroxide KOH (30 wt%). The latter allows the conduction of ions through the electrodes and it's one of most utilized electrolytes, because of its high conductivity and corrosion resistance of stainless steel in this range of concentration [31]. The components included in the simulation are indicated in Table 2.2. In addition to water, hydrogen and oxygen, ions (K^+, H^+ and OH^-) are added. The latter, in fact, migrate through the electrodes of the electrolyser and lead to the formation of hydrogen and oxygen. The thermodynamic method chosen is ELECNRTL (*Electrolyte non-random two liquid*).

Table 2.2. Chemical compounds inserted in the simulation for hydrogen production.

Chemical compound	**Type**	**Conventional name**
H_2O	Conventional	Water
H_2	Conventional	Hydrogen
O_2	Conventional	Oxygen
KOH	Conventional	Potassium hydroxide
K^+	Conventional	Ion K^+
H^+	Conventional	Ion H^+
OH^-	Conventional	Ion OH^-

The simulation has been carried out using the approach developed by Sánchez et al., 2020 [30].

The stoichiometry of the reaction is given by Equation 2.1.

$$H_2O \rightarrow \ H_2 + \frac{1}{2}\ O_2 \tag{2.1}$$

The model involves the calculation of the Faraday efficiency (η_F), defined as the ratio between the actual moles of hydrogen produced ($H_{2,prod}$) to the theoretical moles that should be synthetised stoichiometrically ($H_{2,th}$), as shown in Equation 2.2.

$$\eta_F = \frac{H_{2,prod}}{H_{2,th}} \tag{2.2}$$

According to this approach, the Faraday efficiency is calculated by using an empirical expression at a given temperature (T) and current density (i) utilizing 4 empirical parameters, as reported in Equation 2.3.

$$\eta_F = \left(\frac{i^2}{f_{11} + f_{12} * T + i^2}\right)(f_{22} * T + f_{21}) \tag{2.3}$$

The theoretical hydrogen produced ($H_{2,th}$) has been calculated as indicated in Equation 2.4.

$$H_{2,th} = \frac{P_{stack}}{V_{cell} * z * F} \tag{2.4}$$

where P_{stack} is the power associated to the stack (equal to 0.5 MW), V_{cell} is the cell potential, z is the number of transferred electrons and F is the Faraday constant.

The cell potential (V_{cell}) has been obtained by applying Equation 2.5. This enables to obtain the polarization curve of the electrolyser and, therefore, the necessary potential difference, knowing the operating temperature (T), pressure (P) and current density (i).

$$V_{cell} = V_{rev} + [(r_1 + d_1) + T * r_2 + P * d_2] * i + s * \log\left[\left(\frac{t_3}{T^2} + \frac{t_2}{T} + t_1\right) * i + 1\right] \tag{2.5}$$

In particular, V_{rev} represents the potential value that should be applied thermodynamically to drive the reaction, assuming no dissipations.

The energy required for the reaction is delivered to the electrolyser through the current flow and a portion of this is dissipated in the form of heat. The heat flow is calculated with a thermochemical model based on the Theory of Ulleberg [30].

Once the cell potential (V_{cell}) is known, the excess heat can be calculated using Equation 2.6:

$$Q_{excess} = N * I * (V_{cell} - V_{tn}) \tag{2.6}$$

Here, the excess heat (Q_{excess}) depends on the number of electrochemical cells (N), the current intensity (I), cell potential (V_{cell}) and thermoneutral potential (V_{tn}). The latter is obtained by applying Equation 2.7 and depends on enthalpy variation in the occurring reaction (ΔH), the number of transferred electrons (z) and Faraday constant (F).

$$V_{tn} = \frac{\Delta H}{z * F} \tag{2.7}$$

The empirical parameters and process variables employed the Equations 2.3, 2.4, 2.5, 2.6, 2.7 are reported in Table 2.3.

Table 2.3. Empirical parameters and process variables used for the simulation of hydrogen production.

Variable	Value	Units of measurement
r_1	$4.45153*10^{-5}$	$\Omega.m^2$
r_2	$6.88874*10^{-9}$	$\Omega.m^2.°C^{-1}$
d_1	$-3.12996*10^{-6}$	$\Omega.m^2$
d_2	$4.47137*10^{-7}$	$\Omega.m^2.bar^{-1}$
s	0.33824	V
t_1	-0.01539	$m^2.A^{-1}$
t_2	2.00181	$m^2.A^{-1}.°C$
t_3	15.24178	$m^2.A^{-1}.°C^2$
P (scelta)	5.16	bar
T (scelta)	70	°C
z	2	-
F	96480	$C.mol^{-1}$
V_{rev}	1.2300	V
ΔH	285.83	$kJ.mol^{-1}$
N	600	-
f_{11}	478645.74	$A^2.m^{-4}$
f_{22}	-0.00104	$°C^{-1}$
f_{21}	1.03960	-
f_{12}	-2953.15	$A^2.m^{-4}.°C^{-1}$

The PFD of hydrogen production section is shown in Figure 2.2.

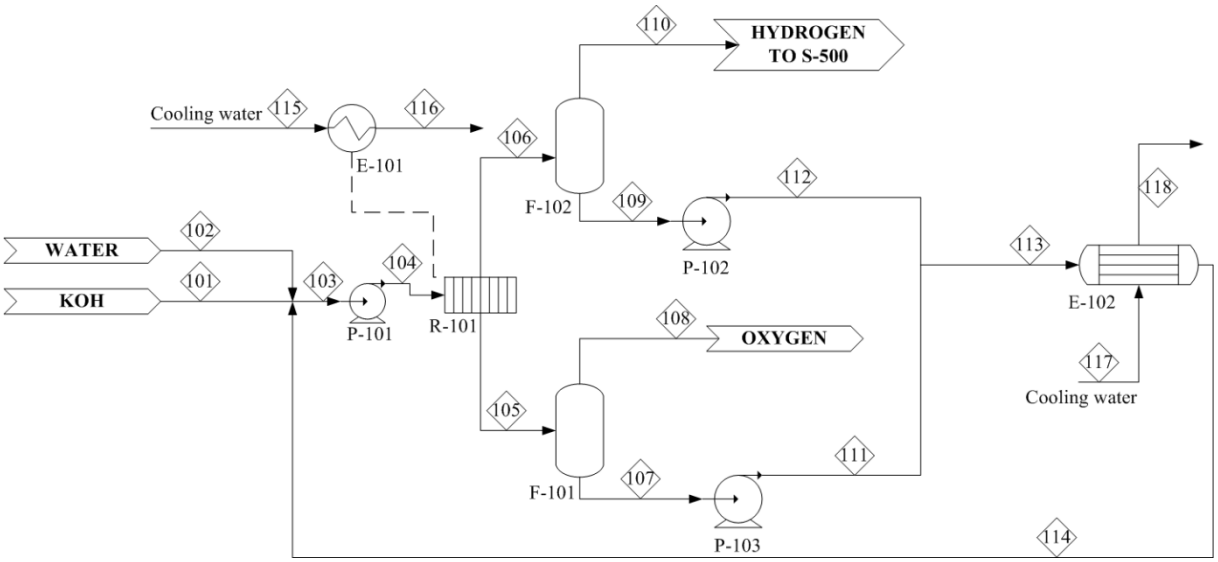

Figure 2.2. PFD of section S-100 for the production of hydrogen.

The simulation included both the equipment necessary for the conversion of the reactants into the products of interest and their separation, as well as the heat exchangers and pumps that allow the movement of the fluids.

The electrolyser (R-101) is simulated as an RSTOIC type reactor. The specified pressure (*P*) is set to match the conditions at which fermentation occurs, while the temperature (*T*) corresponds to the typical operating value of most alkaline electrolysers. The fractional conversion inserted in this block is set after having imposed a ratio of 1 L of water per Nm^3 of produced hydrogen, calculated by combining Equations (2.3) and (2.4) [80].

The streams exiting from the electrolyser (stream 105 and 106) consist of the remaining unreacted liquid solution and the produced gases, oxygen in stream 105 and hydrogen in stream 106. Both enter a flash separator, respectively F-101 and F-102, to allow the separation of the gaseous streams (stream 108 and 110) from the liquid ones (107 and 109). The separated liquid streams are at first brought to the pressure of the incoming stream via pumps P-102 and P-103 and afterwards are cooled to the temperature of the feed via a coaxial tube heat exchanger (E-102). A second heat exchanger (E-101) is necessary to dissipate the heat generated by the electrolyser.

For the sizing of the electrolyser, the model proposed by Sánchez et al., 2020 is employed. Through it the construction characteristics of a single stack were defined, starting from some preliminary assumptions [30]:

- the electrical power absorbed by the single stack is less than 0.5 MW, which aligns with the current state-of-the-art for alkaline electrolysers on the market;
- the current density is set at 0.4 $A.cm^{-2}$, a value that also reflects the state-of-the-art for this type of electrolysis;
- the active area of each cell is equal to 1000 cm^2.

2.3 CO_2 capture

The selected process for CO_2 capture is benchmark chemical absorption with MEA. Given that the objective of this work is the simulation of an industrial-scale process, the intention was to implement the most commonly utilized technology at present.

The simulation and modelling of CO_2 capture process, as well as the resolution of material and energy balances is performed using Aspen Plus® Version 10 (AspenTech, Inc.). The thermodynamic method chosen is ENRTL-RK (*Electrolyte Non-Random Two-Liquid with Redlich-Kwong equation of state*).

The incoming gaseous stream composition comes from the ACEA Pinerolese Industriale Spa biodigester located near Turin. It converts OFMSW into methane and carbon dioxide through anaerobic digestion. Subsequently, methane is purified and the remaining part of the gaseous stream, made up of approximately 60% of CO_2, constitutes the waste that needs to be valorised. The composition of the incoming gas was chosen based on data provided by Acea Pinerolese and Table 2.4 summarizes the gas composition data for different periods of the year. In this case, a hybrid composition was selected, reflecting a worst-case scenario compared to the actual average. Specifically, a composition with the minimum percentage of carbon dioxide and the maximum concentration of pollutants to be eliminated was chosen. Table 2.5 illustrates the selected composition.

Table 2.4. Data provided by Acea Pinerolese Industriale Spa on the gaseous stream to be treated.

Period	January-March	March-May	May-August	August-November
Sulfuric acid (ppm)	132	39,6	37,4	132
Oxygen (%)	5,22	7,44	5,6	4,18
Carbon dioxide (%)	72,9	60,9	74,6	75,7
Hydrogen (%)	<0,035	<0,035	<0,035	<0,035
Methane (%)	0,57	1,07	0,934	0,505
Nitrogen (%)	21,3	30,6	18,9	19,6
Carbon monoxide (%)	<0,0036	<0,0036	<0,0036	<0,0036

Table 2.5. Composition of the input stream to the simulated process for CO_2 capture.

Compound	Composition
Hydrogen sulphide (ppm)	132
Oxygen (%)	7,44
Carbon dioxide (%)	60,9
Hydrogen (%)	<0,035
Methane (%)	1,07
Nitrogen (%)	30,6
Carbon monoxide (%)	<0,0036

The flowrate of the incoming gas is 6830.56 $Nm^3.h^{-1}$ and is mainly made up of carbon dioxide and nitrogen, with traces of methane, hydrogen, carbon monoxide and hydrogen sulphide. Being CO_2 the product of interest, it must have the highest purity for the fermentation step. However, due to its acidic properties similar to CO_2, H_2S would also be absorbed in the amine solution. To address this issue, H_2S is removed in the purification section S-200, as represented in Figure 2.3.

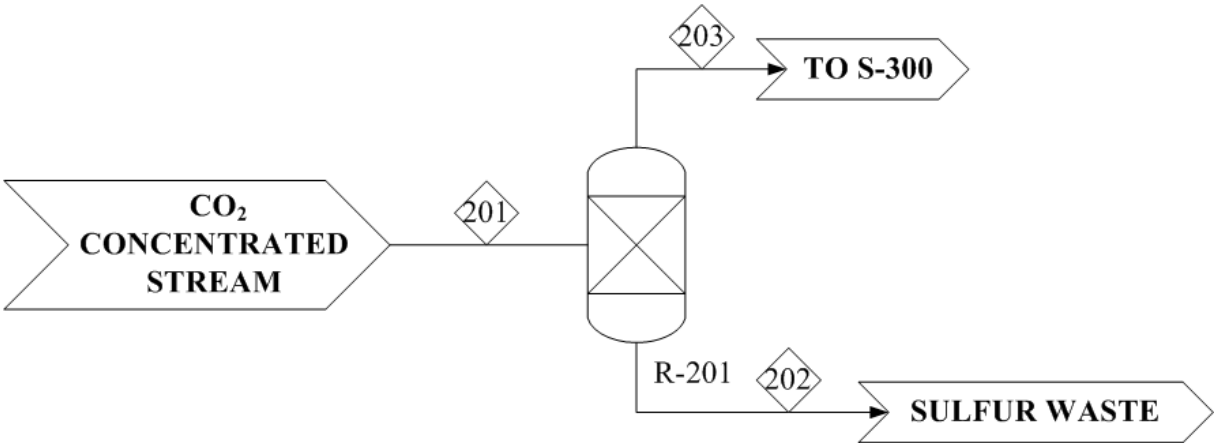

Figure 2.3. PFD of section S-200 for the removal of H_2S.

When H_2S concentration is low, as in the case under consideration, using the conventional Claus process is not convenient [81]. Alternative approaches should then be considered, such as the innovative LO-CAT process. The latter employs an iron-based catalytic solution to oxidise H_2S to elemental sulphur, facilitating its separation and elimination. A key advantage of this process is that the catalytic solution is environmentally friendly and does not produce any dangerous by-products [82].

The removal of H_2S occurs inside an absorption column, where the gas to be treated reacts with a solvent which captures H_2S. The solvent is then regenerated in an oxidative unit, where air is introduced. The regenerated solvent can be recirculated, while the solid sulphur produced in the reactor is separated into a waste stream.

Due to the unknown composition of the solution, the reduction of H_2S is simulated in a RSTOIC (R-201) reactor, where pollutant conversion and removal occur are based on the LO-CAT process yields, achieving a 99.9% H_2S removal efficiency [82]. This process takes place at ambient temperature and does not require additional heating or cooling utilities. A sulphur-rich slurry (stream 202) exits the oxidative unit, which must then be disposed of. Once this pre-treatment has been carried out, the gas can enter the absorption section to capture carbon dioxide (S-300).

Carbon dioxide absorption process employs two packed columns in series, one used for CO_2 capture and the other for solvent regeneration.

The components inserted in the simulation are summarized in Table 2.6. The ionic forms of the compounds present were included in the simulation, since the reactions depend on their concentration in the solution.

Table 2.6. Chemical species inserted in the simulation for CO_2 capture.

Compound	Type	Conventional name
MEA	Conventional	Methyl-diethanolamine
H_2O	Conventional	Water
CO_2	Conventional	Carbon dioxide
H_3O^+	Conventional	Ion
OH^-	Conventional	Ion
HCO_3^-	Conventional	Ion
CO_3^{2-}	Conventional	Ion
$MEAH^+$	Conventional	Ion
$MEACOO^-$	Conventional	Ion
N_2	Conventional	Nitrogen
O_2	Conventional	Oxygen
H_2	Conventional	Hydrogen
CO	Conventional	Carbon monoxide
CH_4	Conventional	Methane

The solvent composition is detailed in Table 2.7. It consists of 30 wt% MEA, which represents the best compromise for increasing CO_2 absorption while simultaneously minimizing issues associated with corrosion and losses [83]. Additionally, a non-negligible amount of CO_2 is present (6.5 wt%), as it is assumed that the solvent regeneration process does not completely remove CO_2 from the amine solution.

Table 2.7. Composition of the solvent employed for CO_2 capture.

Compound	Composition (wt %)
MEA	30
Water	63.5
Carbon dioxide	6.5

A chemical model, called *GLOBAL*, was developed and serves as calculation basis for the software. This model treats all reactions as equilibrium ones.

GLOBAL

$$MEAH^+ + H_2O \rightleftarrows MEA + H_3O^+ \quad (2.8)$$

$$MEACOO^- + H_2O \rightleftarrows MEA + HCO_3^- \quad (2.9)$$

$$2\,H_2O \rightleftarrows H_3O^+ + OH^- \quad (2.10)$$

$$CO_2 + 2\,H_2O \rightleftarrows HCO_3^- + H_3O^+ \quad (2.11)$$

$$HCO_3^- + H_2O \rightleftarrows CO_3^{2-} + H_3O^+ \quad (2.12)$$

However, within the absorption and stripping columns a more detailed model was implemented, *ABS* and *STRIP* respectively, in which equilibrium and kinetically governed reactions appear, as reported in Table 2.8 [84]. These two models differ only in the kinetic of reaction 2.16.

ABS/ STRIP

$$MEAH^+ + H_2O \rightleftarrows MEA + H_3O^+ \quad (2.8)$$

$$2\,H_2O \rightleftarrows H_3O^+ + OH^- \quad (2.10)$$

$$HCO_3^- + H_2O \rightleftarrows CO_3^{2-} + H_3O^+ \quad (2.12)$$

$$CO_2 + OH^- \rightleftarrows HCO_3^- \quad (2.13)$$

$$HCO_3^- \rightleftarrows CO_2 + OH^- \quad (2.14)$$

$$MEA + CO_2 + H_2O \rightleftarrows MEACOO^- + H_3O^+ \quad (2.15)$$

$$MEACOO^- + H_3O^+ \rightleftarrows MEA + CO_2 + H_2O \quad (2.16)$$

Table 2.8. Stoichiometry and stoichiometric coefficients of the reactions inserted in the model *STRIP*.

Reaction	Type	E_a (cal.mol^{-1})	k
(2.8)	Equilibrium	-	-
(2.10)	Equilibrium	-	-
(2.12)	Equilibrium	-	-
(2.13)	Kinetics	13249	1.33e^{17}
(2.14)	Kinetics	25656	6.63e^{16}
(2.15)	Kinetics	9855.8	3.02e^{14}
(2.16) absorber	Kinetics	16518	5.52e^{23}
(2.16) stripper	Kinetics	22782	6.5e^{27}

The following targets have been established for this process:

- CO_2 capture efficiency greater than 90%;
- specific energy consumption for regeneration below 5 MJ.kg^{-1} captured CO_2, a value that reflects the state-of-the-art for chemical absorption with MEA [45];
- CO_2 purity above 99%;
- absence of oxygen in the output stream.

The PFD of CO_2 capture unit (S-300) is presented in Figure 2.4.

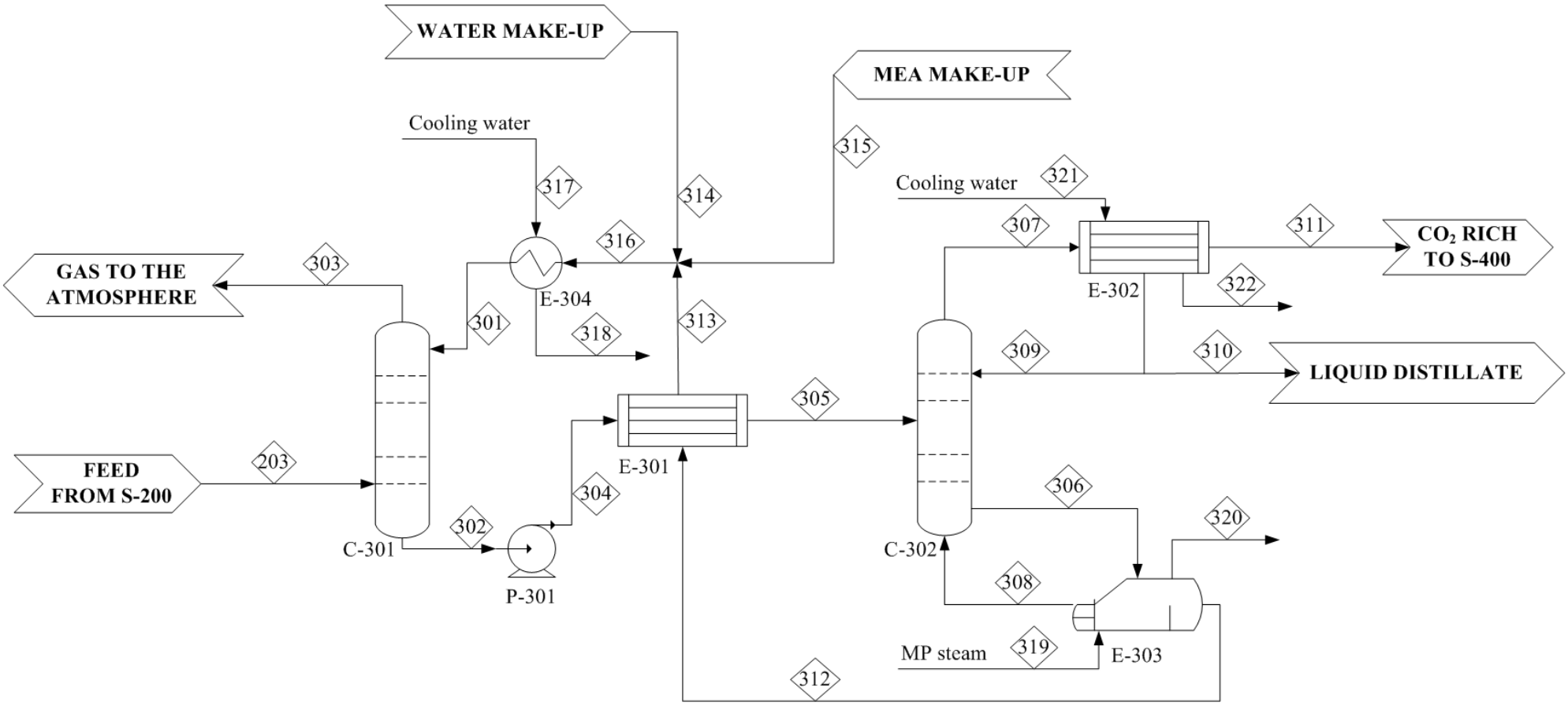

Figure 2.4. PFD of section S-300 for CO_2 capture.

The absorber and the stripper were modelled following the procedure indicated by Madeddu et al., 2019 [84].

The design requirement for the absorber (C-301) is that 90% of the incoming carbon dioxide is transferred to the liquid solution exiting from the bottom of the column (stream 301). This unit was initially simulated with an infinite height to determine the minimum solvent quantity needed to reach the target. Subsequently, the height was gradually reduced, and the final sizing of the column was optimized taking into account three different factors: capital cost of the column, solvent consumption and maintenance of a linear temperature profile within the liquid phase. In this way, all stages contribute effectively to the reaction.

The absorber works at ambient pressure, whereas regeneration is more efficient at higher pressure. Therefore, a pump (P-301) was added between the absorber and the stripper to increase the pressure to 1.8 bar. In the case of mixtures of MEA and CO_2 it is advisable to work at pressures above atmospheric levels to facilitate stripping. However, pressures exceeding 2 bar can lead to MEA degradation [84]. In fact, increasing the pressure also raises the mixture's saturation temperature, resulting in an overall temperature increase. In addition, in accordance to the guidelines specified in the work of Madeddu et al., 2019, to enhance the efficiency of the stripping process it's recommended to keep the inlet stream (stream 305) at 2 °C below the saturation temperature [84].

The stripper (C-302) was sized by adjusting the reboiler duty and the distillate-to-feed ratio. The former was manipulated to ensure that the regenerated solvent exiting the bottom of the column (stream 312) contained a maximum of 6.5 wt. % CO_2, making sure at the same time not to exceed the imposed specific consumption of the reboiler. The latter was varied to achieve the desired purity in the distillate (stream 307). Initially, the column was simulated at infinite height to determine the minimum reboiler duty to meet the target. The height was then progressively decreased, and the final design was developed considering the capital cost, maintenance of a linear temperature profile in the liquid phase and minimization of the reboiler duty. Regarding the feed stage, it was observed that feeding the inlet stream (stream 305) at stage 7 was the optimal solution to reach the set targets minimizing the duty demand at the reboiler.

One of the main challenges of the process is the high energy demand of the reboiler (E-303) in the stripping column. To address this issue, the thermal energy of the regenerated solvent (stream 312) is employed to preheat the stream to be regenerated (stream 301) through a heat exchanger (E-301). This approach not only preheats the amine solution but also cools the solvent returning to the absorption column. However, the regenerated solvent is not cooled sufficiently and an additional heat exchanger (E-304) is required to bring the temperature down to the column inlet value. The process is cyclical and to compensate the unavoidable losses a replenishment both of water and amine, stream 314 and 315 respectively, is necessary.

Excluding CO_2 and H_2S, which is removed in section S-200, the other gaseous species present in the feed stream will be found in the gaseous stream exiting the absorber (stream 303). In the liquid stream exiting the absorber (stream 301), in addition to CO_2 and water, a low quantity of oxygen (0.07 wt. %) is detected, due probably to its solubility in captured

CO_2. Since the current exiting the process (stream 311) will be metabolised by anaerobic bacteria, it is necessary to eliminate the oxygen present. This is achieved in the second purification section (S-400), reported in Figure 2.5.

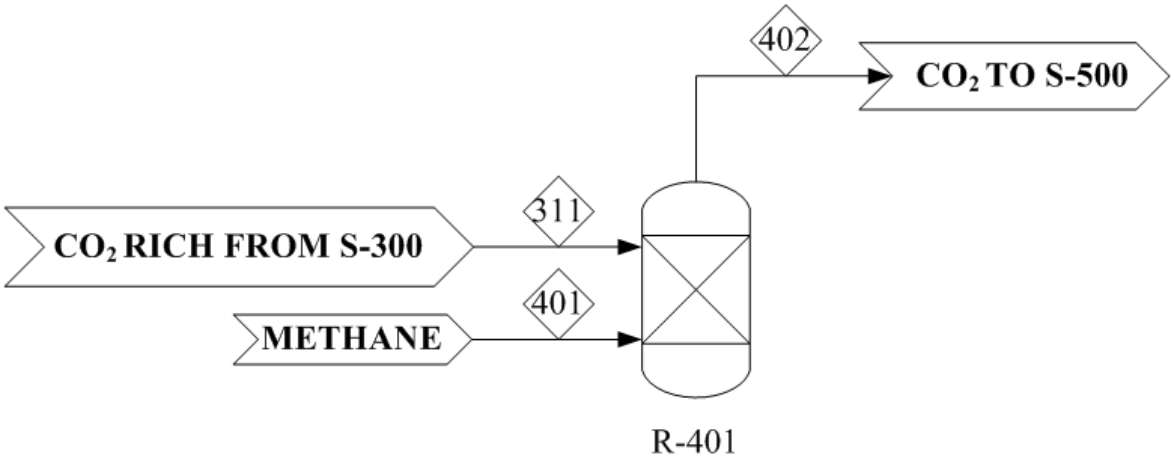

Figure 2.5. PDF of section S-400 for oxygen removal.

A highly effective method for reducing oxygen involves the utilization of a catalytic oxidation process with a platinum-based catalyst [85]. This process is simulated inside a R-STOIC reactor (R-401), where the reaction indicated in Equation 2.17 is inserted:

$$CH_4 + 2O_2 \rightleftarrows \quad CO_2 + 2H_2O \tag{2.17}$$

The reactor works under adiabatic conditions, with a set pressure of 5.16 bar, which is the pressure requested at the inlet of the fermenter in section S-500. To convert all the oxygen present in stream 311, 365.7 $L.h^{-1}$ of methane are needed.

2.4 Fermentation

The simulation and modelling of the fermentation process, along with the resolution of material and energy balances, is carried out using Aspen Plus® Version 10 (AspenTech, Inc.). Specifically, the process has been simulated at two different headspace pressure in the fermenter, 2 bar and 10 bar, basing on the work conducted by Regis, 2024 [58]. In this study, a fully coupled industrial-scale model of a bubble column fermenter was developed. More specifically, the research focused on identifying the optimal conditions of pressure, gas and liquid inlet flow rates and the inlet gas composition to maximise acetic acid productivity under steady-state conditions. It was concluded that the optimal biomass concentration is 5 $g.L^{-1}$. Under this scenario, it was possible to identify two optimal pressure values in the column headspace.

According to this model, at a headspace pressure of 10 bar, acetic acid productivity along with the conversion rates of H_2 and CO_2 are maximised. However, purifying the fermentation broth is challenging due to the non-negligible presence of formic acid. Conversely, at a pressure of 2 bar, formic acid production is insignificant, and compression costs are lower. However, in the latter case acetic acid specific production rate in the column is 63% of what is achieved when fermentation occurs at 10 bar, and the converted flow rates of H_2 and CO_2 are approximately 65% of what is obtained under the same conditions.

In both scenarios, the model enables the calculation of the conversion of the supplied gas. Furthermore, the amounts of CO_2 and H_2 needed to produce acetic acid, biomass and formic acid can be determined, as well as the amount of each gas species dissolved in the medium at steady state. In particular, at 2 bar, to produce 1 kg of acetic acid, 1.71 kg of CO_2 and 0.14 kg of H_2 are required, while at 10 bar, to synthesize 1 kg of acetic acid, 1.85 kg of CO_2 and 0.15 kg of H_2 are necessary. The gas quantities required in the two cases are slightly different due to variations in the dissolved substrate quantities in the medium with changes in pressure, influencing bacterial kinetics for the production of acetic acid, biomass, and formic acid.

The thermodynamic method employed is NRTL (*Non-Random Two-Liquid*). The components included in the simulation are carbon dioxide, hydrogen, water, acetic acid and formic acid, as reported in Table 2.11.

Table 2.11. Chemical compounds inserted in the simulation of fermentation for acetic acid production.

Chemical compound	Type	Conventional name
CO_2	Conventional	Carbon dioxide
H_2	Conventional	Hydrogen
H_2O	Conventional	Water
CH_3COOH	Conventional	Acetic acid
HCOOH	Conventional	Formic acid

In the case of fermentation conducted at 2 bar, the process flow diagram is shown in Figure 2.6, whereas when fermentation is carried out at 10 bar, the corresponding diagram is illustrated in Figure 2.7

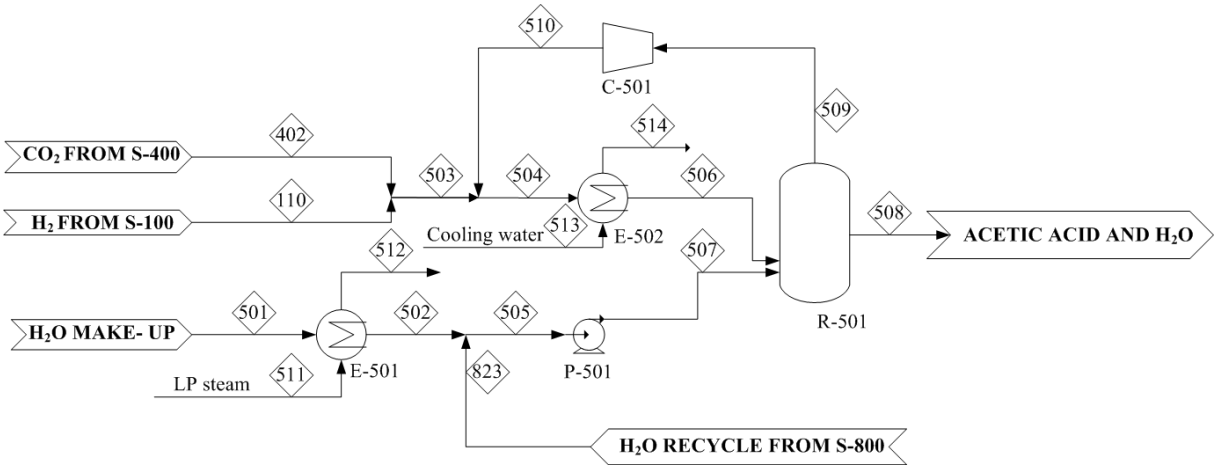

Figure 2.6. PFD S-500 for fermentation section with 2 bar headspace pressure in the fermenter.

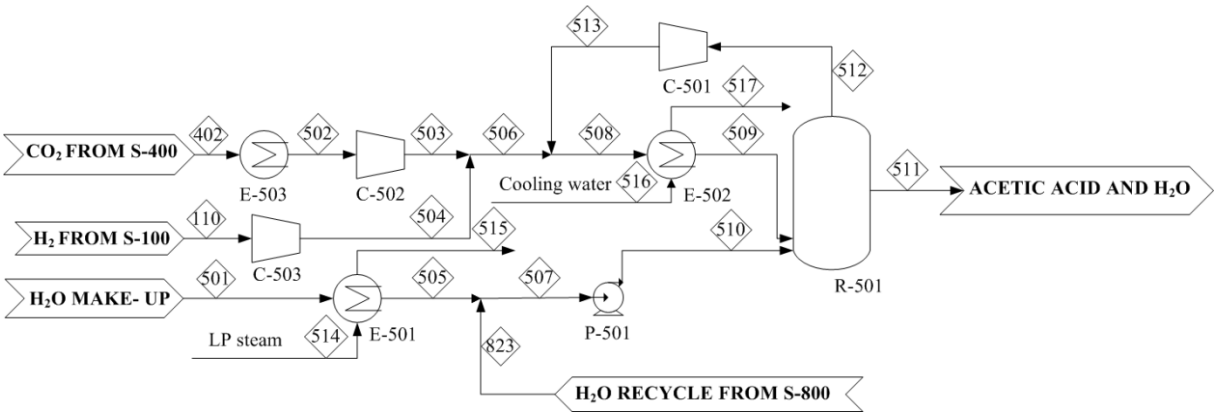

Figure 2.7. PFD S-500 for fermentation section with 10 bar headspace pressure in the fermenter.

The bubble column fermenter (R-501) is simulated as an RSTOIC type reactor. The operating temperature is 66 °C, with the headspace pressure in the column at either 2 bar or 10 bar depending on the simulated conditions.

The reference reaction for acetic acid production is defined in Equation 2.17.

$$2CO_2 + 4H_2 \rightarrow CH_3COOH + 2H_2O \quad (2.17)$$

When fermentation occurs at a headspace pressure of 2 bar in the column, only the previous reaction is considered, as the amount of formic acid produced is negligible compared to acetic acid. However, when the headspace pressure is increased to 10 bar, the reaction for formic acid production, defined in Equation 2.18 must also be included.

$$CO_2 + H_2 \rightarrow HCOOH \quad (2.18)$$

For simplification, *T. kivui* and its medium are excluded from the simulation. However, although the water entering the reactor depletes the nutrients required for bacterial growth, the latter are accounted in the economic analysis.

The unconverted gas is recirculated to the reactor after being recompressed. In particular, the gases entering the reactor are brought to a pressure level 10% higher than that at the bottom of the column to compensate the pressure drop across the sparger and are heated to a temperature of 66 °C in the heat exchanger E-502. When fermentation occurs with a headspace pressure of 2 bar in the column, the H_2 and CO_2 streams are already at the desired pressure. Conversely, if fermentation is carried out at a head pressure of 10 bar, two compressors (C-502 and C-503) are required to further compress the incoming gas streams to the fermentation section. Additionally, in the latter case a heat exchanger (E-503) is necessary on the CO_2 stream to raise the water vapour above the dew point. Finally, water is recirculated from the acetic acid purification section (stream 823) and a make-up of water is necessary to compensate the losses (stream 501). Both flows must be brought to the pressure at the bottom of the reactor using a pump (P-501).

2.5 Purification of acetic acid

Effective purification of acetic acid from a fermentative broth involves two key preliminary steps: filtration and ion exchange.

First, filtration is used to remove solid components, such as residual cellular material. For this purpose, a crossflow filter with ceramic membranes is used. These filters are characterized by a hydrophilic nature, that helps minimize irreversible fouling, a common problem with other materials. With a pore size typically less than 0.2 μm, these filters efficiently separate bacterial biomass. Additionally, ceramic membranes exhibit high resistance to low pH values, ensuring a long lifespan of over 10 years, requiring then only one replacement during the system's operational life.

Subsequently, the fermentation broth undergoes acidification, which is carried out to lower the pH below the pKa of acetic acid, making easier the dissociation of salts and the release of ions that the resins can then remove. The resins involved are first cationic and then anionic ones. In particular, ion exchange operates continuously by alternating between two units: one in operation and one undergoing regeneration. It is assumed that ions are completely removed, with no significant pressure drops of acetic acid during the passage. Cations such as Mg^{2+}, Ca^{2+}, Na^{+}, K^{+} and NH_4^{+} in cationic resins and anions such as SO_4^{2-}, Cl^{-} and HPO_4^{2-} in anionic resins are removed. Back-washing is performed using process water. During regeneration, the cationic resins are treated with an aqueous solution containing 37 % HCl, while for the anionic ones a 30 % NaOH solution is used. The regeneration ends with the passage of air into both resins. Cationic exchange resins are characterized by a lifespan of about 3 years, whereas for anionic ones this value is usually 2 years.

The actual purification of acetic acid from water occurs via HEDP process (hybrid extraction/ distillation process), which combines liquid-liquid extraction with azeotropic distillation.

According to Chilev et al., 2021 the hybrid process is the most efficient one among conventional methods due to several advantages [76]:

- lower loss of product and solvent;
- fewer stages needed in the distillation column;
- lower energy impact in relation to heating and cooling.

In the hybrid process, extraction is employed to separate acetic acid from water using an organic solvent. The choice of the solvent is a crucial point for the process' success, since it must be characterized by a high extraction capacity, allowing the recovery of all the product from the aqueous solution, as well as the capability to form an azeotrope with water, permitting an easy separation in the distillation process. The choice of the solvent fell on methyl *tert*-butyl-ether (MTBE), given its low temperature and concentration of formation of the azeotrope with water, which reduce energy consumption during azeotropic distillation. Specifically, when operating with MTBE the azeotrope forms at 51.6 °C and 4 wt% [76].

Azeotropic distillation is a separation process that involves the use of a third component able to form an azeotrope with water. In particular, acetic acid, being the higher boiling component, is recovered in the bottom with a purity of 99.9% by weight, as required by GAA market. On the other hand, water and MTBE constitute the distillate and are subsequently separated using a decanter. To reduce its external demand, the solvent is thus recirculated upstream of the extraction process. Water is also purified in a distillation column, with the aim to be recirculated in the fermentation section (S-500).

The simulation and modelling of the purification section is carried out using Aspen Plus® V10 (AspenTech, Inc.).

The components included in the simulation are water, acetic acid and MTBE, as reported in Table 2.12.

Table 2.12. Chemical compounds inserted in the simulation for the purification of acetic acid and water.

Chemical compound	**Type**	**Conventional**
H_2O	Conventional	Water
CH_3COOH	Conventional	Acetic acid
MTBE	Conventional	Methyl *tert*-butyl ether

The thermodynamic method chosen is NRTL-HOC (*non-random two liquids- Hayden O'Connel*), which appears to be the most suitable one when dealing with organic acids [76]. In the entire process no pressure losses were considered.

Figure 2.8 shows the process diagram of the extraction section.

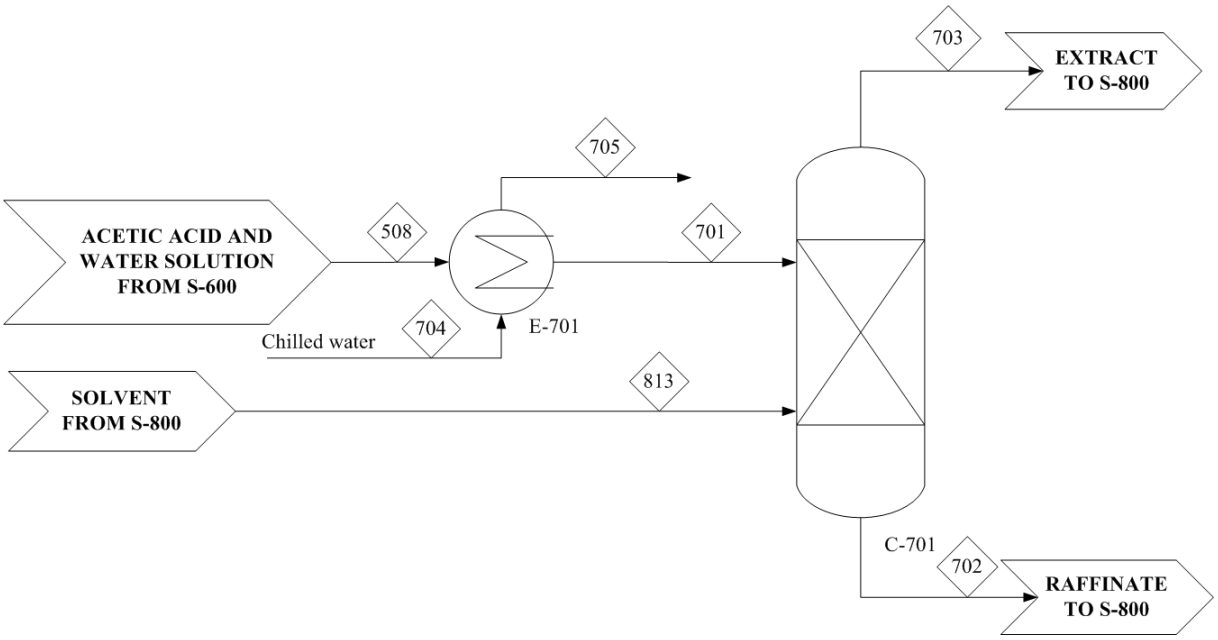

Figure 2.8. PFD S-700 of the extraction section.

The fed stream (508) consists only of acetic acid and water (1.5 wt% CH_3COOH and 98.5 wt% H_2O) and derives from the fermentation section when conducted with a headspace pressure of 2 bar (S-500). Salts and soluble components of the bacterial medium are not considered in this stream, as it is assumed they are completely removed in the ionic exchange resins. The flowrate to be treated is equal to 284923 $kg.h^{-1}$.

The extraction column (C-701) was modelled by implementing the EXTRACT module. It was designed with the aim of recovering 100% of acetic acid present in the feed in the organic extract. In particular, the column was simulated acting on the following parameters: total number of equilibrium stages, solvent flowrate and operating temperature. The latter was specified using an exchanger (E-701) upstream of the column and the result showed that the optimal temperature was 20 °C. It was also assumed that there were no thermal variations along the column and no pressure drops were considered. To achieve the desired total acid recovery, 25 equilibrium stages were necessary. The feed stream (701) entered the column at the top, at stage 1, whereas MTBE (704) was introduced at the bottom of the column at stage 25. Aspen simulations indicated that acetic acid recovery increased with the solvent quantity. Specifically, to meet the target set, the simulator determined a necessary MTBE flowrate of 585000 $kg.h^{-1}$. The extraction column was then sized using Aspen Process Energy Analyzer (APEA), providing as input the number of stages and the mass flowrate fed and considering the extraction column as a vertical tower.

However, an excessively large diameter was generated by the software, which would have been impractical to implement in the reality. Consequently, 5 extractors were implemented to operate in parallel, each of them handling a reduced flowrate. By setting the same targets and confirming the previously described hypotheses, a smaller diameter emerged. To simplify the reading, a single extraction block in Figure 2.8 is represented.

In Table 2.13 are summarized the numerical results.

Table 2.13. Details of the single column in parallel for extraction section (C-701).

	Single column operating in parallel
Flowrate at stage 1 ($kg.h^{-1}$)	56985
Flowrate at stage 20 ($kg.h^{-1}$)	117000

The PFD of acetic acid, water and solvent recovery section (S-800) of the hybrid process is represented in Figure 2.9.

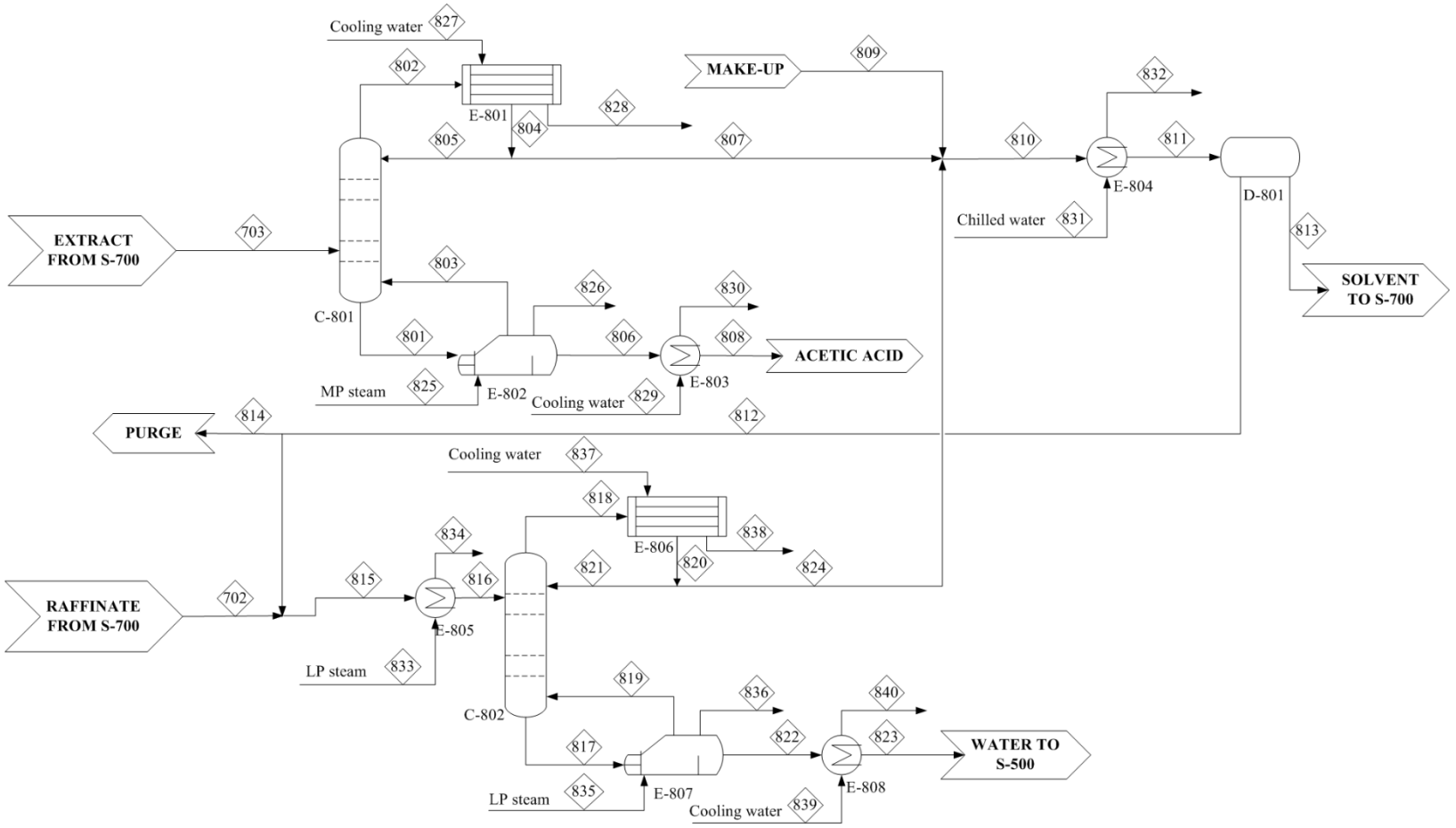

Figure 2.9. PFD of S-800 for acetic acid, water and solvent recovery section.

The modelling of the azeotropic distillation column (C-801) was performed by implementing the RADFRAC module. For the optimal design, the target was set to achieve 99.9% purity of acetic acid at the bottom of the column (GAA target). The ideal number of equilibrium stages is 22. The column performance was also investigated based on the reflux ratio, inlet temperature and feed stage. In particular, the reflux ratio showed no significant effect on achieving the desired concentration of product. Similarly, the inlet temperature was found to have a little effect, therefore it was chosen to feed the column at the extraction column's outlet temperature, i.e. 20 °C. Contrariwise, the feed stage location had a more pronounced impact. By selecting stage 16 as feed stage, the 99.9% purity target was fully achieved. Regarding the sizing of the column, the Aspen *internals* function was used to determine the diameter and height. Similarly to liquid-liquid extraction, the diameter was found to be very large. To address this, a configuration with multiple azeotropic distillation columns operating in parallel was chosen. In this way, the capacity that each column is required to handle is reduced. After carrying out simulations with an increasing number of columns, it was concluded that by introducing 5 columns it was possible to achieve the purity and recovery targets with a reasonable column diameter. Since the reflux ratio significantly affects the sizing, an optimal value of 0.5 was determined. An overview of the sizing details is provided in Table 2.14. From the bottom of the azeotropic distillation column, acetic acid stream is recovered (stream 806). This is cooled to 30 °C in the heat exchanger E-803, preparing it for the transport and sale.

Table 2.14. Details of the single column in parallel for azeotropic distillation section (C-801).

	Single column in parallel
Flowrate stage 16 (kg. h^{-1})	116760
Reflux ratio	0.5

From the head of the azeotropic distillation columns (807), a stream consisting of MTBE and water comes out. This is sent to a decanter (D-801) to obtain separation between the two components. Before decantation, the MTBE-water stream is mixed with the overhead product (stream 824) of the distillation column (C-802) used to treat the aqueous raffinate coming from the extraction section. In addition, a make-up of MTBE (stream 809) is introduced in this section of the plant to compensate the losses. The decanter operates at a temperature of 20 °C, specified through the use of an upstream heat exchanger (E-804). Downstream of the decanter the solvent is recirculated to the extraction column C-701. Instead, water (stream 812) is combined with the previously mentioned raffinate (stream 702) coming from the extraction section and purified through distillation. For this purpose, a distillation column (C-802) is used with the aim of obtaining water with a purity of 99.99% from the bottom. The column was implemented using the RADFRAC module, similarly to azeotropic distillation. Once the target water concentration of the current exiting the bottom was set, the number of equilibrium stages, any pre-heating and the reflux ratio were evaluated. The target water concentration is obtained with a 22-stage column, feeding the raffinate at stage 2 with a reflux ratio of 1. In this case, it is also necessary to pre-heat the

feed to a temperature of 50 °C, in exchanger E-805, as inserting it at a temperature of 20 °C alters the operation of the column. The sizing of the column is performed using the Aspen *internals* function. Unlike the liquid-liquid extraction and azeotropic distillation, the resulting diameter is relatively small compared to earlier cases. Therefore, it was not necessary to implement multiple columns in parallel. From the bottom of the distillation column, a stream (stream 822) constituted of high purity water (99.99%) is recovered. After having been cooled to 66 °C in the heat exchanger E-808, the optimal temperature for fermentation, this water is recycled for the medium preparation in the fermentation section (S-500).

It is important to highlight that, in order to respect the mass balance of water in the control volume of the system, it was necessary to purge upstream of the distillation column (stream 814) so as not to alter its functioning and not have problems with the recirculation.

In Table 2.15 operating conditions are summed up.

Table 2.15. Operating conditions of extraction and distillation columns of the hybrid process.

	Extraction column (C-301) ***(Data refer to a single column in parallel)***	**Azeotropic distillation column (C-401)** ***(Data refer to a single column in parallel)***	**Distillation column (C-402)**
Number of stages	25	22	22
Feed stage	1	16	2
Solvent stage	20	-	-
Temperature (°C)	20	52.37/117.92	37.02/100.03
Pressure (bar)	1.01	1.01	1.01
Condenser	-	Total	Total
Reboiler	-	Partial Kettle	Partial Kettle
Reflux ratio	-	0.5	1

2.6 Thermal integration

To maximise the energy efficiency of the process, an energy analysis was conducted using the Pinch Analysis Method in the software Aspen Energy Analyzer (HX-Net). It's a procedure which is employed to reduce energy consumption in chemical processes through the optimization of heat recovery systems. In this way, the maximum potential energy recovery from the process streams can be achieved, maximizing the heat exchange between them and minimizing the use of utilities. Despite this, lowering utility usage can come at the expense of the fixed costs associated with heat exchangers.

In Aspen Energy Analyzer, the streams are defined with their flowrate, enthalpy and inlet and outlet temperature from the equipment. The software provides the set of hot and cold flows present in the process through composite curves. In particular, the hot composite curve represents the relationship between temperature and enthalpy for heat streams to be removed from streams to be cooled, whereas the cold composite curve represents the same concept for heat streams to be supplied to streams to be heated. These curves allow the identification of the *pinch point*, where the distance between hot and cold curves is minimum.

Utility requirements are minimized by avoiding:

- heat transfer between streams with a temperature difference equal to or lower than the pinch temperature;
- the use of cold utilities to cool streams above the pinch
- the use of hot utilities to heat streams below the pinch.

In the entire process a minimum temperature difference between the hot and cold sides (ΔT_{min}) was set equal to 10 °C.

2.7 Economic analysis and KPIs

The objective of the economic analysis is to determine a minimum selling price for acetic acid produced by CO_2 fermentation. This price refers to the price necessary to cover all investments expenses during the useful life of the system.

2.7.1 Total project investment evaluation

The first step to conduct the economic analysis of the process involves the evaluation of the Total Project Investment (TPI). This is achieved by evaluating the Purchase Equipment Costs (PEC), which represent the cost of each equipment used in the process. This was obtained by sizing the equipment using the Aspen Process Economic Analyzer (APEA) included in Aspen Plus® V10 (AspenTech, Inc.). Leveraging a comprehensive database collected by Engineering, Procurement and Construction (EPC) companies, the program maps out the plant and estimates costs.

For certain plant sections, a different approach was required for assessing the PEC.

In particular, the relationship given in Equation 2.19 was used to scale each PEC according to its size when pricing was known for a different size (or capacity) than what was required.

$$\frac{PEC_a}{PEC_b} = (\frac{A_a}{A_b})^{\gamma} \tag{2.19}$$

In Equation 2.19 A is the equipment cost attribute (size or capacity) and γ is a cost exponent factor depending on the equipment. In particular, γ was considered equal to 0.6 for the six-tenths rule [86].

As regards the hydrogen production section (S-100), the PEC associated to the electrolyser is calculated starting from the reference value of 510 €.kW^{-1} from the year 2023 [87].

For the LO-CAT process, the PEC of the H_2S removal reactor (R-201) was scaled based on the information provided in the supplementary materials of the work published by Bressanin et al., 2020 [88]. As concerns O_2 removal section, the PEC of the catalytic reactor (R-401) was scaled following the work conducted by Peppel et al., 2017a [89]. The catalyst used consists of 99% γ-allumina and 1% platinum and its cost derives from literature data [90] [91]. As for the fermentation section, the PEC associated to the bubble column fermenter was calculated basing on the research of Humbird et al., 2017 [92]. In relation to section S-600, the capital expenditure associated to the employment of filters and ionic exchange resins were provided by selected companies.

To scale all the PECs from the year for which they were available to 2023, which was chosen as the base year, Equation 2.20 was used.

$$\frac{PEC_1}{PEC_2} = \frac{CEPCI_1}{CEPCI_2} \tag{2.20}$$

In Equation 2.20 CEPCI is the Chemical Engineering Plant Cost Index, while subscripts 1 and 2 refer respectively to the year when the cost is available and the base year [86].

The next step is to calculate the cost of each piece of equipment following installation. This quantity, obtained from the PEC using Equation 2.21 is referred to as the IEC (Installed Equipment Cost).

$$IEC = \frac{PEC}{1-\alpha_1-\alpha_2} \quad (2.21)$$

In Equation 2.21 α_1 and α_2 are two coefficients that take into account the installation cost, materials and labour. Their respective values are 0.24 and 0.08 [90].

The Total Equipment Cost (TEC) was obtained from the sum of all the IECs of the equipment. To this, the costs related to the warehouse (estimated at 1.5% of the TEC) and site development (estimated at 9% of the TEC) are added. The sum of these three cost components constitutes the Total Installed Cost (TIC). All the expenses mentioned so far are defined as direct costs because they are directly associated with the construction of the equipment that enables the production of the desired product. Subsequently, the Total Capital Investment (TCI) was assessed. This involves adding indirect expenses, represented as a percentage of the Total Installed Cost (TIC), to the total installation cost. Specifically, considerations were made for site expenses (20 % of the TCI), offices and construction taxes (25 % of the TCI), and contractual contingencies (3 % of the TCI). Finally, to obtain the Total Project Investment (TPI), the TCI was added to other generic expenses such as permits and start-up costs. These expenses were estimated at 10% of the TIC [86]. The calculated costs apply to the construction of a plant from the ground up. The various contributions to the calculation of the TPI are summarized in Table 2.18.

Table 2.18. Contribution used for the calculation of the TPI.

Item	Estimation
Total Equipment Cost (TEC)	Sum of the IEC of all units
Warehouse	1.5% of TEC
Site development	9% of TEC
Total Installed Cost (TIC)	Sum of TEC, warehouse and site development
Field expenses	20% of TIC
Home office & construction fee	25% of TIC
Project contingency	3% of TIC
Total indirect expenses	48% of TIC
Total Capital Investment (TCI)	Sum of indirect expenses and TIC
Other costs	10% of TIC
Total Project Investment (TPI)	Sum of TCI and other expenses

2.7.2 Operational cost evaluation

To evaluate the total operating costs, two contributions were examined: variable operating costs and fixed operating costs. The former were considered only during plant operation and include raw materials, utilities and waste handling. Regarding the procurement of raw materials for hydrogen production process, the price of water (0.021 €.m^{-3} from APEA) and KOH (465 €.ton^{-1} [93]) were assesed. For CO_2 capture, MEA (1.1 \$.kg^{-1} [47]) and the chemicals for H_2S removal were regarded, as well as the cost of methane (.0.13 \$.Nm^{-3} [94])

for the removal of O_2 in section S-400. As for the fermentation section, the cost of water and the nutrients required for bacterial growth were factored in. Moreover, the cost of the inoculum of the bacterium from a microbial bank was included in the analysis. As concerns the downstream phase, the cost of MTBE (653 €.t^{-1} [94]) was taken into account. In addition, regarding section S-600 the cost of the reactants employed for the regeneration of resins was considered, respectively 630 €.ton^{-1} for HCl 37% solution and 130 €.ton^{-1} for NaOH. Furthermore, it was supposed to replace MEA solution and MTBE once a year, to deal with their possible degradation. Also, KOH was set to be substituted with the same frequency due to possible contamination. Therefore, the total cost of raw materials also includes these considerations.

Regarding thermal utilities, the most suitable for performing the required thermal operations were implemented (considering a ΔT_{min} of 10°C). Their cost, along with electrical expenses, was assessed using APEA.

Moreover, among other variable costs wastewater treatment and waste chemicals treatment were regarded. The least involves the treatment of the acqueous stream purged in the recovery section (S-800) which contains traces of MTBE as well as water soluble components not eliminated in the preliminary purification phase, which could accumulate along the process. This cost amounts to 3 €.m^{-3} [86]. The latter is carried out on the volume of solvent replaced, i.e. KOH in Section S-100, MEA in section S-300 and MTBE in section S-700 with an presumed cost of 200 \$.ton^{-1} [86].

Whether the plant was working at full capacity or not, fixed operating costs were charged completely. Labour and several overhead elements were included in these costs. Wages were calculated considering that the plant worked 365 days.year^{-1} for 24 hours.day^{-1} divided into 3 shifts of 8 hours, for a total of 1095 shifts.year^{-1}. Each operator worked 49 weeks.year^{-1}, five 8 hours shifts.week^{-1} for a total of 245 shifts.year^{-1} which were about 2000 hours. By dividing the number of annual shifts by those carried out by each worker, it was obtained that must be hired 4.5 operators for any operator needed in the plant at any time. The number of operators necessary for each shift (N_{OS}) was obtained through Equation 2.22 [86].

$$N_{OS} = (6.29 + 31.7\, P_{SH} + 0.23\, N_{EQ})^{0.5} \qquad (2.22)$$

In Equation 2.22, P_{SH} is the number of operations in the process that require the handling of particulate solids, while N_{EQ} is the sum of compressors, towers, reactors and heat exchangers present in the plant. The number of necessary operators was therefore given by 4.5 times *Nos*. A chemical worker hourly wage was considered equal to 17 € [95]. Consequently, it was possible to calculate the number of operators required and multiply it for the number of annual hours and the hourly wage to obtain the annual salary. This provides the cost required for the operational staff but not included support or supervisory staff. To obtain the fixed operating costs must be added to the salaries the costs related to general overhead, maintenance, insurance and taxes, the estimate of which is presented in Table 2.19. Within the overhead category, expenses for research and development, support equipment, and the use of patented technologies are included. All of these items are collectively quantified as 60 % of the salaries costs. Maintenance expenses and those related to taxes and insurance are assessed at 2 % of the Total Equipment Cost and 1.5 % of the Total Installed Cost, respectively.

Table 2.19. Estimation of indirect contributions used for the assessment of operating costs.

Item	Estimation
General overhead	60% of salaries
Maintenance	20% of TEC
Insurance & Taxes	1.5% of TIC

2.7.3 Discounted cash flow analysis

After determining the total investment costs and operational expenses, a discounted cash flow rate of return analysis can be applied to derive a minimum selling price for acetic acid produced via fermentation, ensuring the recovery of all investments and expenses. The discounted cash flow analysis involved iterating the final prices of the chemicals produced until reaching a net present value (NPV) for the process equal to zero. To calculate the NPV, it is necessary to subtract Total Plant Investment (TPI) from the sum of cash flows over the plant's lifespan, as outlined in Equation 2.23.

$$NPV = \sum_{t=1}^{PL} \frac{TAS - TPC - IT}{(1 + DR)^t} - TPI \tag{2.23}$$

In Equation 2.23 within the sum constituting the total cash flow, the Total Annual Sales (TAS), representing the annual revenue from product sales and having a positive sign, is subtracted by the Total Production Costs (TPC) and Income Taxes (IT). The term in the denominator represents an interest factor, which varies annually and depends on the discount rate (DR). The index 't' denotes the operating year of the plant and varies from 1 to Plant Life (PL). For the process under consideration, a plant lifespan of 20 years has been assumed, consistent with the majority of chemical plants. The parameters for the discounted cash flow analysis were chosen in accordance with the recommendations provided by Short et al., 1995 [96]. The geographic location of the plant considered is Europe, where the applicable tax rate is set at 33% [97].

The startup duration considered is 6 months. During this period, compared to the nominal values of the plant, the revenues are at 50%, fixed operating expenses are at 100%, and variable operating expenses are at 75%. In the three years prior to the plant's startup, the total project investment is spent in the following proportions: 8% of TPI in year -3, 60% of TPI in year -2, and 32% of TPI in year -1. In the last year, the contribution of working capital, amounting to 5% of TPI, has been considered.

Depreciation expenses are assessed at a rate of 200%, over a recovery period of 7 years, utilizing the declining balance method. During this period, revenues from product sales are lower than depreciation expenses, hence no taxation is anticipated. Local taxes have not been considered in as the precise location of the plant in Europe has not been determined.

Table 2.20 summarizes the parameters used for the discounted cash flow rate of return analysis.

Table 2.20. Discounted cash flow analysis parameters.

Plant life	20 years
Discount rate	10%
General plant depreciation	200% declining balance
General plant recovery period	7 years
Federal tax rate	33%
Financing	100% equity
Construction period	2.5 years
First 6 months' expenditures	8%
Next 12 months' expenditures	60%
Last 12 months' expenditures	32%
Working capital	5% of TPI
Start-up time	0.5 years
Revenues during start-up	50% of normal
Variable cost during start-up	75% of normal
Fixed cost during start-up	100% of normal

2.7.4 Key performance indicators

Alongside assessing the profitability of the process under examination, Key Performance Indicators (KPIs), i.e. parameters measuring energy performance and process efficiency, have been evaluated. These parameters enable an analytical basis for comparison among various technologies and are crucial to consider during the decision-making phase. In addition, they highlight areas where further development and improvement are possible.

For alkaline electrolysis, the chosen KPI is the specific consumption per kilogram of hydrogen produced, calculated according to Equation 2.24.

$$Specific\ consumption\ \left(\frac{kWh}{kg}\right) = \frac{P_{stack}(kW)}{H_2\ productivity\ \left(\frac{kg}{h}\right)} \tag{2.24}$$

The current state-of-the-art for alkaline electrolysers indicates an average specific consumption ranging between 55 and 60 kWh per kilogram in industrial scale plants [98].

In the carbon dioxide absorption process, three key objectives must be met: the specific consumption, the percentage of captured carbon dioxide and the purity of the obtained stream. Specific energy consumption is calculated as the ratio between the energy expenditure at the reboiler of the stripping column and the amount of carbon dioxide produced per unit of time, as reported in Equation 2.25.

$$Specific\ consumption\ (\frac{MJ}{kg}) = \frac{Reboiler\ duty(MW)}{CO_2\ productivity\ (\frac{kg}{s})} \quad (2.25)$$

The percentage of captured carbon dioxide and the purity of the obtained stream are obtained as indicated by Equations 2.26 and 2.27.

$$CO_2\ capture\ efficiency\ (\%) = \frac{\dot{m}_{CO_2,product}\ (kg.h^{-1})}{\dot{m}_{CO_2feed}\ (kg.h^{-1})} * 100 \quad (2.26)$$

$$Purity\ (\%) = \frac{\dot{m}_{CO_2,product}\ (kg.h^{-1})}{\dot{m}_{product}\ (kg.h^{-1})} * 100 \quad (2.27)$$

Literature references for the chemical absorption process of CO_2 report specific consumptions ranging between 3.5 and 5 MJ.kg^{-1} [45] . The chosen recovery target is 90% of the incoming carbon dioxide to the absorption column. For the purity of the outgoing stream, a target value of 99% has been selected.

As for downstream section, the parameters reported in Equations 2.28, 2.29, 2.30 and 2.31 were chosen as indicators.

In Equation 2.28, the purity of the produced acetic acid stream is defined as the ratio between its flowrate ($\dot{m}_{AA,product}$) and the total product flowrate ($\dot{m}_{product}$).

$$Purity\ (\%) = \frac{\dot{m}_{AA,product}\ (kg.h^{-1})}{\dot{m}_{product}\ (kg.h^{-1})} * 100 \quad (2.28)$$

In Equation 2.29, the recovery is defined as the ratio between the flowrate of acetic acid obtained in the product stream ($\dot{m}_{AA,product}$) and that present in the feed, i.e. the stream that exits from the fermentation section (S-500) ($\dot{m}_{AA,feed}$).

$$Recovery\ (\%) = \frac{\dot{m}_{AA,product}\ (kg.h^{-1})}{\dot{m}_{AA,feed}\ (kg.h^{-1})} * 100 \quad (2.29)$$

In Equation 2.30, the solvent consumption is indicated, referring to the ratio between the flowrate of MTBE and the product flowrate.

$$Solvent\ recovery\ (g.kg^{-1}) = \frac{\dot{m}_{make-up}\ (g.h^{-1})}{\dot{m}_{product}\ (kg.h^{-1})} \quad (2.30)$$

In Equation 2.31, the specific energy consumption related to heating and cooling utilities is reported. The consumption is defined as the ratio between the sum of the thermal power related to heating and cooling ($\dot{Q}_{hot} + \dot{Q}_{cold}$) and the obtained product flowrate ($\dot{m}_{product}$).

$$Utilities\ energy\ consumption\ (MJ.kg^{-1}) = \frac{\dot{Q}_{hot} + \dot{Q}_{cold}\ (MW)}{\dot{m}_{product}\ (kg.s^{-1})} \quad (2.31)$$

For the overall process, carbon efficiency was selected as KPI. It is defined in Equation 2.32 as the ratio of the flowrate of carbon in the product (stream 808) as acetic acid ($\dot{m}_{C,AA,product}$) and the flowrate of carbon in the carbon dioxide stream that enters the CO_2 capture section (stream 203), indicated as $\dot{m}_{C,CO_2,capture\ inlet}$.

$$Carbon\ efficiency = \frac{\dot{m}_{C,AA,product}\ (kg.h^{-1})}{\dot{m}_{C,CO_2,capture\ inlet}\ (kg.h^{-1})} * 100 \quad (2.32)$$

3. Results of the simulations

3.1 Hydrogen production

The alkaline electrolysis plant for hydrogen production has been described in Section 2.2. The simulation enabled the sizing and quantification of the flows and equipment necessary for the balance of plant. The process occurs continuously and water is recirculated. In Table 3.1 the specifications of the hydrogen stream produced (stream 110) are summarized. In particular, stream 110 is only made up of hydrogen and water. Since hydrogen is not intended for sale but requested with water in the fermentation section (S-500), it is not necessary to produce high purity hydrogen.

Table 3.1. Description of hydrogen flow (stream 110) produced from each stack in hydrogen production section (S-100).

Flowrate ($kg.h^{-1}$)	17.39
Mass fraction of hydrogen (wt%)	80.17
Mass fraction of water (wt%)	19.83
Temperature (°C)	70
Pressure (bar)	5.16
Vapor fraction	1

The productivity of a single stack is 166.39 $ton.y^{-1}$ of hydrogen. The specific consumption calculated with Equation 2.24 is 56.68 $kWh.kg^{-1}$ and falls within the range of current alkaline electrolysers (48.96-58.98 $kWh.kg^{-1}$) [99]. When performing fermentation with a headspace pressure of 2 bar, according to the model developed by Regis, 2024, the productivity of the single fermenter is 36.94 $kton.y^{-1}$ of acetic acid and 5.67 $kton.y^{-1}$ of H_2 are requested [58]. Therefore, 35 modules similar to the one just described are necessary.

3.2 CO_2 capture

The carbon dioxide capture process via chemical absorption with MEA has been illustrated in Section 2.3. It operates continuously and the regenerated solvent is recirculated. However, due to the unavoidable losses, a fresh amine and water make-up respectively equal to 0.10 $kg.h^{-1}$ and 1073 $kg.h^{-1}$ are necessary. Table 3.2 summarizes the results of the sizing and details of absorption and stripping columns.

Table 3.2. Sizing and details of absorption (C-301) and stripping columns (C-302) of CO_2 capture section (S-300).

	Absorber (C-301)	**Stripper (C-302)**
Height (m)	9	9
Diameter (m)	1.56	1.66
Packing	Mellapack 250Y	Mellapack 250Y
Condenser	\	Partial-Vapor-Liquid
Reboiler	\	Kettle
D:F	0.37	0.03
Reboiler duty (MW)	\	10.25

91.90 wt% of carbon dioxide present in the stream entering the plant is recovered through absorption process. The purity target is also respected with a carbon dioxide concentration in the final stream (stream 402) equal to 99.50 wt%. The specific consumption evaluated according to Equation 2.25 is 4.98 $MJ.kg^{-1}$, which is in line with the results from the literature [45]. Moreover, the stream 402 exiting from the last purification section (S-400) and employed as reactant in the fermentation section (S-500) does not contain oxygen. Its main specifications are reported in Table 3.3.

Table 3.3. Description of CO_2 stream (stream 402) produced through chemical absorption in CO_2 capture section (S-300).

Flowrate ($kg.h^{-1}$)	7407.87
Mass fraction of CO_2 (wt%)	99.50
Mass fraction of water (wt%)	0.50
Temperature (°C)	31.08
Pressure (bar)	5.16

3.3 Fermentation

The fermentation section for the production of acetic acid has been outlined in Section 2.4. According to the model developed by Regis, 2024, when operating with a headspace pressure of 2 bar in the bubble column fermenter, 37.41 kton.y^{-1} of acetic acid are produced. Instead, when the headspace pressure is equal to 10 bar, 53.94 kton.y^{-1} are synthesized with the same column dimensions [58]. The details of the products which are obtained from fermentation are listed in Table 3.4.

Table 3.4. Details of the products when fermentation occurs with a headspace pressure of 2 bar and 10 bar.

Item	**Fermentation with a headspace pressure of 2 bar**	**Fermentation with a headspace pressure of 10 bar**
Acetic acid produced (kton.y^{-1})	37.41	53.94
Acetic acid concentration (%wt)	1.50	1.50
Formic acid concentration (%wt)	-	0.17
H_2O concentration (%wt)	98.50	98.33

The process operates continuously and 100% of the unconverted CO_2 and H_2 are recycled back to the inlet of the fermenter. This is advantageous because it allows the optimal use of the reactants, avoiding waste and/or emissions in the atmosphere.

Part of the water necessary for the fermentation phase is provided by purified water from the recovery section (S-800). A make-up of water in the fermentation section is necessary to completely satisfy the water demand of fermentation. Table 3.5 summarizes the requested raw materials and CO_2 and H_2 conversion in the case of fermentation occurring with a headspace pressure of 2 bar and 10 bar. Both for fermentation occurring with a headspace pressure of 2 and 10 bar, the recovery of water is assumed to be 97.50 wt%, as the recovery of water in the recovery section (S-800).

Table 3.5. Raw material requested and conversion when fermentation occurs with a headspace pressure of 2 bar and 10 bar.

Item	Fermentation with a headspace pressure of 2 bar	Fermentation with a headspace pressure of 10 bar
CO_2 requested ($kg.h^{-1}$)	7308.33	11374.90
H_2 requested ($kg.h^{-1}$)	586.36	895.55
H_2O make-up ($kg.h^{-1}$)	4335.45	6230.02
CO_2 conversion (%)	63.46	78.41
H_2 conversion (%)	61.17	26.67

3.4 Downstream

The modelling of the purification process of acetic acid from the fermentation broth has been depicted in Section 2.5. The process operates continuously and solvent MTBE is recirculated, while purified water is used as a reactant in the fermentation section (S-500). However, due to the unavoidable losses, a make-up of solvent of 305 $kg.h^{-1}$ is needed. In addition, a purge is necessary to avoid the accumulation of inert and problems with the recirculation, although it is responsible for the losses of MTBE.

The recovery of acetic acid in stream 808 is 99.80 wt% while its purity is 99.90 wt%, hence the concentration requirements for the sale of GAA are respected. Moreover, the consumption of the solvent, according to Equation 2.30, is equal to 71.56 $g.kg^{-1}$, whereas utilities energy consumption, evaluated with Equation 2.31, is 124.57 $MJ.kg^{-1}$. The water stream exiting from the purification section (stream 823) is characterized by a purity of 99.99 wt% and the recovery is 97.50 wt% compared to the inlet stream (stream 508).

The sizing was performed with the *internals* function for the distillation columns and with the *interactive sizing* for the extraction column and the decanter. The results referring to the single column are summarized in Table 3.5.

Table 3.5. Sizing of the equipment of the HEDP process of extraction (S-700) and recovery section (S-800).

Extraction column C-701	
Number of stages	25
Height (m)	8.38
Diameter (m)	2.38
Azeotropic distillation column C-801	
Type of internals	Trayed
Number of trays	22
Number of stages	20
Height (m)	12.19
Diameter (m)	4.06
Water-MTBE distillation column C-802	
Type of internals	Trayed
Number of trays	22
Number of stages	20
Height (m)	10.97
Diameter (m)	4.21
Decanter D-401	
Diameter (m)	3.35

3.5 Thermal integration

As reported in Section 2.6, an energy analysis was performed using the Pinch Analysis Method in the software Aspen Energy Analyzer (HX-NET). Its objective is the reduction of energy consumption through the optimization of heat recovery systems.

The energy integration was carried out on the exchangers, excluding those of distillation columns, of sections that had more than one heat flow to exploit, i.e. the fermentation section (S-500) and the purification section (S-700 and S-800).

After indicating the specifications of the process streams and utilities, the software generated alternative heat exchangers designs to the one implemented in Aspen Plus. Among those that were feasible to implement, the choice fell on the design that offered the greatest savings in terms of total costs.

As concerns the fermentation process carried out with a headspace pressure of 2 bar, the selected design is represented in Figure 3.1.

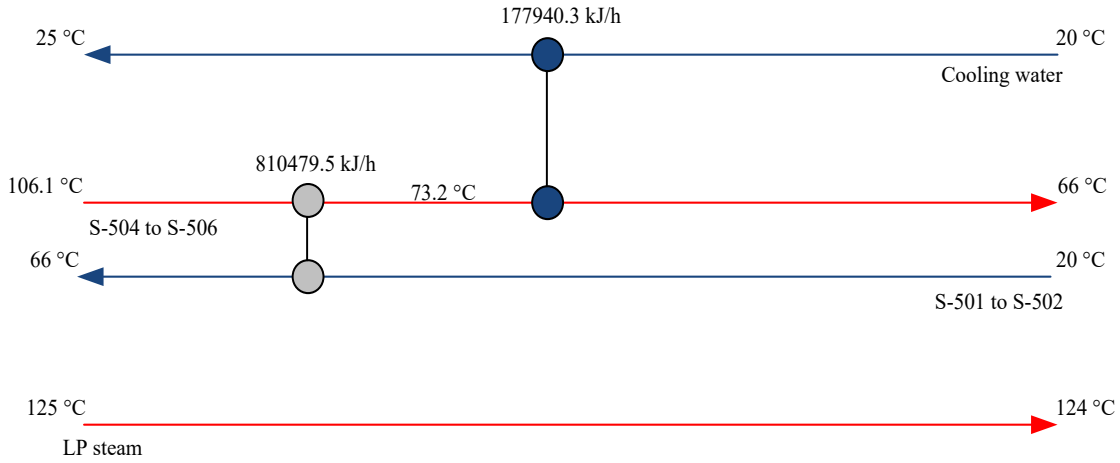

Figure 3.1. Heat exchanger diagram representative of the alternative design chosen for the fermentation process (S-500) occurring with a headspace pressure of 2 bar.

This design involves higher capital costs than the others proposed by the software. This is caused by the greater area required for the heat exchangers. However, significantly reduced operating costs offset the initial investments, resulting in an overall reduction in total costs in the long term.

In fact, the demand of hot utilities, specifically *low-pressure steam* (LPS) is completely eliminated, whereas the saving in cold utility is 82% at the expense of a 20% raise in capital costs compared to the initial situation. In the original design, the demand for hot utility required from E-501 exchanger was completely satisfied by LPS, while the E-502 exchanger relied completely on cooling water (CW) to cool the inlet stream to 66°C at which fermentation occurs. Instead, the proposed design allowed a coupling between the two heat exchangers involved in the process. In particular, the hot process stream 504 is employed to heat the water make up (stream 501) to the temperature of 66 °C. To carry out this exchange, stream 504 is cooled to a temperature of 73.2 °C and using CW reaches the required temperature of 66 °C.

When fermentation occurs with a headspace pressure of 10 bar, the alternative heat exchangers design is illustrated in Figure 3.2.

In this instance as well, operating costs are reduced at the expense of higher capital costs leading, nevertheless, to a net reduction in total costs.

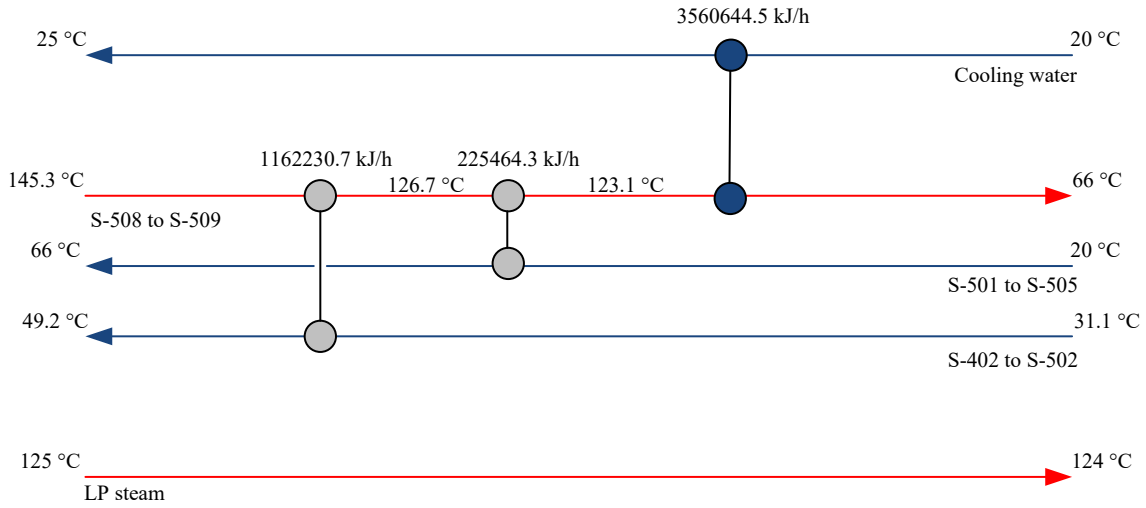

Figure 3.2. Heat exchanger diagram representative of the alternative design chosen for the fermentation process (S-500) occurring with a headspace pressure of 10 bar.

The coupling of the heat exchangers eliminates the demand for hot utilities and reduces the request for cold utilities by 28% at the loss of a 5% raise in capital costs compared to the initial situation. The original design involved the utilization of LPS to heat the incoming streams of E-501 and E-503 exchangers to 66 °C and 49.2 °C respectively. Instead, the cold utility request necessary for E-502 exchanger to bring the reactants to the fermentation temperature was completely satisfied by the utilization of CW. With the proposed coupling, both the temperature increase required to stream 501 and to stream 402 are realized employing the hot process stream (stream 508). In particular, water make-up (stream 501) is raised to 66 °C exploiting stream 508, which goes from 145.3 °C to 126.7 °C. At this point, to raise the water vapour of stream 402 above the dew point, stream 508 undergoes a further drop in temperature. The final temperature of 66 °C is reached by stream 508 with the aid of CW.

Regarding the downstream section, the alternative design chosen is shown in Figure 3.3.

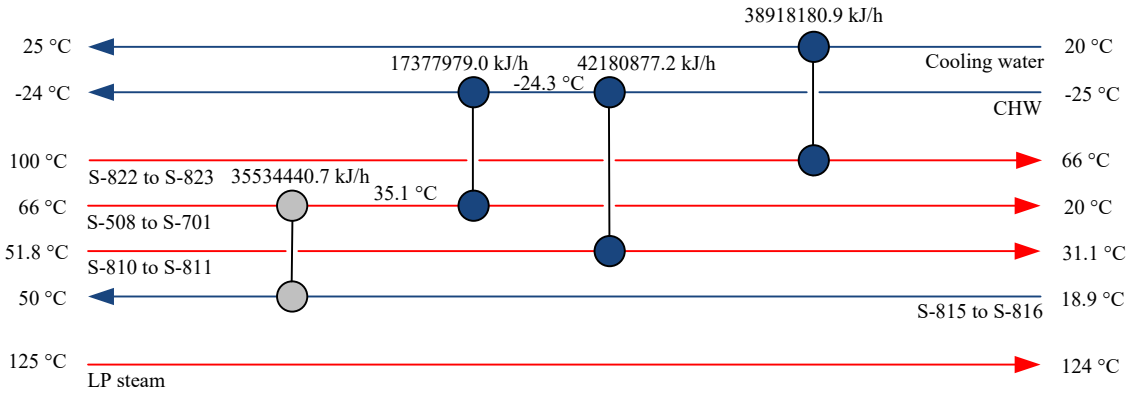

Figure 3.3. Heat exchanger diagram representative of the alternative design chosen for the downstream section (S-700 and S-800).

The selected design permits a reduction in operating costs, at the expense of higher capital costs (21% compared to the initial simulation).

This design allows the elimination of the demand for hot utilities, i.e. LPS. The latter, in fact, was necessary to heat stream 815 to a temperature of 50 °C before being fed to the water purification column (C-802). Instead, with the selected design this temperature difference is achieved by exploiting the hot stream 508 coming from the fermentation section, which must be cooled to a temperature of 20 °C, required for the extraction process.

In particular, stream 508 is first cooled to a temperature of 35.1 °C, transferring heat to stream 815. The latter is heated from 18.9 °C to 50 °C. Subsequently, stream 508 is further cooled to 20 °C using the cold utility *chilled water* (CHW). As a result, the overall demand for cold utility is significant lower, with a saving of 93% compared to the initial simulation.

Beyond the integrations of the individual units, an attempt was made to integrate the entire process, i.e. sections S-100 (hydrogen production), S-300 (CO_2 capture), S-500 (fermentation), S-700 (extraction) and S-800 (recovery section). However, they were found to be non-integrable. In fact, the combination of these sections led to nearly vertical lines in the composite curve, indicating a change in temperature with a low variation in enthalpy. This suggests that there is insufficient heat available for effective heat exchange to carry out an energy integration between the various sections of the plant. Therefore, in the economic analysis outlined in Chapter 4, the capital and operating costs related to the heat exchangers are those resulting from the thermal integration described in this chapter.

4. Results of the economic analysis

4.1 Hydrogen production

The hydrogen production process is discussed in Section 2.2, while the results of the simulation are reported in Section 3.1.

Table 4.1 summarizes the expenses that make up the Total Project Investment (TPI) for a plant characterized by a productivity of 5.68 kton.y^{-1} of hydrogen.

Table 4.1 Expenses that make up the TPI for section S-100 for a productivity of 5.68 kton.y^{-1} of hydrogen.

Item	Cost (M€)
Total Equipment Cost (TEC)	22.80
Warehouse	0.34
Site development	2.05
Total Installed Cost (TIC)	25.20
Field expenses	5.04
Home office & construction fee	6.30
Project contingency	0.76
Total indirect expenses	12.09
Total Capital Investment (TCI)	37.29
Other costs	2.52
Total Project Investment (TPI)	39.81

The Total Equipment Cost is obtained from the sum of the bare erected costs given by the Purchase Equipment Cost (PEC) of the individual equipment present in the process. Table 4.2 groups the PECs by categories, while Figure 4.1 depicts the percentage distribution of these costs across the equipment present in the system.

Table 4.2. PECs for the electrolysis plant (S-100) with a productivity of 5.68 kton.y^{-1} of hydrogen.

Equipment	PECs (M€)
Electrolyzer	12.15
Separators	1.42
Exchangers	1.38
Pumps	0.56

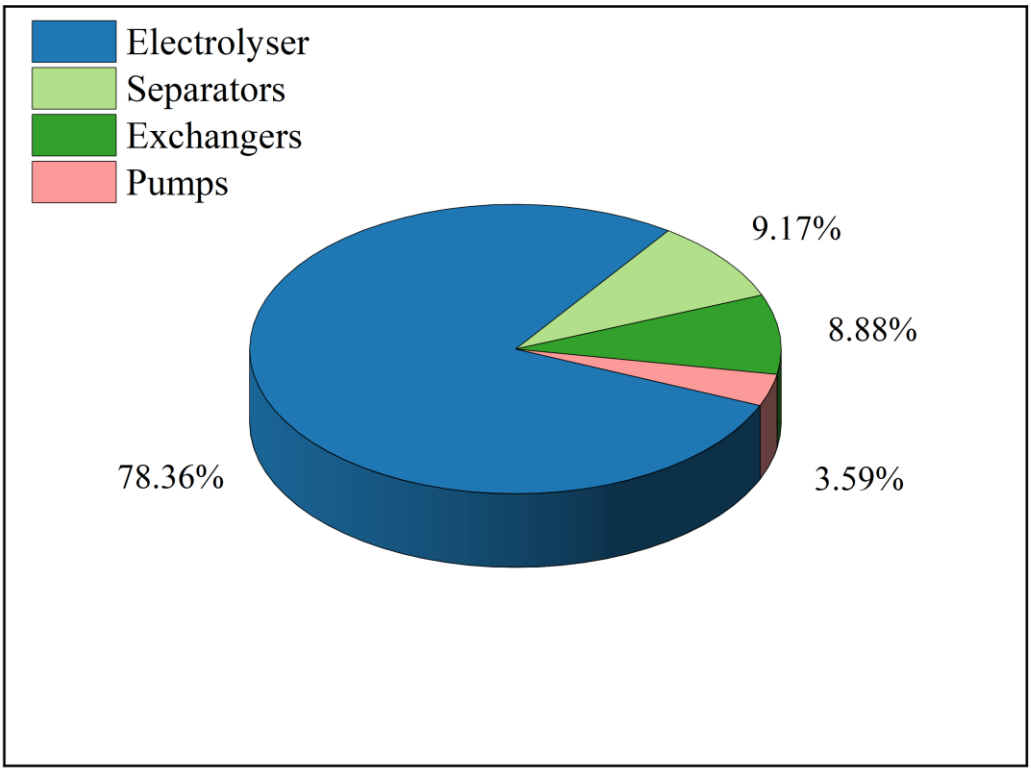

Figure 4.1. Percentage distribution of the PECs regarding the electrolysis plant (S-100) for a productivity of 5.68 kton.y^{-1} of hydrogen.

Expenditure on the electrolyser is predominant compared to other equipment and constitutes more than 78% of capital expenditure. This result reflects the complexity of electrolysers, in addition to the use of specific and expensive corrosion-resistant materials and sophisticated separation systems.

In estimating operating expenses, 8650 h.y^{-1} of plant operation were regarded. The expenses that constitute the OPEX and their costs are specified in Section 2.7.2. In particular, raw materials include water and KOH, while utilities encompass the requested electricity and cold utilities. Table 4.3 shows the operating costs per kilogram of hydrogen produced.

Table 4.3. Operational costs for the electrolysis plant (S-100) with a productivity of 5.68 kton.y^{-1} of hydrogen.

Item	Opex (€.kg^{-1})
Raw Materials	0.01
Utilities	2.06
Overhead	0.11
Maintenance	0.08
Salaries	0.18
Insurance and Taxes	0.07

It is noted that utilities represent the greater share of OPEX. Among them, electricity is the largest contributor and it's necessary for converting water molecules into hydrogen and oxygen. However, a portion of it is dissipated as heat by the electrolyser. Moreover, a small amount of electricity is required to operate the pumps, but it is limited.

In this regard, in Figure 4.2 the distribution of variable operating costs per kilogram of hydrogen produced for the electrolysis process is depicted.

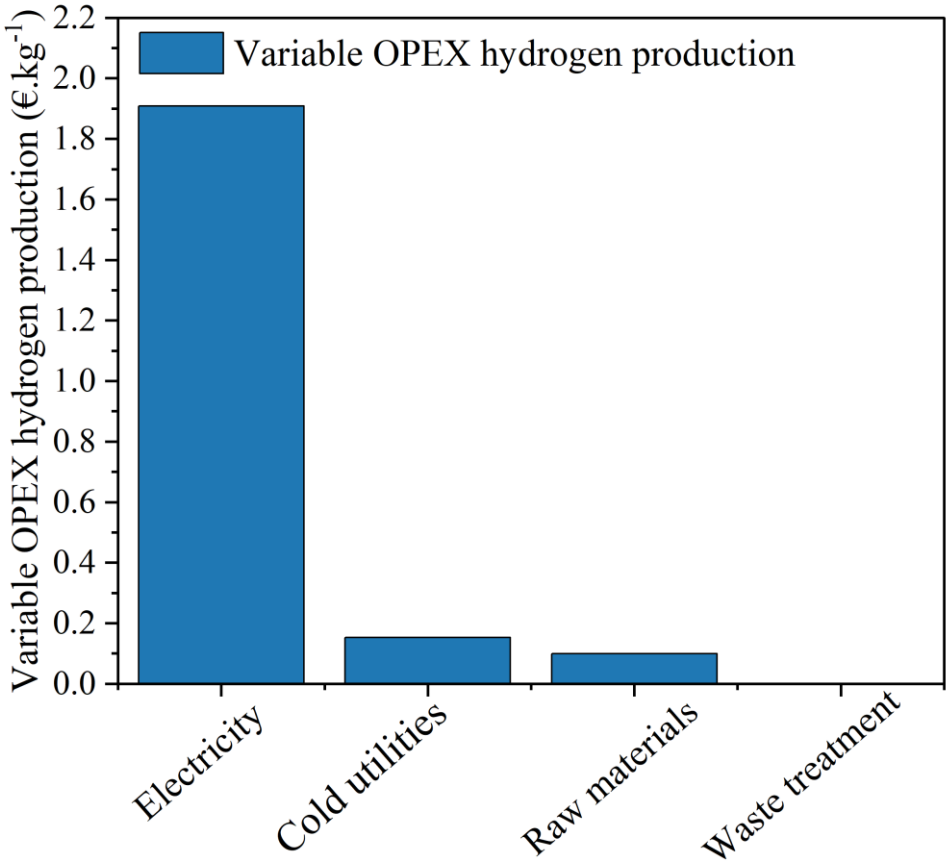

Figure 4.2. Comparison between variable operating costs per unit of hydrogen produced regarding the electrolysis plant (S-100) for a productivity of 5.68 kton.y^{-1} of hydrogen.

The total investment required for a plant producing 5.68 kton.y^{-1} of hydrogen is 39.81 M€. Fixed operating costs are 2.50 M€.y^{-1} while variable operating costs amount to 12.28 M€.y^{-1}. These expenses include amortization, interest and taxes. During the start-up phase of the plant, it is assumed that the revenue from hydrogen sales will be 50% of the normal value. By applying the iterative procedure comprehensively described in Section 2.7.3 that results in a zero NPV, a minimum selling price of hydrogen of 3.77 €.kg^{-1} is obtained.

The simulation was repeated considering an additional scenario: hydrogen production in 2030. In fact, the European Union has established future targets to be achieved by 2030 regarding the technological advancement of electrolysers. These targets are set within the *Strategic and Innovation Agenda 2021-2027* and aim to greater process efficiency and lower management costs, in addition to a lower employment of raw materials, in particular critical ones. Table 4.4 compares these targets with the 2021 state-of-the-art in alkaline electrolysis technology [87].

Table 4.4. 2030 European targets and 2021 values regarding the development of alkaline electrolysers.

Key Performance Indicator	State of the art (2021)	Target (2030)
Electric consumption ($kWh.kg^{-1}$)	50	48
Capital cost (€.kW^{-1})	600	400
Operating costs O&M (€.$(kg.d^{-1})^{-1}.y^{-1}$)	50	35
Start-up time (sec)	3600	300
Degradation (%.$1000h^{-1}$)	0.12	0.1
Current density ($A.cm^{-2}$)	0.6	1
Use of critical raw materials ($mg.W^{-1}$)	0.6	0

The higher current density requires fewer cells within the stack to achieve the same hourly productivity. This contributes, together with the expected drop in capital cost up to 400 €.kW^{-1}, to an overall decrease in CAPEX. Furthermore, the demand for electricity is reduced which is reflected in a decrease in OPEX. In addition, the heat to be eliminated by the electrolyser is cut, turning into a lower cold utility demand by exchanger E-101, as well as a reduction of its capital expense. In particular, for a productivity of 5.68 $kton.y^{-1}$ of hydrogen, the specific PEC associated to the electrolyser drops to 1.81 € per kilogram of hydrogen produced in a year, compared to the previous value of 2.13 €.kg^{-1}.y. Regarding variable operating costs, electricity cost decrease from 1.91 €.kg^{-1} to 1.58 €.kg^{-1}, while expenses associated with cold utilities from 0.15 €.kg^{-1} to 0.12 €.kg^{-1}.

As a result, the minimum selling price is 3.17 €.kg^{-1}, instead of 3.77 €.kg^{-1}.

The prices obtained have been compared to those present in the scientific literature, as evidenced in Table 4.5.

Table 4.5. Comparison of costs for green hydrogen as production technology and energy source vary.

Technology	Plant size ($ton.y^{-1}$)	Hydrogen cost (€.kg^{-1})	Source
AEL	5680	3.77	This study
AEL (2030)	5680	3.17	This study
AEL	2500	8.12	[100]
PEM	2500	7.72	[101]
AEL	900	7.60	[102]

PEM	900	8.55	[103]
SOEC	900	10.16	[104]
PEM	230	8.02	[105]
PEM	560	5.14	[106]
PEM powered by photovoltaic panels	5000	7.27	[107]
PEM powered by wind turbines	10000	4.99	[108]
AEL powered by wind turbines	10000	3.74	[109]
AEL powered by photovoltaic panels	5000	5.74	[107]

Literature prices generally refer to smaller plant sizes compared to the 5.68 ton.y^{-1} target to ensure the requested productivity to the fermenter. Therefore, to enable an effective comparison with literature data, it was decided to scale-up the AEL section starting from the productivity of a single stack equal to 166.39 ton.y^{-1}, as described in Chapter 2, then increased to cover the literature range. To scale up, the CAPEX were evaluated using Equation 2.19, while the OPEX were scaled proportionally based on the requested productivity.

The results of the scaling-up are depicted in Figure 4.3, which shows also the literature data reported in Table 4.5.

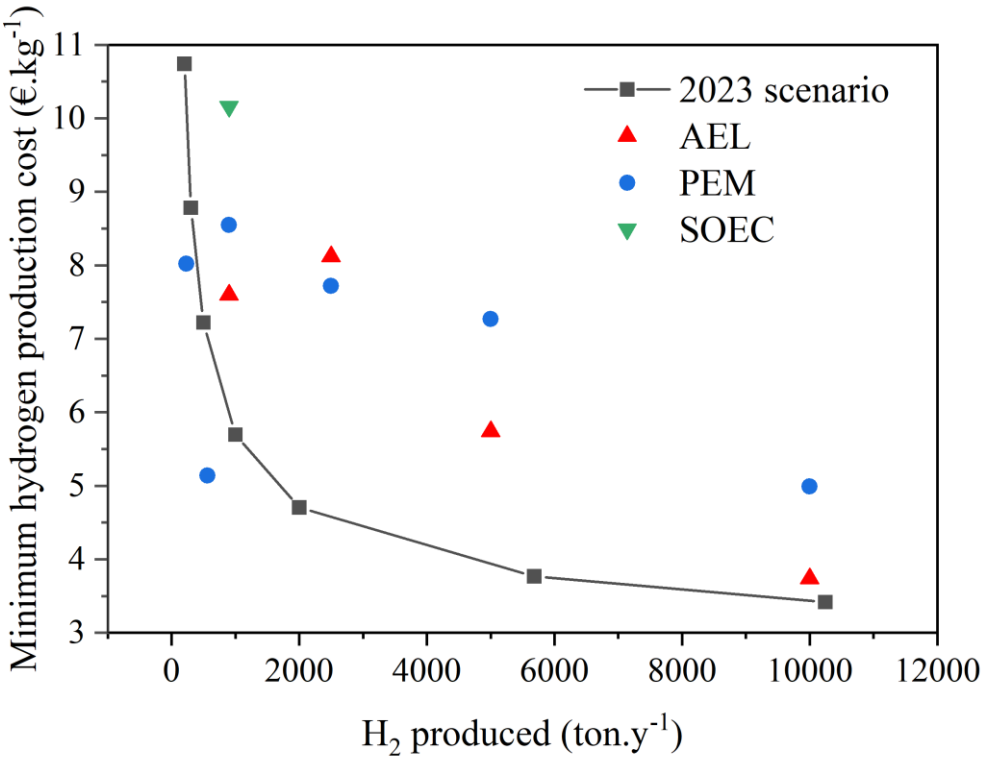

Figure 4.3. Effect of plant scale on the minimum selling price of hydrogen (black squares). Also depicted are the selling costs from the literature of hydrogen produced through various electrolysis technologies (Red triangles: AEL; Blue dots: PEM; Green triangles: SOEC) at different scales.

From the results it emerges that the calculated sales price of hydrogen remains roughly below most literature values. However, the produced hydrogen has a purity of 80.17 wt%, since it is not necessary to dehydrate hydrogen for the following fermentation.

4.2 CO_2 capture

The carbon dioxide capture process is described in Section 2.3, while the results of the simulation are reported in Section 3.2.

In Table 4.6 the expenses that make up the Total Project Investment (TPI) for the carbon dioxide capture process are listed.

Table 4.6. Expenses that make up the TPI for H_2S removal (S-200), CO_2 capture process (S-300) and oxygen removal (S-400).

Item	Cost (M€)
Total Equipment Cost (TEC)	1.21
Warehouse	0.02
Site development	0.11
Total Installed Cost (TIC)	1.34
Field expenses	0.27
Home office & construction fee	0.34
Project contingency	0.04
Total indirect expenses	0.64
Total Capital Investment (TCI)	1.98
Other costs	0.13
Total Project Investment (TPI)	2.12

The Total Equipment Cost (TEC) is the sum of the bare erected costs obtained from the Purchase Equipment Cost (PEC) of each component within the system. Table 4.7 outlines the cumulative bare erected costs of the different sections of the plant. The percentage distribution of these prices across the plant sections is illustrated in Figure 4.4.

Table 4.7. Sum of the bare erected costs for H_2S removal section (S-200), CO_2 capture section (S-300) and oxygen removal section (S-400) in CO_2 capture plant.

Section	Sum of the bare erected costs (M€)
H_2S removal (S-200)	0.35
CO_2 capture (S-300)	0.80
O_2 removal (S-400)	0.06

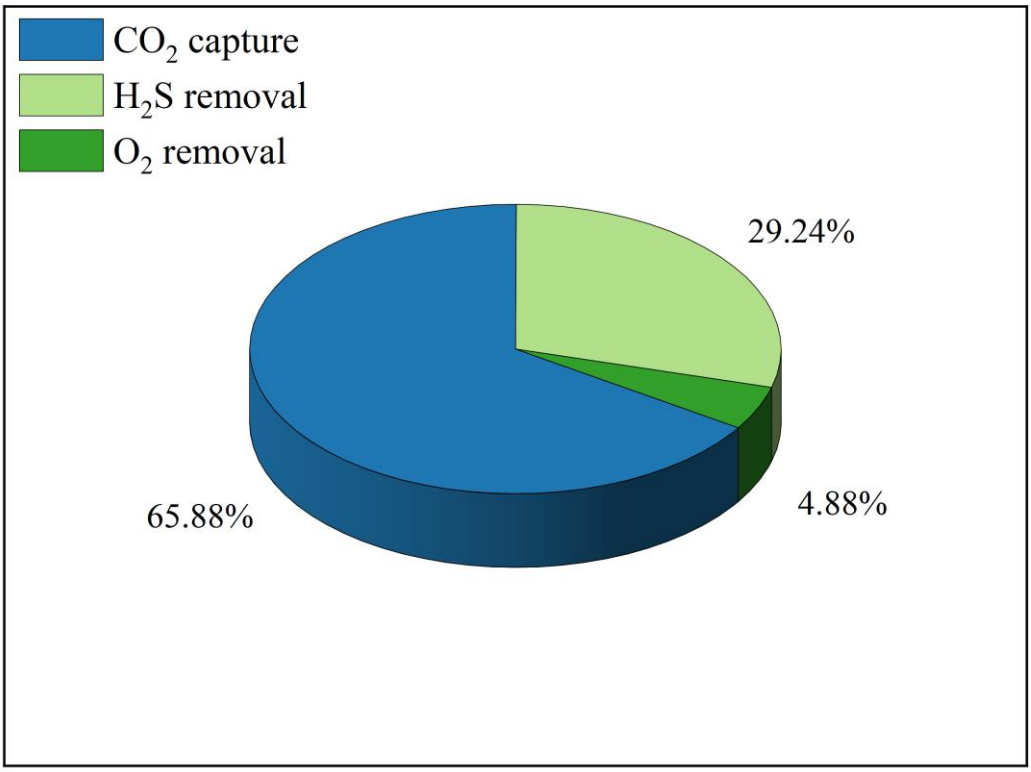

Figure 4.4. Percentage contribution to the Total Equipment Cost (TEC) of H_2S removal section (S-200), CO_2 capture section (S-300) and oxygen removal section (S-400) in CO_2 capture plant.

As shown in Figure 4.3, the higher costs are related to CO_2 capture section (S-300). Specifically, the absorber (C-301) and the stripper (C-302) account respectively for 17% and 27% to the TEC. The impact of H_2S removal section is smaller but still significant. Instead, the capital costs related to oxygen abatement section (S-400) are lower, despite the employment of a platinum-based catalyst, due to the low amount of O_2 to be eliminated.

In the evaluation of the manufacturing costs, 8650 $h.y^{-1}$ of plant operation were considered. Raw materials include MEA and water make-up cost, as well as the *una tantum* cost, associated with replacing the solvent annually to deal with any degradation. Additionally, this category encompasses the chemicals employed in the LO-CAT process and methane requested for O_2 removal. Instead, the utilities cost is provided by APEA, while costs associated with the chemical treatment on the spent solvent belong to the category of other variable costs. The respective costs are described comprehensively in Section 2.7.2.

Table 4.8 shows the specific operating costs for the carbon dioxide capture process. As expected, utilities make up the higher contribution, i.e. 76.52 % of operational expenses.

Table 4.8. Operating costs related to sections S-200, S-300 and S-400 for CO_2 capture plant.

Item	Opex (€.kg^{-1})
Raw Materials	0.0010
Utilities	0.0436
Overhead	0.0041
Maintenance	0.0004
Salaries	0.0068
Insurance and Taxes	0.0003
Waste treatment	0.0007

Figure 4.5 shows the annual variable operating expenses normalized on the productivity of the plant. The stripping process for the regeneration of the solvent is energy intensive, requiring then a high amount of medium pressure steam (MPS) as hot utility. In fact, the request of this utility is predominant over the other variable expenses contributing approximately 88.18% of the total. No negligible is the impact of cold utilities, required by the condenser E-302 and the exchanger E-304, accounting for 7.76% of the total variable operating expenses.

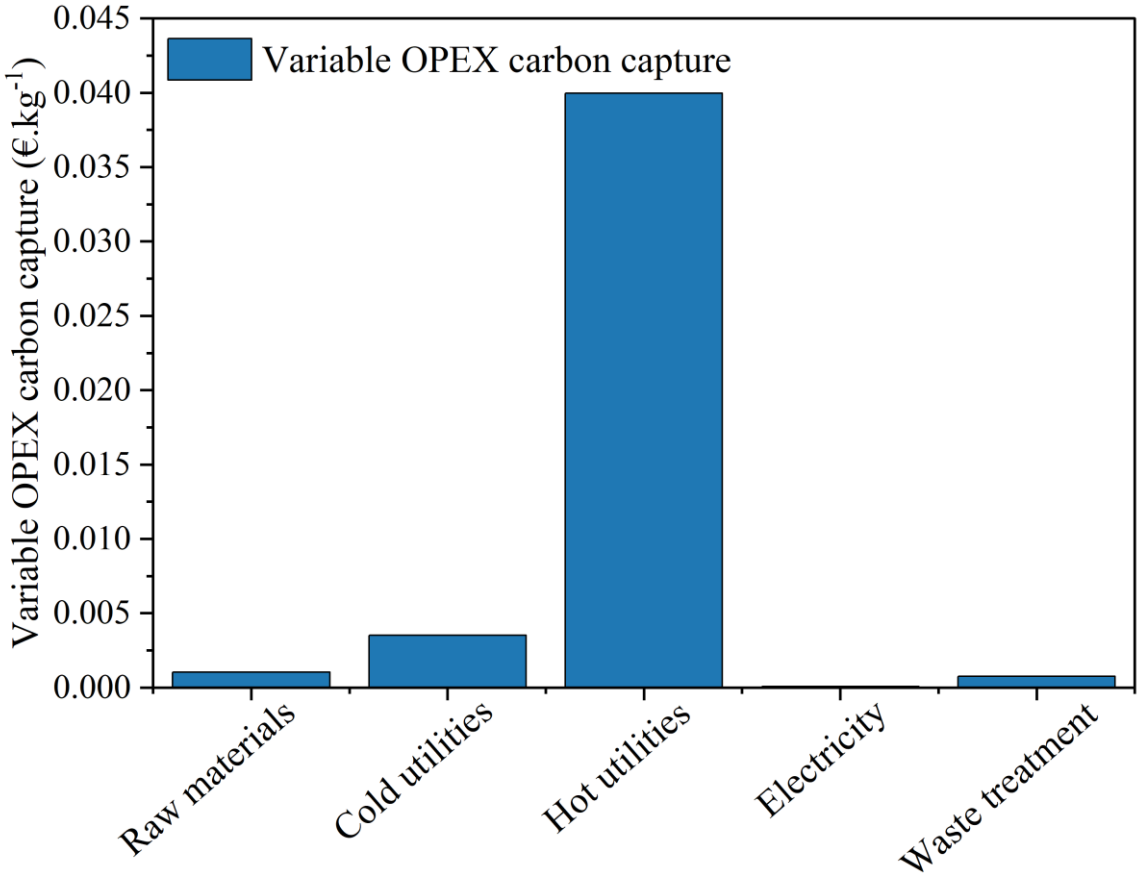

Figure 4.5. Comparison among variable operating cost of H_2S removal section (S-200), CO_2 capture section (S-300) and oxygen removal section (S-400) in CO_2 capture plant.

The minimum carbon dioxide capture cost is calculated through the iterative procedure explained in Section 2.7.3 that results in a NPV equal to 0.

In this case the total investment necessary for a plant that captures 64.02 kton.y^{-1} of CO_2 is 2.12 M€, the annual fixed operating costs are equal to 0.74 M€.y^{-1} and the variable operating costs are equal to 2.90 M€.y^{-1}. A minimum CO_2 selling price of 0.063 €.kg^{-1} is achieved.

Table 4.9 summarizes the selling cost of CO_2 obtained through chemical absorption as well as other post-combustion and pre-combustion technologies, along with their corresponding plant size.

Table 4.9. Comparison of costs for carbon dioxide capture as production technology and plant size varies.

Technology	**Plant size (Mton.y^{-1})**	**Cost (€.kg^{-1})**	**Source**
Chemical absortion (MEA)	0.064	0.063	This study
Chemical absortion (MEA)	4.1	0.077	[110]
Oxy-combustion	1.3	0.060	[111]
Oxy-combustion	1.3	0.046	[112]
Physical absortion	3.8	0.036	[113]
Chemical absortion (MDEA)	5.6	0.053	[114]
Chemical absortion (MEA+MDEA)	2.3	0.111	[115]
Rectisol	6	0.112	[116]
Purisol	3.3	0.042	[111]
Selexol	3	0.053	[117]
Chemical absortion(MEA)	1.1	0.048	[118]
Physical absortion	3.1	0.028	[119]

Carbon dioxide capture plants are usually located downstream of cement factories, metallurgical plants or energy production plants and no economic analysis referring to a waste stream from a biodigester was found in the literature. Furthermore, the capacities of these plants are much greater than those of biodigesters.

Therefore, it was decided to scale up the carbon capture section to larger sizes to cover the literature size range. To pursuit this, the CAPEX was evaluated basing on Equation 2.19, while the OPEX were scaled proportionally according to the requested productivity. The results are represented in Figure 4.6, which also shows the literature data reported in Table 4.9.

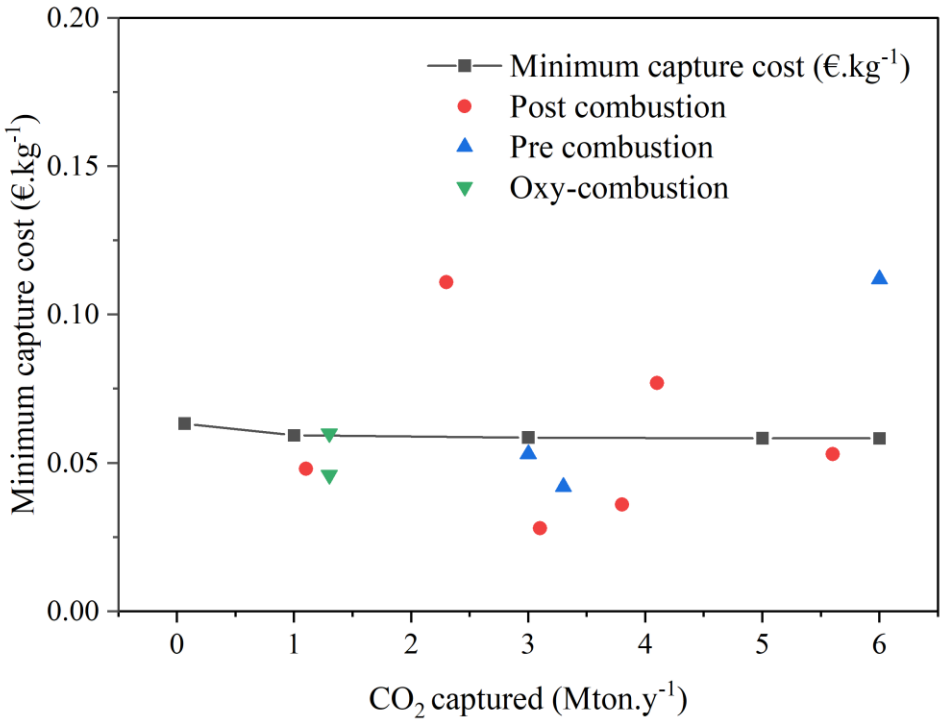

Figure 4.6. Effect of plant size on the minimum selling price of carbon dioxide varying with plant size (black squares). Also depicted are the selling costs from the literature of CO_2 captured through other technologies (Red dots: post-combustion capture; Blue triangles: pre-combustion capture; Green triangles: oxy-combustion) at different scales.

From the results, it is observed that the price obtained from the scale-up appears to be within the range of other carbon dioxide capture technologies.

4.3 Fermentation

As discussed in Section 2.4, the fermentation step is simulated at two distinct headspace pressures in the fermenter, 2 bar and 10 bar, to identify the optimal configuration. The results of the simulations are detailed in Section 3.3.

In Table 4.10 the expenses that make up the Total Project Investment (TPI) for the fermentation process with headspace pressure of 2 bar and 10 bar are listed.

Table 4.10. Expenses contributing to the TPI for the fermentation process (S-500) with headspace pressures of 2 bar and 10 bar.

Item	Headspace pressure of 2 bar cost (M€)	Headspace pressure of 10 bar cost (M€)
Total Equipment Cost (TEC)	7.99	21.72
Warehouse	0.12	0.33
Site development	0.72	1.96
Total Installed Cost (TIC)	8.83	24.01
Field expenses	1.77	4.80
Home office & construction fee	2.21	6.00
Project contingency	0.26	0.72
Total indirect expenses	4.24	11.52
Total Capital Investment (TCI)	13.07	35.53
Other costs	0.88	2.40
Total Project Investment (TPI)	13.95	37.93

The Total Equipment Cost is obtained by summing the bare erected costs starting from the Purchase Equipment Cost (PEC) of the single equipment employed in the process. In both cases, the fermenter is the main contributor to the definition of the TEC, accounting for more than 76.79% and 69.41% when fermentation occurs with a headspace pressure respectively of 2 bar and 10 bar. In particular, when fermentation is carried out with a headspace pressure of 10 bar, the TPI is more than the double than that of fermentation when conducted with a headspace pressure of 2 bar. This is caused by the higher capital expenses associated with working at a higher pressure not only regarding the fermenter but also compressors and heaters. In fact, an additional heater (E-503) and two compressor (C-502 and C-503) are needed. Moreover, the amount of acetic acid produced and the request of reactants is increased for the same column size. Consequently, the higher flowrates lead to higher PECs for other shared equipment across both processes.

As regards operational expenses, the cost associated to raw materials and utilities was investigated considering 8650 $h.y^{-1}$ of plant operation. A thermal integration was conducted on Aspen Energy Analyser (HX-Net) and deeply described in Section 3.5. This analysis reduced the hot utility demand to zero, contributing to a reduction of operating costs.

In Figure 4.7 the distribution of variable operating costs per kilogram of acetic acid produced for the fermentation process with a headspace pressure of 2 bar and 10 bar is

shown. It is observed that the contribution of utilities is significantly lower compared to that of raw materials, i.e. nutrients, water make-up and bacterial inoculum. Among them, the nutrients required for the bacterial growth account for almost the entire cost associated to raw materials. The high cost of nutrients is also explained by the way their prices were obtained. In fact, they refer to a very small quantity compared to the amount required in the process under examination.

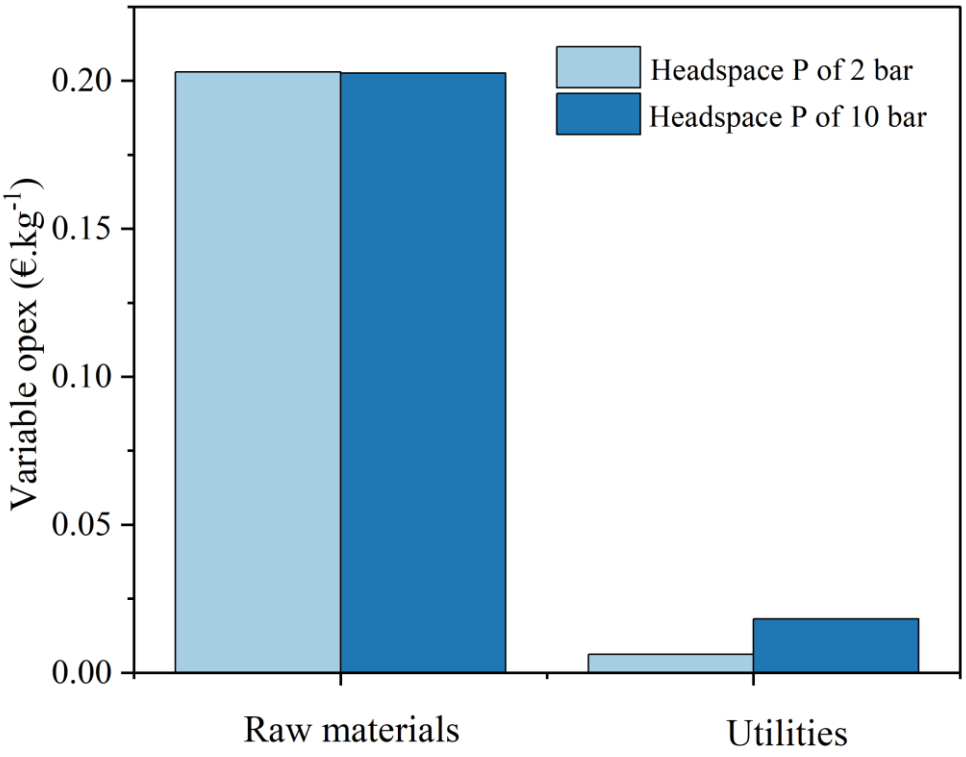

Figure 4.7. Comparison of variable operating costs per kilogram of acetic acid produced for the fermentation process (S-500) with headspace pressures of 2 bar and 10 bar.

Table 4.11 outlines the operational and capital costs per kilogram of acetic acid produced for the fermentation process with headspace pressures of 2 bar and 10 bar.

Table 4.11. Operational and capital costs per kilogram of acetic acid produced for fermentation process (S-500) with headspace pressures of 2 bar and 10 bar.

Item	Headspace pressure of 2 bar cost (€.kg^{-1})	Headspace pressure of 10 bar cost (€.kg^{-1})
Variable operating costs	0.209	0.221
Fixed operating costs	0.025	0.027
CAPEX	0.019	0.035

When comparing variable operating costs, the difference arises from the higher electricity and cold utility demand when working with a headspace pressure of 10 bar. However, this difference is low because raw materials constitute a much larger portion of these costs. Fixed operating costs are higher at 10 bar due to the increased labour required for operation since the number of equipment is higher. Regarding capital expenses, at 10 bar these costs are significantly higher due to the increasing number of equipment and the need for the reactor to operate under a higher pressure.

The minimum fermentation cost is calculated through the iterative procedure explained in Section 2.7.3 that results in a NPV equal to 0.

The minimum fermentation cost for the process with headspace pressures of 2 bar is 0.298 €.kg^{-1}, while for the process with headspace pressure of 10 bar is 0.365 €.kg^{-1}.

Table 4.12 provides an overview of the capacities of traditional acetic acid plants, sugar fermentation-based facilities and plants involved in the production of various chemicals through gas fermentation.

Table 4.12. Product capacities of conventional acetic acid plants, those employing sugar fermentation, and of plants producing other chemicals via gas fermentation.

Product	Production route	Capacity (ton.y^{-1})	Feasibility study/ existing plant	Source
Acetic acid	Gas fermentation	37 407	Feasibility study	This study
Acetic acid	Gas fermentation	53 941	Feasibility study	This study
Acetic acid	Fossil	500 000	Existing plant	[120]
Acetic acid	Fossil	255 000	Existing plant	[121]
Acetic acid	Fossil	150 000	Existing plant	[122]
Acetic acid	Sugar fermentation	120 000	Feasibility study	[68]
Ethanol	Gas fermentation	180 000	Feasibility study	[18]
Methane	Gas fermentation	2 000	Existing plant	[66]
Ethanol	Gas fermentation	45 000	Existing plant	[63]
Ethanol	Gas fermentation	64 000	Existing plant	[64]
Ethanol	Gas fermentation	10 000	Existing plant	[78]
Ethanol	Gas fermentation	180 000	Existing plant	[123]

Comparing the amount of pure acetic acid obtainable from a single fermenter with the data in Table 4.12 it is observed that these capacities are of small to medium size compared to existing plants and feasibility studies on gas fermentation, with the maximum being 180000 ton.y^{-1}. For acetic acid production from fossil sources, industrial plants can reach 500000 ton.y^{-1}. Based on these data it was decided to scale up the fermentation process to reach 500000 ton.y^{-1} by adding multiple fermenters in parallel, analysing then how the minimum price varied. At 2 bar, 14 fermenters are needed to reach 500000 ton.y^{-1}, while at 10 bar only 10 fermenters are requested. In Figure 4.8 the trend of the minimum fermentation cost as a function of plant size for fermentation processes with headspace pressures of 2 bar and 10 bar is depicted. For sizes above 500000 ton.y^{-1}, the minimum fermentation cost is 0.238 €.kg^{-1} for processes with a headspace pressure of 2 bar, while it is 0.277 €.kg^{-1} when fermentation occurs with a headspace pressure of 10 bar.

Even when scaling to larger capacities, the minimum fermentation costs are higher for fermentation carried out with a headspace pressures of 10 bar compared to those at 2 bar. Although fewer fermenters in parallel are needed at 10 bar to achieve the same acetic acid output, the high pressures result in higher capital costs and operating costs for the fermentation section, leading to a higher minimum fermentation cost.

For this reason, the other steps from S-100 to S-800 were simulated basing on the operative conditions and results associated to fermentation occurring with a headspace pressure of 2 bar.

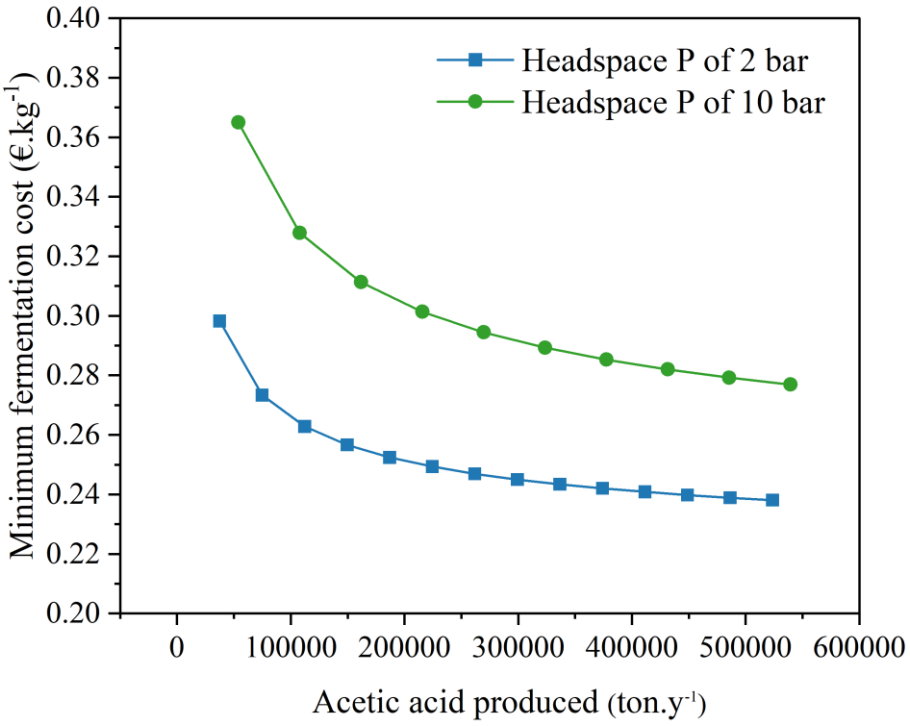

Figure 4.8. Trend of the minimum gas fermentation cost as the plant size varies for fermentation processes with headspace pressures of 2 bar and 10 bar.

4.4 Purification of acetic acid

The modelling of the purification section is described in Section 2.5, whereas the results of the simulation are presented in Section 3.5.

In Table 4.13 the expenses that make up the total investment for the purification process are listed.

Table 4.13. Expenses that make up the Total Project Investment (TPI) for acetic acid purification process, including filtration and ion exchange section (S-600), liquid-liquid extraction section (S-700) and solvent, acid and water recovery section (S-800).

Item	Cost (M€)
Total Equipment Cost (TEC)	19.45
Warehouse	0.29
Site development	1.75
Total Installed Cost (TIC)	21.50
Field expenses	4.30
Home office & construction fee	5.37
Project contingency	0.64
Total indirect expenses	10.31
Total Capital Investment (TCI)	31.80
Other costs	2.15
Total Project Investment (TPI)	33.95

The Total Equipment Cost is obtained from the sum of the bare erected costs given by the Purchase Equipment Cost (PEC) of the individual equipment present in the process.

Figure 4.9 shows the percentage contribution of the bare erected costs for the HEDP process, divided by type of equipment.

The largest contributor is the one associated to azeotropic distillation columns (C-801) contributing approximately 38% of the total. Moreover, filtration and ion exchange section (S-600) plays a significant role, accounting roughly 34% of the overall total. This is justified by the high flowrate that must be purified, requiring then a significant quantity of resins that must be substituted often during the useful plant life. Instead, the contribution of the decanter and exchangers is negligible. Moreover, it must be underlined that the CAPEX of the exchangers and the respective OPEX, even though their contribution is minimal in comparison to the whole process, derive from the results of the energy integration carried out, explained in Section 3.5.

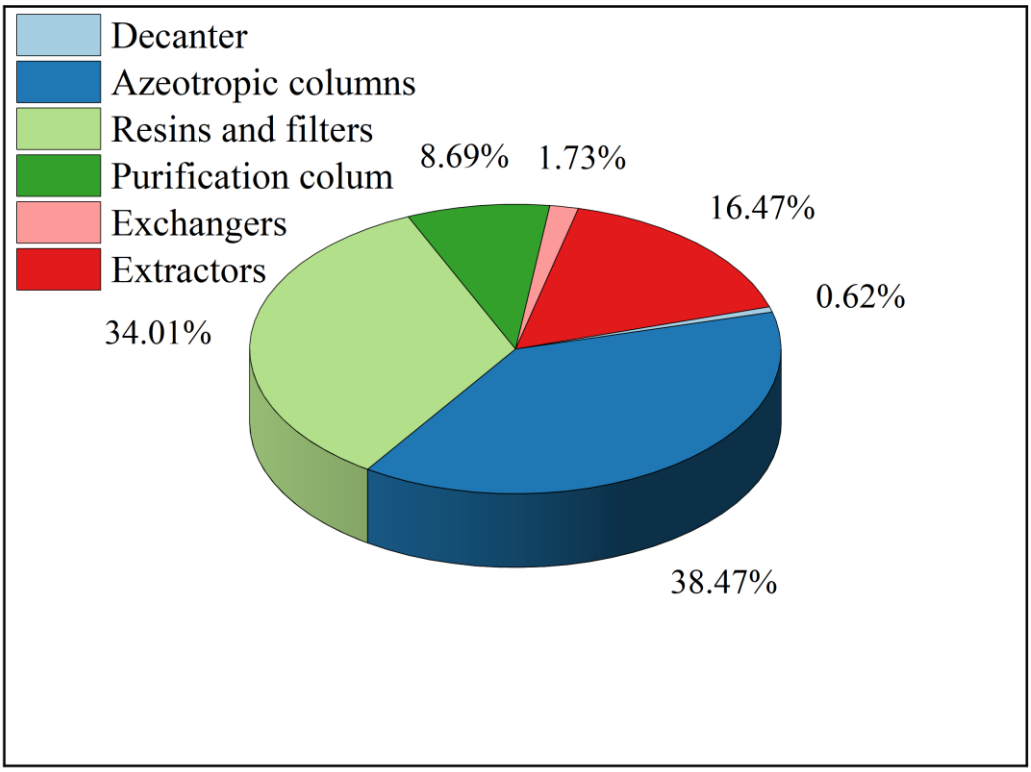

Figure 4.9. Percentage contribution of the bare erected cos for the HEDP process, divided by type of equipment for filtration and ion exchange section (S-600), liquid-liquid extraction section (S-700) and solvent, acid and water recovery section (S-800).

The OPEX evaluation was performed considering 8650 $h.y^{-1}$ of plant operation. For raw materials, the cost of MTBE make-up and the *una tantum* cost were accounted, assuming that the solvent was replaced once a year to address any potential degradation. In addition, the cost of the chemicals for resins regeneration, i.e. NaOH and HCl, were factored in. Moreover, the wastewater treatment and waste chemical treatment cost were taken into account. The former is carried out on the purged water stream in Section S-800, both to avoid issues with recirculation during the simulation of the process but also to prevent the accumulation of soluble components over time. The latter, instead, is performed on MTBE which is replaced once a year. The respective costs are reported in Section 2.7.2. As for the cost of hot and cold utilities, the costs were provided by APEA. Table 4.14 shows the specific operating costs for acetic acid purification process.

Table 4.14. Operating costs related to the purification process of acetic acid, including filtration and ion exchange section (S-600), liquid-liquid extraction section (S-700) and solvent, acid and water recovery section (S-800).

Item	Opex (€.kg^{-1})
Raw Materials	0.149
Utilities	0.246
Overhead	0.009
Maintenance	0.010
Salaries	0.015
Insurance and Taxes	0.009
Other variable costs	0.006

As can be observed from Table 4.14, utilities constitute the largest contributor to OPEX with 55.53% of the total. This is due to the high demand of utilities required by the distillation columns, especially the azeotropic one. An important share is given by raw materials, 33.52% of OPEX, justified by the high flowrate of solvent needed as well as the significant amount of chemicals for the regeneration of resins.

Figure 4.10 shows the annual variable operating expenses normalized on the productivity of the plant.

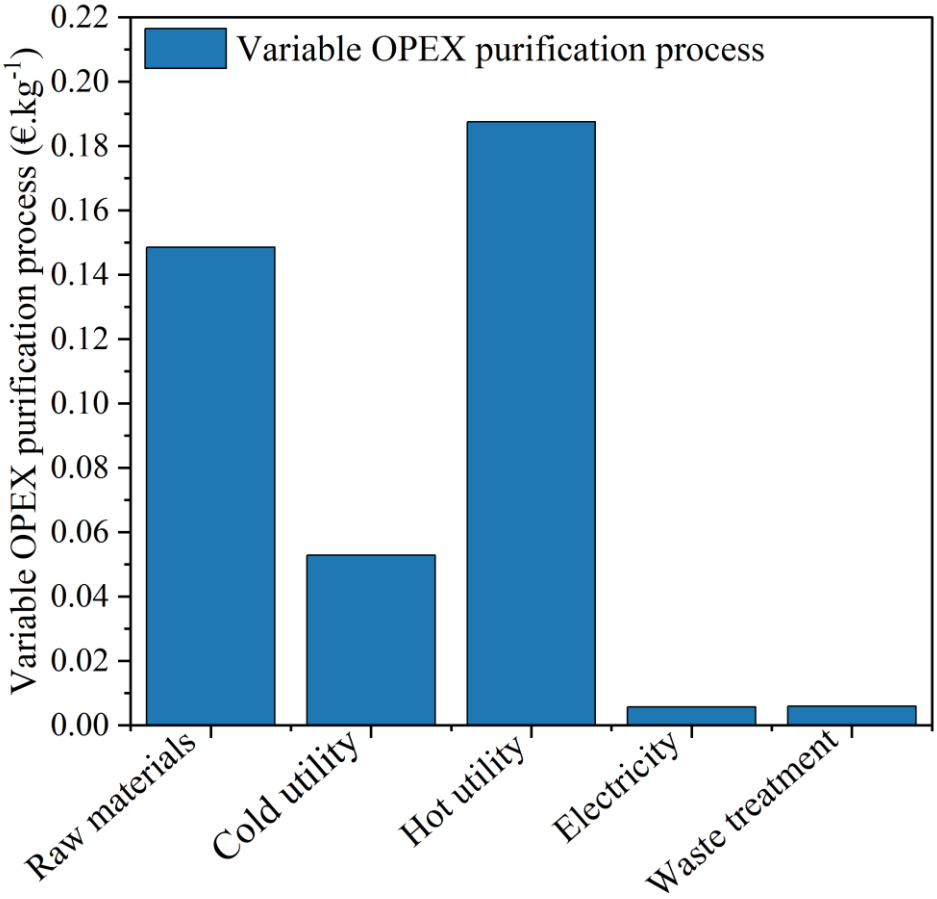

Figure 4.10. Comparison among variable operating costs for acetic acid purification process, including filtration and ion exchange section (S-600), liquid-liquid extraction section (S-700) and solvent, acid and water recovery section (S-800).

As expected, the expense relating to heating is the highest. This is due to the consumption of medium pressure steam in the reboilers of the azeotropic distillation columns (C-801) and the consumption of low-pressure stream in the solvent recovery section in column (C-802). Also cooling has an important impact, given that the expense of the condenser of the various columns is high. Furthermore, there are several exchangers used for cooling the process streams. Although the energy integration carried out and described in depth in Section 3.5 has reduced the demand for cold utilities, the associated expense is not negligible. Instead, the contribution of electricity is certainly insignificant compared to the others.

To obtain the minimum selling price for the purification process, the iterative procedure explained in Section 2.7.3 was applied. In this case the total investment necessary for a plant that produces 37.41 kton.y^{-1} of CH_3COOH is 33.95 M€, the annual fixed operating costs are equal to 1.59 M€.y^{-1} and the variable operating costs are equal to 14.98 M€.y^{-1}. As a result, the cost of purification for this scale is 0.60 € per kilogram of acetic acid produced.

4.5 Overview of the entire process

By combining prices calculated in Alkaline Electrolysis Section (S-100), Removal of H_2S Section (S-200), CO_2 capture Section (S-300), Removal of O_2 Section (S-400), Fermentation Section (S-500), Filtration ad Ion Exchange Section (S-600), Liquid-liquid Extraction Section (S-700) and Solvent, acid and water recovery Section (S-800), a minimum selling price of acetic acid equal to 1.56 €.kg^{-1} for a productivity of 37.41 kton.y^{-1} was determined. Details of the individual contributions are provided in Table 4.15.

Table 4.15. Prices of hydrogen production, CO_2 capture, fermentation with a headspace pressure of 2 bar, purification per kilogram of acetic acid produced, and the overall acetic acid price. These prices refers to a plant productivity of 37.41 kton.y^{-1} in 2023.

ITEM	**Price in 2023 (€.kg^{-1} of acetic acid)**
H_2 (S-100)	0.573
CO_2 (S-200, S-300 and S-400)	0.108
Fermentation with a headspace pressure of 2 bar (S-500)	0.298
Purification (S-600, S-700 and S-800)	0.596
Entire process	1.575

The percentage contribution of the individual sections of the process to the definition of acetic acid price is shown in Figure 4.11.

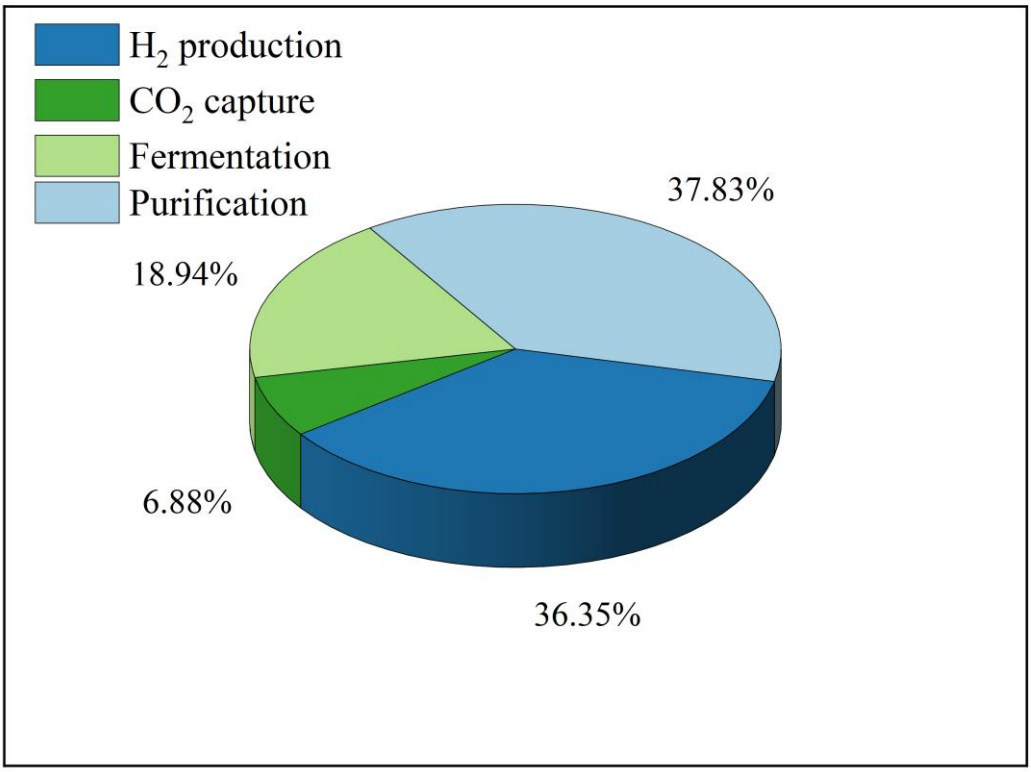

Figure 4.11. Contribution of H_2 production (S-100), CO_2 capture (S-200, S-300 and S-400), fermentation process (S-500) and purification process (S-600, S-700 and S-800) to the definition of acetic acid price in the 2023-scenario with a plant productivity of 37.41 kton.y^{-1}.

It is observed that the highest-cost sections are the purification process and hydrogen production. Specifically, the former contributes 37.8% to the final price, while the latter accounts for 36.4 %.

In terms of capital expenditure, electrolysers are the most expensive equipment, contributing alone to more than 34% of the TEC. The purification section has also a significant impact, as the azeotropic columns and resins contribute respectively to 14.54% and 12.85% of the TEC. Another critical item is the fermenter, which represents 11.93% of the TEC.

The entire process was then analysed and compared in terms of operational expenditure, with the results depicted in Figure 4.12.

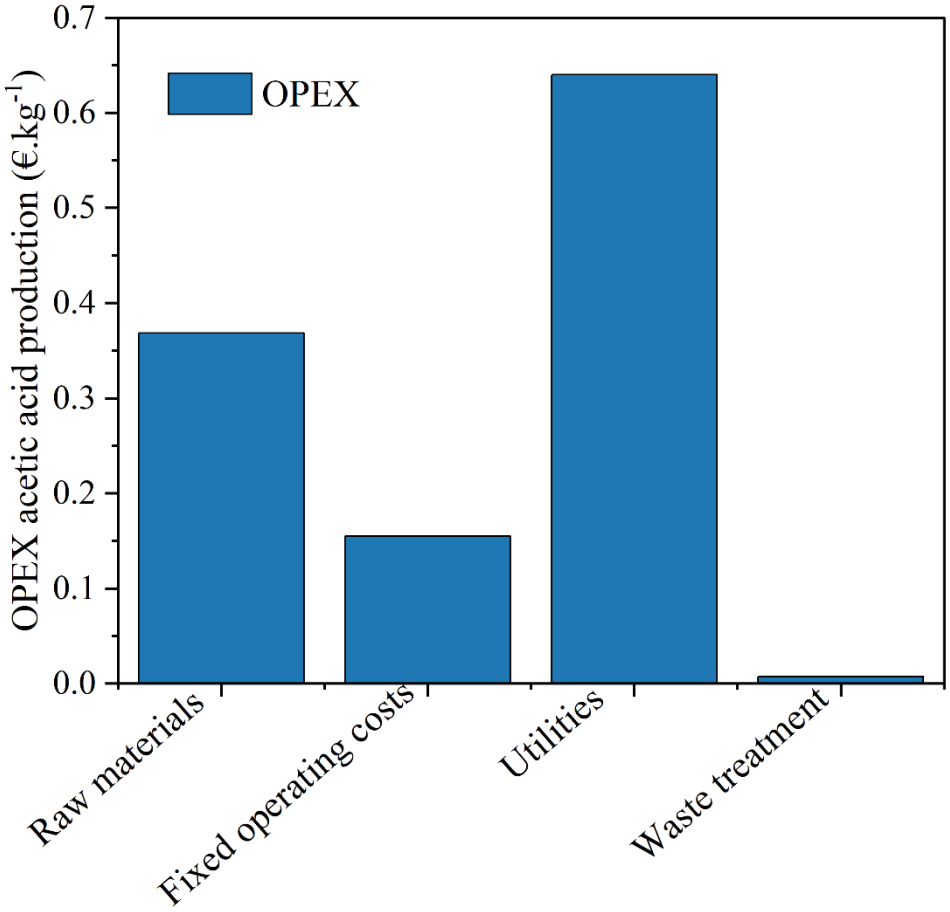

Figure 4.12. Distribution of operating expenses of acetic acid production for a plant characterized by a productivity of 37.41 kton.y^{-1}.

From Figure 4.10 it is observed that the largest impact is that of utilities, which contribute more than the half to the OPEX. Specifically, in terms of utilities, hydrogen production is the most significant section, since the high consumption of electricity accounts for over 45% of total utility cost. Moreover, the purification phase contributes 38%, due to the high demand for both hot and cold utilities, which represent 29.29% and 8.25% of the total respectively. In addition, the cost of MPS for amine regeneration in the carbon dioxide capture process makes up 10.69% of total utility cost.

With respect to raw materials, the greatest contributor is given by the fermentation section, due to the high expense for nutrients, representing more than 55% of the total. Instead, 40.3% of the total cost of raw materials is attributable to the purification phase due to the high cost of chemicals for the regeneration of resins and MTBE make-up.

No-negligible are fixed operating costs, as a result of the elevated number of equipment and the significant TPI. Instead, the impact of waste treatment is low.

A scale-up was further carried out to examine how acetic acid price varied as the size of the plant increased, by adopting multiple fermenters in parallel. To scale up, the CAPEX were evaluated using Equation 2.19, while the OPEX, including wages, were scaled proportionally based on the requested productivity.

The largest size was chosen based on the maximum sizes of green hydrogen production plants via alkaline electrolysis of projects soon to be commercialized. Among these, notable is the HYSYNERGY PROJECT which aims to reach a production of around 20 kton.y^{-1} of

hydrogen by 2025 [124]. Therefore, accordingly on these considerations it was decided to scale-up to the use of 4 fermenters in parallel, which correspond to a productivity of 149.63 kton.y^{-1} of GAA and a request of hydrogen of 20.49 kton.y^{-1}. Moreover, in analogy with the approach outlined in Section 4.3, it was desired to estimate the cost implications of a progressive scaling up until reaching a scale comparable to that of large-scale plants that utilize methanol carbonylation, as showed in Table 4.12. This corresponds to the employment of up to 14 fermenters in parallel. However, a scaling up to this number of fermenters would require significantly higher amounts of hydrogen, up to 71.70 kton.y^{-1}, which makes this scenario unrealistic with the current or near-future hydrogen production capacities. Despite this limitation, it remains interesting to analyse how production capacity influences the MSP of acetic acid in large-scale scenarios.

In Figure 4.13 the trend of the minimum selling price of acetic acid as the scale of the system increases for the 2023 scenario is depicted.

Larger capacities correspond to lower acetic acid prices. This is because capital costs don't increase proportionally with the size of the plant and, consequently, fixed operating expenses do not either. By increasing the size, the MSP tends to stabilize, ultimately approaching a limit value of approximately 1.17 €.kg^{-1}.

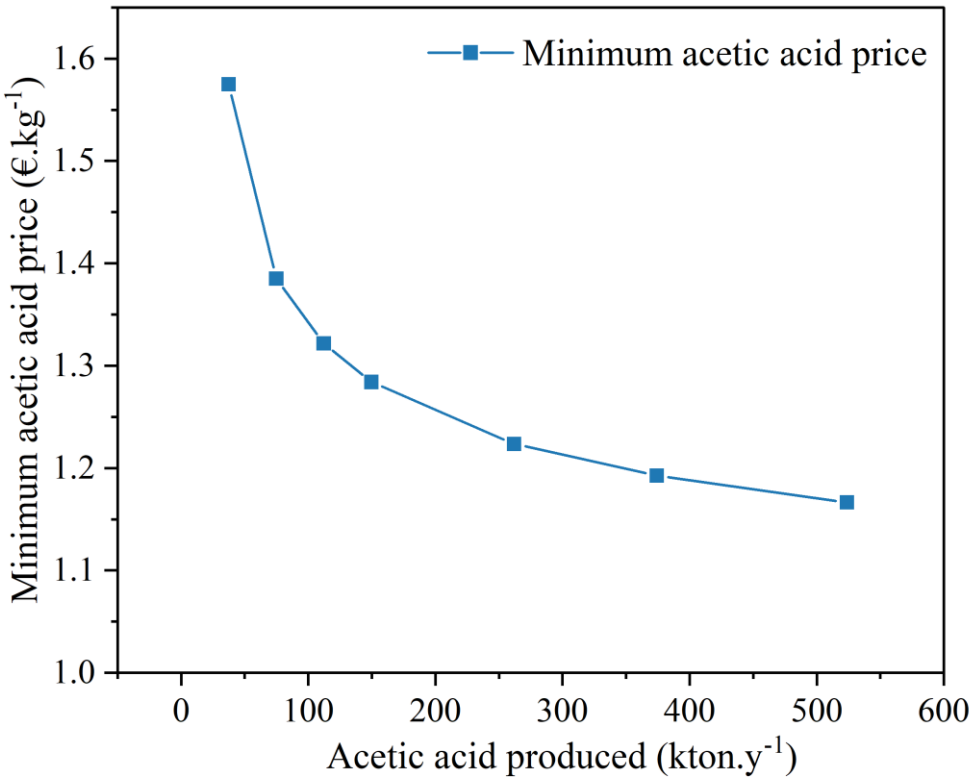

Figure 4.13. Trend of the minimum price of acetic acid as the plant size varies in the 2023 scenario.

Moreover, it was evaluated how acetic acid price changed considering the production of hydrogen according to projected values for 2030. As expected, for the size of 37.41 kton.y^{-}

[1] of acetic acid, the price of acetic acid in the 2030 scenario reduces due to a 14.62% fall in the price of hydrogen production per kilogram of acetic acid, which drops the final price of acetic acid from 1.576 €.kg^{-1} to 1.492 €.kg^{-1}. In this scenario, the purification section accounts 39.95% to the final price, whereas hydrogen production represents 32.80% of the total.

Furthermore, a comparison between the cost implications resulting from the scaling up in 2023 and in 2030 was carried out. The results are represented in Figure 4.14.

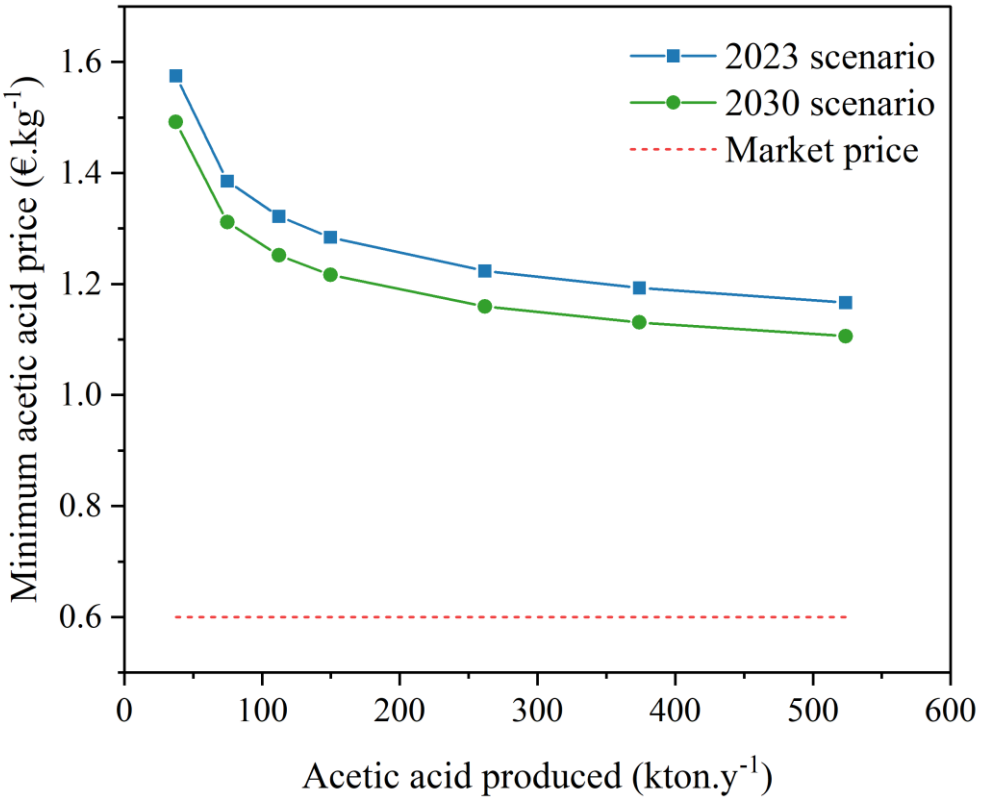

Figure 4.14. Trend of the minimum price of acetic acid as the plant size varies for the 2023 and 2030 scenarios in addition to the comparison with the market price.

The comparison shows how the MSP of acetic acid for the 2030 scenario stabilizes in the largest scale at a price that is 5.20% lower than the previous one, specifically 1.11 €.kg^{-1}. In any case, although at higher sizes acetic acid price drops significantly, it remains decidedly superior than the market value of GAA in 2023, equal to 0.6 €.kg^{-1} [125].

Furthermore, for the entire process the carbon efficiency was evaluated according to Equation 2.32 and is equal to 78.54 %. This indicates that almost 80% of the carbon entering Section S-200 as CO_2 is effectively converted into the product of interest, i.e. acetic acid. This result is justified by the recirculation of all unreacted CO_2 in the fermenter, in addition to the high capture efficiency and the good recovery of acetic acid in the purification step. Moreover, including in the carbon contained in the product not only acetic acid but all carbon dioxide which is converted into acetic acid, formic acid, biomass and dissolved int the liquid, this value increases to 91.04%.

5. Conclusions and future prospects

5.1 Conclusions

Acetic acid is a compound widely used in numerous industrial applications. Its synthesis via gas fermentation could be an interesting alternative both to the synthetic route and sugar fermentation process.

Acetic acid production via gas fermentation uses as raw materials H_2 and CO_2: the first is synthesized via AEL, while the second is captured via chemical absorption with MEA. These substrates are fed to a bioreactor. Since the fermentation produces a highly diluted acetic acid solution, a purification step is required. This is carried out using the HEDP process.

The hydrogen produced has a purity of 80.17 wt% and water electrolysis plant was sized to achieve a productivity of 5.67 kton.y^{-1} of hydrogen.

Carbon dioxide is captured from a waste stream derived from the upgrade process of biogas into bio-methane starting from OFMSW. Upstream of the CO_2 capture process, a purification stage is necessary to remove traces of H_2S present in the feed. Downstream of the absorption process, an additional purification unit is needed to eliminate residual oxygen from the output stream. The capture process was sized to absorb at least 90% of the CO_2 available in the incoming stream and reach a productivity of 70.97 kton.y^{-1} of 99.5 wt% carbon dioxide. The vapor fraction excluding CO_2 and H_2 is water. Since fermentation takes place in an aqueous environment high purity of the substrates is not required, lowering then their production costs.

The fermentation process was simulated at two distinct headspace pressures, 2 bar and 10 bar, to identify the optimal configuration. It was found that at 2 bar, the cost of acetic acid was reduced, despite a lower productivity for the single fermenter. In addition, only a negligible quantity of formic acid was synthesized, facilitating the following purification step. With a single bubble column with a headspace of 2 bar, 37.41 kton.y^{-1} of acetic acid was produced with a concentration in the fermentation broth of 1.5 wt%.

Purification is performed with a hybrid process that integrates solvent extraction with azeotropic distillation (HEDP), utilizing MTBE as a solvent. This turns into a 99.8% of recovery of acetic acid, with a final purity of 99.9 wt%, respecting the concentration requirements for the sale of GAA.

Through an energy analysis, the heat exchange between process streams was maximised in order to reduce energy consumption.

For the entire process, an economic analysis was conducted to determine a minimum selling price of acetic acid. To accomplish this, both total investment expenses and operating costs were evaluated.

As concerns hydrogen production, more than 78% of the sum of the PECs is attributable to the electrolyser, while the largest share of OPEX is given by the high electricity demand. As a result, a price of hydrogen equal to 3.77 €.kg^{-1} for a plant size of 5.68 kton.y^{-1} is obtained. The simulation was repeated using projected hydrogen production values for 2030. With the same plant size, the final price drops to 3.17 €.kg^{-1}.

Regarding carbon dioxide capture, in terms of CAPEX the absorber and the stripper are the most impactful equipment, contributing to more than 40% of the TEC. Instead, among operational expenses hot utility demand for the regeneration of the solvent is predominant.

For a plant that captures 64.02 kton.y^{-1} of CO_2, a minimum selling price of 0.063 €.kg^{-1} is achieved.

In relation to the fermentation section, whether conducted with a headspace pressure of 2 bar or 10 bar, the highest capital investment is attributable to the bubble column fermenter. In terms of OPEX, the nutrients required for the bacterial growth account for almost the entire cost of operating costs. The minimum fermentation cost for the process with headspace pressures of 2 bar is 0.298 €.kg^{-1} for a plant size of 37.41 kton.y^{-1}, while for the process with headspace pressure of 10 bar is 0.365 €.kg^{-1} for a plant capacity of 53.94 kton.y^{-1}. By increasing the quantity of acetic acid produced using multiple fermenters in parallel, until reaching the productivity of the largest conventional plants, the fermentation cost is lower when fermentation occurs at 2 bar. Given the economic advantage, the decision was made to operate at the lower pressure.

With regard to the purification section, the largest contributor to the TEC is given by azeotropic distillation columns and ion exchange resins, together accounting roughly 72% of the total. Concerning OPEX, the high demand of hot utility requested by the reboilers of the columns as well as the large request of MTBE and chemicals for the regeneration of resins contribute to the biggest share of operational expenses.

Combining all sections, for a productivity of 37.41 kton.y^{-1} a price of acetic acid equal to 1.58 €.kg^{-1} is obtained. In addition, a scale-up was further carried out to asses how price might vary as the size approaches that of traditional large-scale plants. It was observed that the price stabilizes at a value of around 1.17 €.kg^{-1}. Moreover, it was evaluated how acetic acid price varied considering the production of hydrogen according to projected values for 2030. In this scenario, at larger scales the price steadies at 1.11 €.kg^{-1}, which remains significantly higher than the 2023 acetic acid market price, i.e. 0.6 €.kg^{-1}.

However, although less economical than traditional methods, gas fermentation offers a sustainable alternative reducing fossil fuels consumption and utilizing CO_2 otherwise emitted to the atmosphere. In fact, almost 80% of carbon entering the capture section is converted into acetic acid.

5.2 Future prospects

Considering the sections that make up the entire fermentation process leading to the synthesis of acetic acid, some prospects can be explored.

Regarding hydrogen production via electrolysis, it represents a promising alternative for synthesizing green hydrogen. However, despite the optimization planned for 2030, there are numerous challenges still to address to make this technology technically, economically and environmentally sustainable. These include reducing the capital cost of the electrolysers and improving energy efficiency. In addition, the electricity employed must come from renewable sources. Also, the progress in the development of new electrolysers, including SOEC, represent an area of interest. To minimize the consumption of water as raw material, as it's a limited and precious resource, research is ongoing to develop electrolysers capable of using directly seawater. This would enable the use of abundant water resources lowering related costs.

With respect to the carbon dioxide absorption process, future challenges concern the utilization of new solvents. The latter must not be toxic and corrosive and should require less energy for regeneration. In this regard, amino blends could represent an alternative to the benchmark MEA.

In relation to the fermentation section, optimizing the composition of the bacterial medium could significantly reduce the elevated associated costs.

As for the purification process, efforts could be focused on reducing the high costs related to the use of azeotropic distillation columns through process intensification. In this regard, acetic acid could be purified with these columns up to an intermediate level of purity, with the final GAA target purity achieved using hydrophilic membranes. Among the latter, hollow fibres membrane could be employed. In particular, the selected material for these membranes should have a great affinity with water and allow the rejection of organic acids, as acetic acid. Their main advantage lies in their high material exchange surface that enables, by modulating the number of fibres inside them, their potential application to purify large flowrates.

Finally, to assess the sustainability of the overall process, a Life Cycle Assessment (LCA) study could be conducted. This methodology evaluates the environmental footprint of a product or service throughout its entire life cycle and identifies its bottlenecks to minimize the environmental impact. For the examined process, it would be particularly valuable to evaluate the Global Warming Potential and Fossil Fuels Consumption.

List of symbols

Parameters

A	Equipment cost attribute
CAPEX	Capital expenses, €
DR	Discount Rate, €
d_1	Empirical parameter, $\Omega.m^2$
d_2	Empirical parameter, $\Omega.m^2.bar^{-1}$
E_a	Activation Energy, $cal.mol^{-1}$
F	Faraday constant
FCI	Fixed capital investment, €
f_{11}	Empirical parameter, $A^2.m^{-4}$
f_{12}	Empirical parameter, $A^2.m^{-4}.°C^{-1}$
f_{21}	Empirical parameter
f_{22}	Empirical parameter, $°C^{-1}$
$H_{2,prod}$	Actual moles of hydrogen produced
$H_{2,th}$	Theoretical moles of hydrogen that should be synthetised
i	Current density, $A.cm^{-2}$
I	Current intensity, A
IEC	Installed Equipment Cost, €
IT	Income Taxes, €
k	Kinetic constant
$\dot{m}$	Mass flowrate, $kg.h^{-1}$
N	Number of electrochemical cells
N_{EQ}	Number of compressors, towers, reactors and heat exchangers
N_{OS}	Number of operators necessary for each shift
NPV	Net present value, €
OPEX	Operating expenses, $€.y^{-1}$
P	Pressure, bar
PEC	Purchase Equipment Cost, €
PL	Plant life, years
P_{SH}	Number of operations that requires the handling of solids
P_{stack}	Power associated to the stack, kW
$\dot{Q}_{cold}$	Cold thermal power, kW
Q_{excess}	Excess heat, kW

$\dot{Q}_{hot}$	Hot Thermal power, kW
r_1	Empirical parameter, $\Omega.m^2$
r_2	Empirical parameter, $\Omega.m^2.°C^{-1}$
s	Empirical parameter, V
T	Temperature, °C
TAC	Total annualized costs, €
TAS	Total Annual Sales, €
TCI	Total Capital Investment, €
TEC	Total Equipment Cost, €
TIC	Total Installed Costs, €
TPC	Total Production Costs, €
TPI	Total Project Investment, €
t_1	Empirical parameter, $m^2.A^{-1}$
t_2	Empirical parameter, $m^2.A^{-1}.°C$
t_3	Empirical parameter, $m^2.A^{-1}.°C^2$
V_{cell}	Cell potential, Volt
V_{rev}	Thermodynamic potential , Volt
V_{tn}	Thermoneutral potential, Volt
z	Number of transferred electrons

Greek symbols

α_1	Installation labour factor
α_2	Building, material and labour factor
γ	Cost exponent factor
ΔH	Enthalpy variation, $kJ.mol^{-1}$
ΔT_{min}	Minimum temperature difference, °C
η_F	Faraday efficiency

Acronyms and abbreviations

ABS	Absorber
AEL	Alkaline electrolyser
AEM	Anion exchange membrane
APEA	Aspen Process Economic Analyzer
C	Column
CEPCI	Chemical Engineering Plant Cost Index

CFD	Computational fluid dynamics
CHW	Chilled water
CSS	Carbon capture and storage
CSTR	Continuous stirred tank reactor
CW	Cooling water
D	Decanter
DAC	Direct air capture
DEA	Diethanolamine
DIBK	Di-iso-butyl kerosene
E	Heat exchanger
EA	Ethyl acetate
ELECNRTL	*Electrolyte non-random two Liquids*
ELECNRTL-RK	*Electrolyte non-random two Liquids with Ridley-Kwong Equation of State*
EPC	Engineering Procurement and Construction
F	Flash separator
GAA	Glacial acetic acid
GGE	Greenhouse gas emissions
GHG	Greenhouse gas
GWP	Global Warming Potential
HEDP	Hydrid extraction/distillation process
HER	Hydrogen Evolution Reaction
IBA	Isobutyl acetate
IPA	Isopropyl acetate
IPCC	Intergovernmental Panel on Climate Change
ITC	International Test centre for CO_2 Capture
KPI	Key performance indicator
LPS	Low pressure steam
MA	Methyl acetate
MDEA	Methyldiethanolamine
MEA	Monoethanolamine
MPS	Medium pressure steam
MSP	Minimum Selling Price
MTBE	Methyl-tert-butyl ether
NOAA	National Oceanic and Atmospheric Administration

NRTL	*Non-random two Liquids*
NRTL -HOC	*Non-random two Liquids-Hayden O'Connel*
OER	Oxygen evolution Reaction
O&M	Operation and maintenance
OFMSW	Organic Fraction of Municipal Solid Waste
P	Pump
PEC	Purchase Equipment Cost
PEM	Proton exchange membrane
PFD	Process Flow Diagram
PZ	Piperazine
R	Reactor
S	Section
STRIP	Stripper
SOEC	Solid oxide water electrolysis cell
THF	Tetrahydrofolate
TPA	Terephthalic acid
TRL	Technological Readiness Level
VA	Vinyl acetate
VAM	Vinyl acetate monomer
VFAA	Volatile carboxylic acids
WLP	Wood-Ljungdahl Pathway

Subscripts

1	Reference year
2	Base year
t	Plant operating year

References

[1] J. L. Martín-Espejo, J. Gandara-Loe, J. A. Odriozola, T. R. Reina, and L. Pastor-Pérez, "Sustainable routes for acetic acid production: Traditional processes vs a low-carbon, biogas-based strategy," *Sci. Total Environ.*, vol. 840, no. February, 2022, doi: 10.1016/j.scitotenv.2022.156663.

[2] A. C. Dimian and A. A. Kiss, "Enhancing the Separation Efficiency in Acetic Acid Manufacturing by Methanol Carbonylation," *Chem. Eng. Technol.*, vol. 44, no. 10, pp. 1792–1802, 2021, doi: 10.1002/ceat.202100230.

[3] ReportLinker, "Chemical Sector Insights: Acetic Acid and Ethyl Acetate Market Trends and Opportunities." Accessed: Apr. 22, 2024. [Online]. Available: https://www.reportlinker.com/plpcluster/5576197

[4] Z. M. Research, "Acetic Acid Market Growth, Size, Share, Trends, and Forecast 2030." Accessed: Apr. 22, 2024. [Online]. Available: https://www.zionmarketresearch.com/report/acetic-acid-market

[5] C. Le Berre, P. Serp, P. Kalck, and G. P. Torrence, "Acetic acid in Ullmann's encyclopedia of industrial chemistry," *Wiley, Weinheim. doi*, vol. 10, no. 1002, p. 14356007, 2011.

[6] P. Pal and J. Nayak, "Acetic Acid Production and Purification: Critical Review Towards Process Intensification," *Sep. Purif. Rev.*, vol. 46, no. 1, pp. 44–61, 2017, doi: 10.1080/15422119.2016.1185017.

[7] F. P. Rosenbaum and V. Müller, "Moorella thermoacetica: A promising cytochrome- and quinone-containing acetogenic bacterium as platform for a CO2-based bioeconomy," *Green Carbon*, vol. 1, no. 1, pp. 2–13, 2023, doi: 10.1016/j.greenca.2023.06.002.

[8] F. M. Liew, M. E. Martin, R. C. Tappel, B. D. Heijstra, C. Mihalcea, and M. Köpke, "Gas Fermentation-A flexible platform for commercial scale production of low-carbon-fuels and chemicals from waste and renewable feedstocks," *Front. Microbiol.*, vol. 7, no. MAY, 2016, doi: 10.3389/fmicb.2016.00694.

[9] A. M. Henstra, J. Sipma, A. Rinzema, and A. J. Stams, "Microbiology of synthesis gas fermentation for biofuel production," *Curr. Opin. Biotechnol.*, vol. 18, no. 3, pp. 200–206, 2007, doi: 10.1016/j.copbio.2007.03.008.

[10] S. Redl, M. Diender, T. Ø. Jensen, D. Z. Sousa, and A. T. Nielsen, "Exploiting the potential of gas fermentation," *Ind. Crops Prod.*, vol. 106, pp. 21–30, 2017, doi: 10.1016/j.indcrop.2016.11.015.

[11] J. Gao, H. K. Atiyeh, J. R. Phillips, M. R. Wilkins, and R. L. Huhnke, "Development of low cost medium for ethanol production from syngas by Clostridium ragsdalei," *Bioresour. Technol.*, vol. 147, pp. 508–515, 2013,

doi: 10.1016/j.biortech.2013.08.075.

[12] J. R. Phillips, R. L. Huhnke, and H. K. Atiyeh, “Syngas fermentation: A microbial conversion process of gaseous substrates to various products,” *Fermentation*, vol. 3, no. 2. MDPI AG, Jun. 01, 2017. doi: 10.3390/fermentation3020028.

[13] Y. C. Ardila, J. E. J. Figueroa, B. H. Lunelli, R. M. Filho, and M. R. W. Maciel, “Simulation of ethanol production via fermentation of the synthesis gas using aspen plustm,” *Chem. Eng. Trans.*, vol. 37, pp. 637–642, 2014, doi: 10.3303/CET1437107.

[14] B. Sirigudi Rahul Rao and A. H. Johannes Thesis Adviser Karen High Sundar Madihally A Gordon Emslie, “BIOMASS TO ETHANOL: PROCESS SIMULATION, VALIDATION AND SENSITIVITY ANALYSIS OF A GASIFIER AND A BIOREACTOR.”

[15] J. Chen, J. A. Gomez, K. Höffner, P. I. Barton, and M. A. Henson, “Metabolic modeling of synthesis gas fermentation in bubble column reactors,” *Biotechnol. Biofuels*, vol. 8, no. 1, Jun. 2015, doi: 10.1186/s13068-015-0272-5.

[16] O. Pardo-Planas, H. K. Atiyeh, J. R. Phillips, C. P. Aichele, and S. Mohammad, “Process simulation of ethanol production from biomass gasification and syngas fermentation,” *Bioresour. Technol.*, vol. 245, pp. 925–932, 2017, doi: 10.1016/j.biortech.2017.08.193.

[17] S. Michailos, D. Parker, and C. Webb, “Design, Sustainability Analysis and Multiobjective Optimisation of Ethanol Production via Syngas Fermentation,” *Waste and Biomass Valorization*, vol. 10, no. 4, pp. 865–876, 2019, doi: 10.1007/s12649-017-0151-3.

[18] C. Piccolo and F. Bezzo, “A techno-economic comparison between two technologies for bioethanol production from lignocellulose,” *Biomass and Bioenergy*, vol. 33, no. 3, pp. 478–491, Mar. 2009, doi: 10.1016/j.biombioe.2008.08.008.

[19] F. Regis, A. H. A. Monteverde, and D. Fino, “A techno-economic assessment of bioethanol production from switchgrass through biomass gasification and syngas fermentation,” *Energy*, vol. 274, Jul. 2023, doi: 10.1016/j.energy.2023.127318.

[20] E. M. de Medeiros, H. Noorman, R. Maciel Filho, and J. A. Posada, “Production of ethanol fuel via syngas fermentation: Optimization of economic performance and energy efficiency,” *Chem. Eng. Sci. X*, vol. 5, Jan. 2020, doi: 10.1016/j.cesx.2020.100056.

[21] R. M. Swanson, J. A. Satrio, R. C. Brown, A. Platon, and D. D. Hsu, “Techno-Economic Analysis of Biofuels Production Based on

Gasification," 2010. [Online]. Available: http://www.osti.gov/bridge

[22] B. Acharya, P. Roy, and A. Dutta, "Review of syngas fermentation processes for bioethanol," *Biofuels*, vol. 5, no. 5, pp. 551–564, Sep. 2014, doi: 10.1080/17597269.2014.1002996.

[23] P. Roy, A. Dutta, and B. Deen, "Greenhouse gas emissions and production cost of ethanol produced from biosyngas fermentation process," *Bioresour. Technol.*, vol. 192, pp. 185–191, 2015, doi: 10.1016/j.biortech.2015.05.056.

[24] D. Choi, D. C. Chipman, S. C. Bents, and R. C. Brown, "A techno-economic analysis of polyhydroxyalkanoate and hydrogen production from syngas fermentation of gasified biomass," *Appl. Biochem. Biotechnol.*, vol. 160, no. 4, pp. 1032–1046, 2010, doi: 10.1007/s12010-009-8560-9.

[25] S. Shiva Kumar and V. Himabindu, "Hydrogen production by PEM water electrolysis – A review," *Mater. Sci. Energy Technol.*, vol. 2, no. 3, pp. 442–454, 2019, doi: 10.1016/j.mset.2019.03.002.

[26] M. Wang, Z. Wang, X. Gong, and Z. Guo, "The intensification technologies to water electrolysis for hydrogen production - A review," *Renew. Sustain. Energy Rev.*, vol. 29, pp. 573–588, 2014, doi: 10.1016/j.rser.2013.08.090.

[27] Nationalgrid, "The hydrogen colour spectrum." Accessed: Jul. 20, 2024. [Online]. Available: https://www.nationalgrid.com/stories/energy-explained/hydrogen-colour-spectrum

[28] S. Shiva Kumar and H. Lim, "An overview of water electrolysis technologies for green hydrogen production," *Energy Reports*, vol. 8, pp. 13793–13813, 2022, doi: 10.1016/j.egyr.2022.10.127.

[29] R. Pinsky, P. Sabharwall, J. Hartvigsen, and J. O'Brien, "Comparative review of hydrogen production technologies for nuclear hybrid energy systems," *Prog. Nucl. Energy*, vol. 123, no. November 2019, p. 103317, 2020, doi: 10.1016/j.pnucene.2020.103317.

[30] M. Sánchez, E. Amores, D. Abad, L. Rodríguez, and C. Clemente-Jul, "Aspen Plus model of an alkaline electrolysis system for hydrogen production," *Int. J. Hydrogen Energy*, vol. 45, no. 7, pp. 3916–3929, 2020, doi: 10.1016/j.ijhydene.2019.12.027.

[31] A. Z. Arsad *et al.*, "Hydrogen electrolyser technologies and their modelling for sustainable energy production: A comprehensive review and suggestions," *Int. J. Hydrogen Energy*, vol. 48, no. 72, pp. 27841–27871, 2023, doi: 10.1016/j.ijhydene.2023.04.014.

[32] Worldometer, "World Population Milestone." Accessed: May 13, 2024. [Online]. Available: https://www.worldometers.info/world-population/#:~:text=8.1 Billion (current),currently living) of the world.

[33] G. carbon Budget, "Fossil CO2 emissions at record high in 2023."

Accessed: May 13, 2024. [Online]. Available: https://globalcarbonbudget.org/fossil-co2-emissions-at-record-high-in-2023/

[34] Rebecca Lindsey, "Climate change: atmospheric carbon dioxide." Accessed: May 13, 2024. [Online]. Available: https://www.climate.gov/news-features/understanding-climate/climate-change-atmospheric-carbon-dioxide#:~:text=Carbon dioxide concentrations are rising,in just a few hundred.

[35] S. Osmanski, "How Do Carbon Emissions Affect the Environment?" Accessed: May 13, 2024. [Online]. Available: https://www.greenmatters.com/p/how-do-carbon-emissions-affect-environment

[36] Y. M. Alshammari, "Scenario analysis for energy transition in the chemical industry: An industrial case study in Saudi Arabia," *Energy Policy*, vol. 150, no. January, p. 112128, 2021, doi: 10.1016/j.enpol.2020.112128.

[37] Climeworks, "Direct air capture: our technology to capture CO_2." Accessed: May 16, 2024. [Online]. Available: https://climeworks.com/direct-air-capture

[38] Climeworks, "Climeworks switches on world's largest direct air capture plant." Accessed: May 16, 2024. [Online]. Available: https://climeworks.com/press-release/climeworks-switches-on-worlds-largest-direct-air-capture-plant-mammoth

[39] Iea50, "Direct air capture." Accessed: May 16, 2024. [Online]. Available: https://www.iea.org/energy-system/carbon-capture-utilisation-and-storage/direct-air-capture

[40] S. Roussanaly, A. L. Brunsvold, E. S. Hognes, J. P. Jakobsen, and X. Zhang, "Integrated techno-economic and environmental assessment of an amine-based capture," *Energy Procedia*, vol. 37, pp. 2453–2461, 2013, doi: 10.1016/j.egypro.2013.06.126.

[41] J. C. M. Pires, F. G. Martins, M. C. M. Alvim-Ferraz, and M. Simões, "Recent developments on carbon capture and storage: An overview," *Chem. Eng. Res. Des.*, vol. 89, no. 9, pp. 1446–1460, 2011, doi: 10.1016/j.cherd.2011.01.028.

[42] J. Gibbins and H. Chalmers, "Carbon capture and storage," *Energy Policy*, vol. 36, no. 12, pp. 4317–4322, 2008, doi: 10.1016/j.enpol.2008.09.058.

[43] W. Y. Hong, "A techno-economic review on carbon capture, utilisation and storage systems for achieving a net-zero CO2 emissions future," *Carbon Capture Sci. Technol.*, vol. 3, no. March, p. 100044, 2022, doi: 10.1016/j.ccst.2022.100044.

[44] X. Zhang, Z. Song, R. Gani, and T. Zhou, “Comparative Economic Analysis of Physical, Chemical, and Hybrid Absorption Processes for Carbon Capture,” *Ind. Eng. Chem. Res.*, vol. 59, no. 5, pp. 2005–2012, 2020, doi: 10.1021/acs.iecr.9b05510.

[45] A. S. Bhown and B. C. Freeman, “Analysis and Status of Post-Combustion Carbon Dioxide Capture Technologies,” pp. 8624–8632, 2020.

[46] W. Gao *et al.*, “Industrial carbon dioxide capture and utilization: State of the art and future challenges,” *Chem. Soc. Rev.*, vol. 49, no. 23, pp. 8584–8686, 2020, doi: 10.1039/d0cs00025f.

[47] X. Ding, H. Chen, J. Li, and T. Zhou, “Comparative techno-economic analysis of CO2 capture processes using blended amines,” *Carbon Capture Sci. Technol.*, vol. 9, no. August, p. 100136, 2023, doi: 10.1016/j.ccst.2023.100136.

[48] A. M. Arias, P. L. Mores, N. J. Scenna, and S. F. Mussati, “Optimal design and sensitivity analysis of post-combustion CO2 capture process by chemical absorption with amines,” *J. Clean. Prod.*, vol. 115, pp. 315–331, 2016, doi: 10.1016/j.jclepro.2015.12.056.

[49] G. T. Rochelle, “Amine Scrubbing for CO2 Capture,” *Science (80-.).*, vol. 325, no. 5948, pp. 1652–1654, 2009, doi: 10.1126/science.1176731.

[50] R. Idem *et al.*, “Pilot plant studies of the CO2 capture performance of aqueous MEA and mixed MEA/MDEA solvents at the University of Regina CO2 capture technology development plant and the boundary dam CO2 capture demonstration plant,” *Ind. Eng. Chem. Res.*, vol. 45, no. 8, pp. 2414–2420, 2006, doi: 10.1021/ie050569e.

[51] L. C. Law, N. Yusoff Azudin, and S. R. Syamsul, “Optimization and economic analysis of amine-based acid gas capture unit using monoethanolamine/methyl diethanolamine,” *Clean Technol. Environ. Policy*, vol. 20, no. 3, pp. 451–461, 2018, doi: 10.1007/s10098-017-1430-1.

[52] A. Vidra and Á. Németh, “Bio-produced Acetic Acid : A Review,” vol. 62, no. 3, pp. 245–256, 2018.

[53] G. Deshmukh and H. Manyar, “Production Pathways of Acetic Acid and Its Versatile Applications in the Food Industry,” *Biotechnol. Appl. Biomass*, 2021, doi: 10.5772/intechopen.92289.

[54] G. Merli, A. Becci, A. Amato, and F. Beolchini, “Acetic acid bioproduction: The technological innovation change,” *Sci. Total Environ.*, vol. 798, p. 149292, 2021, doi: 10.1016/j.scitotenv.2021.149292.

[55] A. Katsyv and V. Müller, “Overcoming Energetic Barriers in Acetogenic C1 Conversion,” *Front. Bioeng. Biotechnol.*, vol. 8, 2020, doi: 10.3389/fbioe.2020.621166.

[56] F. R. Bengelsdorf *et al.*, “Bacterial Anaerobic Synthesis Gas (Syngas) and CO2 + H2 Fermentation,” *Adv. Appl. Microbiol.*, vol. 103, pp. 143–221, 2018, doi: 10.1016/bs.aambs.2018.01.002.

[57] F. Regis, L. Tarraran, A. Monteverde, and D. Fino, “Screening of conditions for the acetic acid production from H2 and CO2 by Thermoanaerobacter kivui in a pressurized stirred tank bioreactor,” *Chem. Eng. J.*, vol. 485, no. November 2023, p. 149685, 2024, doi: 10.1016/j.cej.2024.149685.

[58] F. Regis, “Microbial CO2 Conversion to Acetic Acid: From Laboratory Testing to an Industrial-Scale Model,” Politecnico di Torino, 2024.

[59] A. J. Ungerman and T. J. Heindel, “Carbon monoxide mass transfer for syngas fermentation in a stirred tank reactor with dual impeller configurations,” *Biotechnol. Prog.*, vol. 23, no. 3, pp. 613–620, 2007, doi: 10.1021/bp060311z.

[60] N. Kantarci, F. Borak, and K. O. Ulgen, “Bubble column reactors,” *Process Biochem.*, vol. 40, no. 7, pp. 2263–2283, 2005, doi: 10.1016/j.procbio.2004.10.004.

[61] D. Laupsien, A. Cockx, and A. Line, “Bubble Plume Oscillations in Viscous Fluids,” *Chem. Eng. Technol.*, vol. 40, no. 8, pp. 1484–1493, 2017, doi: 10.1002/ceat.201600690.

[62] X. Li, D. Griffin, X. Li, and M. A. Henson, *Incorporating hydrodynamics into spatiotemporal metabolic models of bubble column gas fermentation*, vol. 116, no. 1. 2019. doi: 10.1002/bit.26848.

[63] H. Province and S. Steel, “Success Stories of Advanced Biofuels for Transport BEIJING SHOUGANG LANZATECH NEW ENERGY SCIENCE & TECHNOLOGY CO ., LTD .: GAS FERMENTATION,” 2018, [Online]. Available: https://artfuelsforum.eu/wp-content/uploads/2020/02/Success-Stories.pdf

[64] CORDIS, “Production of sustainable, advanced bio-ethANOL through an innovative gas-fermentation process using exhaust gases emitted in the STEEL industry.” Accessed: Apr. 21, 2024. [Online]. Available: https://cordis.europa.eu/project/id/656437

[65] V. Ngu, J. Morchain, and A. Cockx, “Spatio-temporal 1D gas–liquid model for biological methanation in lab scale and industrial bubble column,” *Chem. Eng. Sci.*, vol. 251, p. 117478, 2022, doi: 10.1016/j.ces.2022.117478.

[66] E. GmbH, “EIC ACCELERATOR PROGRAM AND THE BIOCAT ROSLEV PROJECT.” Accessed: May 13, 2024. [Online]. Available: https://www.electrochaea.com/projects/

[67] H. Wu, L. Valentino, S. Riggio, M. Holtzapple, and M. Urgun-Demirtas, “Performance characterization of nanofiltration, reverse osmosis, and ion

exchange technologies for acetic acid separation," *Sep. Purif. Technol.*, vol. 265, p. 118108, 2021, doi: 10.1016/j.seppur.2020.118108.

[68] R. Morales-Vera, J. Crawford, C. Dou, R. Bura, and R. Gustafson, "Techno-economic analysis of producing glacial acetic acid from poplar biomass via bioconversion," *Molecules*, vol. 25, no. 18, Sep. 2020, doi: 10.3390/molecules25184328.

[69] K. Li, I. Chien, and C. Chen, "Design and Optimization of Acetic Acid Dehydration Processes," *5th Int. Symp. Adv. Control Ind. Process.*, no. 1998, pp. 126–131, 2014.

[70] L. Petrescu and C. M. Cormos, "Classical and Process Intensification Methods for Acetic Acid Concentration: Technical and Environmental Assessment," *Energies*, vol. 15, no. 21, 2022, doi: 10.3390/en15218119.

[71] D. L. Uribe Santos, J. A. Delgado Dobladez, V. I. Águeda Maté, S. Álvarez Torrellas, and M. Larriba Martínez, "Recovery and purification of acetic acid from aqueous mixtures by simulated moving bed adsorption with methanol and water as desorbents," *Sep. Purif. Technol.*, vol. 237, p. 116368, 2020, doi: 10.1016/j.seppur.2019.116368.

[72] C. S. López-Garzón and A. J. J. Straathof, "Recovery of carboxylic acids produced by fermentation," *Biotechnol. Adv.*, vol. 32, no. 5, pp. 873–904, 2014, doi: 10.1016/j.biotechadv.2014.04.002.

[73] S. Aghapour Aktij, A. Zirehpour, A. Mollahosseini, M. J. Taherzadeh, A. Tiraferri, and A. Rahimpour, "Feasibility of membrane processes for the recovery and purification of bio-based volatile fatty acids: A comprehensive review," *J. Ind. Eng. Chem.*, vol. 81, no. September, pp. 24–40, 2020, doi: 10.1016/j.jiec.2019.09.009.

[74] W. Raza, J. Wang, J. Yang, and T. Tsuru, "Progress in pervaporation membranes for dehydration of acetic acid," *Sep. Purif. Technol.*, vol. 262, no. January, p. 118338, 2021, doi: 10.1016/j.seppur.2021.118338.

[75] I. L. Chien, K. L. Zeng, H. Y. Chao, and J. H. Liu, "Design and control of acetic acid dehydration system via heterogeneous azeotropic distillation," *Chem. Eng. Sci.*, vol. 59, no. 21, pp. 4547–4567, 2004, doi: 10.1016/j.ces.2004.06.041.

[76] C. Chilev *et al.*, "Investigation of acetic acid dehydration by various methods To cite this version : HAL Id : hal-03369925," 2021.

[77] D. D. P. Systems, "Recovery of acetic acid from acqueous waste streams." Accessed: Aug. 01, 2024. [Online]. Available: https://www.dedietrich.com/en/solutions-and-products/extraction/liquid/liquid-extraction/recovery-acetic-acid-aqueous-waste

[78] J. Holmgren, “India: Potential for developing agricultural residues to sustainable ethanol.” Accessed: Apr. 21, 2024. [Online]. Available: https://www.indianchemicalnews.com/opinion/india-potential-for-developing-agricultural-residues-to-sustainable-ethanol-13316

[79] Y. Guo, G. Li, J. Zhou, and Y. Liu, “Comparison between hydrogen production by alkaline water electrolysis and hydrogen production by PEM electrolysis,” *IOP Conf. Ser. Earth Environ. Sci.*, vol. 371, no. 4, 2019, doi: 10.1088/1755-1315/371/4/042022.

[80] AWOE, “Alkaline electrolysers.” Accessed: Jul. 26, 2024. [Online]. Available: https://awoe.net/Water-Electrolysis-Alkaline-Technology.html

[81] L. Hanzon, “Technoeconomic Analysis of the Co-Production of Hydrogen and Power in Thermochemical-Based Biorefineries,” p. 133, 2020, [Online]. Available: https://www.mines.edu/aes/wp-content/uploads/sites/320/2020/01/Hanzon_MS-Thesis-2011.pdf

[82] M. Tecnnologies, “Removing H2S from Gas streams.” Accessed: Sep. 01, 2024. [Online]. Available: https://merichemtech.com/sulfur-recovery-with-lo-cat/?doing_wp_cron=1725191918.7372579574584960937500

[83] A. S. Bhown and B. C. Freeman, “Analysis and status of post-combustion carbon dioxide capture technologies,” *Environ. Sci. Technol.*, vol. 45, no. 20, pp. 8624–8632, 2011, doi: 10.1021/es104291d.

[84] B. R. Madeddu Claudio, Errico Massimiliano, *CO2 Capture by Reactive Absorption-Stripping Modeling, Analysis and Design*, 1st ed. 2019.

[85] T. Peppel *et al.*, “Methods for the Trace Oxygen Removal from Methane-Rich Gas Streams,” *Chem. Eng. Technol.*, vol. 40, no. 1, pp. 153–161, 2017, doi: 10.1002/ceat.201600171.

[86] R. Turton, *Analysis, Synthesis, and Design of Chemical Processes Fourth Edition*, vol. 53, no. 9. 2013.

[87] C. H. Partnership, “Clean Hydrogen JU - SRIA Key Performance Indicators (KPIs).” Accessed: Oct. 31, 2024. [Online]. Available: https://www.clean-hydrogen.europa.eu/knowledge-management/strategy-map-and-key-performance-indicators/clean-hydrogen-ju-sria-key-performance-indicators-kpis_en

[88] J. M. Bressanin *et al.*, “Techno-economic and environmental assessment of biomass gasification and fischer-tropsch synthesis integrated to sugarcane biorefineries,” *Energies*, vol. 13, no. 17, 2020, doi: 10.3390/en13174576.

[89] “Chem Eng Technol - 2016 - Peppel - Methods for the Trace Oxygen Removal from Methane-Rich Gas Streams.pdf.”

[90] M. Hänchen, A. Stiel, Z. R. Jovanovic, and A. Steinfeld, “Thermally driven copper oxide redox cycle for the separation of oxygen from gases,” *Ind. Eng.*

Chem. Res., vol. 51, no. 20, pp. 7013–7021, 2012, doi: 10.1021/ie202474s.

[91] E. Alonso, F. R. Field, and R. E. Kirchain, "Platinum availability for future automotive technologies," *Environ. Sci. Technol.*, vol. 46, no. 23, pp. 12986–12993, 2012, doi: 10.1021/es301110e.

[92] D. Humbird, R. Davis, and J. D. McMillan, "Aeration costs in stirred-tank and bubble column bioreactors," *Biochem. Eng. J.*, vol. 127, pp. 161–166, 2017, doi: 10.1016/j.bej.2017.08.006.

[93] B. Analytiq, "Potassium hydroxide prrice index." [Online]. Available: https://businessanalytiq.com/procurementanalytics/index/potassium-hydroxide-price-index/

[94] Chemanalyst, "Chemanalyst." Accessed: Oct. 25, 2023. [Online]. Available: https://www.chemanalyst.com/

[95] Federchimica, "Federchimica." Accessed: Oct. 31, 2024. [Online]. Available: https://www.federchimica.it/portale-dei-servizi

[96] W. Short, D. Packey, and T. Holt, "A manual for the economic evaluation of energy efficiency and renewable energy technologies," *Renew. Energy*, vol. 95, no. March, pp. 73–81, 1995, doi: NREL/TP-462-5173.

[97] E. Tito *et al.*, "Conceptual design and techno-economic assessment of coupled hydrothermal liquefaction and aqueous phase reforming of lignocellulosic residues," *J. Environ. Chem. Eng.*, vol. 11, no. 1, p. 109076, 2023, doi: 10.1016/j.jece.2022.109076.

[98] S. Dokhani, M. Assadi, and B. G. Pollet, "Techno-economic assessment of hydrogen production from seawater," *Int. J. Hydrogen Energy*, vol. 48, no. 26, pp. 9592–9608, 2023, doi: 10.1016/j.ijhydene.2022.11.200.

[99] M. O. Yangyanh Li, Tao Zhang, Jugang Ma, Mintao Deng, Junjie Gu, Fuyuan Yang, "Study the effect of lye flow rate, temperature, system pressure and different current density on energy consumption in catalyst test and 500W commercial alkaline water electrolysis," *Mater. Today Phys.*, 2022, doi: https://doi.org/10.1016/j.mtphys.2022.100606 Get rights and content.

[100] K. Zouhri and S. Y. Lee, "Evaluation and optimization of the alkaline water electrolysis ohmic polarization: Exergy study," *Int. J. Hydrogen Energy*, vol. 41, no. 18, pp. 7253–7263, 2016, doi: 10.1016/j.ijhydene.2016.03.119.

[101] B. Lee, H. Chae, N. H. Choi, C. Moon, S. Moon, and H. Lim, "Economic evaluation with sensitivity and profitability analysis for hydrogen production from water electrolysis in Korea," *Int. J. Hydrogen Energy*, vol. 42, no. 10, pp. 6462–6471, 2017, doi: 10.1016/j.ijhydene.2016.12.153.

[102] W. Kuckshinrichs, T. Ketelaer, and J. C. Koj, "Economic analysis of improved alkaline water electrolysis," *Front. Energy Res.*, vol. 5, no. FEB,

2017, doi: 10.3389/fenrg.2017.00001.

[103] F. Barbir, “PEM electrolysis for production of hydrogen from renewable energy sources,” *Sol. Energy*, vol. 78, no. 5, pp. 661–669, 2005, doi: 10.1016/j.solener.2004.09.003.

[104] R. Adolph, “済無No Title No Title No Title,” vol. 33, no. 1, pp. 1–23, 2016.

[105] A. Hassanpouryouzband, E. Joonaki, K. Edlmann, and R. S. Haszeldine, “Offshore Geological Storage of Hydrogen: Is This Our Best Option to Achieve Net-Zero?,” *ACS Energy Lett.*, vol. 6, pp. 2181–2186, 2021, doi: 10.1021/acsenergylett.1c00845.

[106] F. Dawood, M. Anda, and G. M. Shafiullah, “Hydrogen production for energy: An overview,” *Int. J. Hydrogen Energy*, vol. 45, no. 7, pp. 3847–3869, 2020, doi: 10.1016/j.ijhydene.2019.12.059.

[107] M. R. Shaner, H. A. Atwater, N. S. Lewis, and E. W. McFarland, “A comparative technoeconomic analysis of renewable hydrogen production using solar energy,” *Energy Environ. Sci.*, vol. 9, no. 7, pp. 2354–2371, 2016, doi: 10.1039/c5ee02573g.

[108] J. L. Fan, P. Yu, K. Li, M. Xu, and X. Zhang, “A levelized cost of hydrogen (LCOH) comparison of coal-to-hydrogen with CCS and water electrolysis powered by renewable energy in China,” *Energy*, vol. 242, p. 123003, 2022, doi: 10.1016/j.energy.2021.123003.

[109] D. Jang, J. Kim, D. Kim, W. B. Han, and S. Kang, “Techno-economic analysis and Monte Carlo simulation of green hydrogen production technology through various water electrolysis technologies,” *Energy Convers. Manag.*, vol. 258, no. November 2021, p. 115499, 2022, doi: 10.1016/j.enconman.2022.115499.

[110] F. Vega, F. M. Baena-Moreno, L. M. Gallego Fernández, E. Portillo, B. Navarrete, and Z. Zhang, “Current status of CO2 chemical absorption research applied to CCS: Towards full deployment at industrial scale,” *Appl. Energy*, vol. 260, no. February, 2020, doi: 10.1016/j.apenergy.2019.114313.

[111] E. Adu, Y. Li, Y. Zhang, Y. Xin, and P. Tontiwachwuthikul, “Optimization and energy assessment of technological process for CO2 capture system of natural gas and coal combustion,” *Energy Reports*, vol. 8, pp. 7612–7627, 2022, doi: 10.1016/j.egyr.2022.06.004.

[112] L. F. De Mello, R. Gobbo, G. T. Moure, and I. Miracca, “Oxy-combustion technology development for Fluid Catalytic Crackers (FCC) - Large pilot scale demonstration,” *Energy Procedia*, vol. 37, pp. 7815–7824, 2013, doi: 10.1016/j.egypro.2013.06.562.

[113] E. S. Rubin, J. E. Davison, and H. J. Herzog, “The cost of CO2 capture and

storage," *Int. J. Greenh. Gas Control*, vol. 40, pp. 378–400, 2015, doi: 10.1016/j.ijggc.2015.05.018.

[114] S. Yun, M. G. Jang, and J. K. Kim, "Techno-economic assessment and comparison of absorption and membrane CO2 capture processes for iron and steel industry," *Energy*, vol. 229, p. 120778, 2021, doi: 10.1016/j.energy.2021.120778.

[115] H. Isogai, C. A. Myers, and T. Nakagaki, "Cost estimation of CCS integration into thermal power plants in Japan," *Proc. Int. Conf. Power Eng. 2021, ICOPE 2021*, vol. 9, no. 4, pp. 1–18, 2021, doi: 10.1299/mej.22-00028.

[116] K. Damen, R. Faber, R. Gnutek, H. A. J. Van Dijk, C. Trapp, and L. Valenz, "Performance and modelling of the pre-combustion capture pilot plant at the Buggenum IGCC," *Energy Procedia*, vol. 63, pp. 6207–6214, 2014, doi: 10.1016/j.egypro.2014.11.652.

[117] M. Bailera, P. Lisbona, B. Peña, and L. M. Romeo, "A review on CO2mitigation in the Iron and Steel industry through Power to X processes," *J. CO2 Util.*, vol. 46, 2021, doi: 10.1016/j.jcou.2021.101456.

[118] Y. Yang *et al.*, "Techno-economic assessment and exergy analysis of iron and steel plant coupled MEA-CO2 capture process," *J. Clean. Prod.*, vol. 416, no. July, p. 137976, 2023, doi: 10.1016/j.jclepro.2023.137976.

[119] IEA Greenhouse Gas R&D Programme (IEA GHG), "Cost and Performance of Carbon Dioxide Capture from Power Generation," *IEA Energy Pap.*, 2011, [Online]. Available: http://www.environmentportal.in/files/costperf_ccs_powergen.pdf

[120] Alan S. Brown, "Celanese opens Singapore acetic acid plant." Accessed: Apr. 21, 2024. [Online]. Available: https://www.chemicalonline.com/doc/celanese-opens-singapore-acetic-acid-plant-0002

[121] ICIS, "BP to handle US acetic acid sales for Eastman." Accessed: Apr. 21, 2024. [Online]. Available: https://www.icis.com/explore/resources/news/2018/07/23/10244014/bp-to-handle-us-acetic-acid-sales-for-eastman/

[122] ICIS, "Chemical profile: Europe acetic acid." Accessed: Apr. 21, 2024. [Online]. Available: https://www.icis.com/subscriber/icb/2020/08/07/10538362/chemical-profile-europe-acetic-acid/#_=_

[123] M. B. M., "Calif. firm to use LanzaTech process." Accessed: Apr. 21, 2024. [Online]. Available: https://cen.acs.org/articles/94/i13/Calif-firm-use-LanzaTech-process.html

[124] N. Muro-Suné, “HySynergy green H2 production plant.” Accessed: Nov. 04, 2024. [Online]. Available: https://www.ramboll.com/projects/energy/hysynergy-green-h2-production-plant

[125] Chemanalyst, “Track acetic acid price trend and forecast in top 10 leading countries worldwide.” Accessed: Nov. 06, 2024. [Online]. Available: https://www.chemanalyst.com/Pricing-data/acetic-acid-9